University of Dundee

University of Dundee

DOCTOR OF PHILOSOPHY

Magnetic Resonance Assessment of Aortic Stiffness in Diabetes and Cardiovascular Disease

Cassidy, Deirdre

Award date:
2014

Link to publication

General rights
Copyright and moral rights for the publications made accessible in the public portal are retained by the authors and/or other copyright owners and it is a condition of accessing publications that users recognise and abide by the legal requirements associated with these rights.

- Users may download and print one copy of any publication from the public portal for the purpose of private study or research.
- You may not further distribute the material or use it for any profit-making activity or commercial gain
- You may freely distribute the URL identifying the publication in the public portal

Take down policy
If you believe that this document breaches copyright please contact us providing details, and we will remove access to the work immediately and investigate your claim.

Download date: 05. May. 2023

Magnetic Resonance Assessment of Aortic Stiffness in Diabetes and Cardiovascular Disease

Deirdre Cassidy

A thesis submitted in fulfilment of the requirements for the degree of Doctor of Philosophy

Division of Cardiovascular and Diabetes Medicine,

Medical Research Institute,

University of Dundee

September 2014

TABLE OF CONTENTS

LIST OF FIGURES

LIST OF TABLES

ABREVIATIONS AND SYMBOLS

A	Area
AA_0	Ascending aorta
ABI	Ankle-brachial index
ACC/AHA	American college of cardiology / American heart association
AD	Aortic distensibility
α_E	Ernst angle
AGE	Advanced glycation end-products
ANOVA	Analysis of variance
AP	Aortic pressure
AUC	Area under curve
B_o	Static magnetic field strength
BSA	Body surface area
bSSFP	Balanced steady state free precession
BMI	Body mass index
BNP	Brain natriuretic peptide
CHF	Chronic heart failure
cIMT	C-reactive protein
CHD	Coronary heart disease
CD	Cardiac death
CF-PWV	Carotid- femoral pulse wave velocity
C-PWV	Conventional pulse wave velocity
CRF	Case report form
C-RP	C-reactive protein
CT	Computed tomography
CVD	Cardiovascular disease
DA_o	Descending aorta
DBP	Diastolic blood pressure
DHS	Dallas Heart Study

E	Young's modulus of elasticity
ECG	Electrocardiogram
EDV	End diastolic volume
EF	Ejection fraction
eGFR	Estimated glomerular filtration rate
eNOS	Endothelial nitric oxide synthase
ESV	End systolic volume
FLASH	Fast low-angle shot
FoV	Field of view
FVE	Fourier velocity encoding
G	Group
Gd-DTPA	Gadolinium-diethylentriaminepentaacetate
GE	Gradient echo
HDL	High density lipoprotein
HIC	Health informatics centre
HR	High resolution
hs-CRP	High sensitivity c-reactive protein
Hz	Hertz
IDL	Intermediate-density lipoprotein
IHD	Ischaemic heart disease
γ	Lamour frequency of spins
LGE	Left gadolinium enhancement
LR	Low resolution
LSD	Least significant difference
LV	Left ventricle
LVEF	Left ventricle ejection fraction
LVH	Left ventricle hypertrophy
LVP	Left ventricle pressure
LVM	Left ventricle mass
MAP	Mean arterial pressure
MESA	Multi-ethnic study of atherosclerosis

MHz	Mega-hertz
MI	Myocardial infarction
M-mode	Motion mode
MR	Magnetic resonance
MRI	Magnetic resonance imaging
MS-PWV	Multi-site pulse wave velocity
MMP	Matrix metalloproteases
MRI	Magnetic resonance imaging
NMR	Nuclear magnetic resonance
NO	Nitric oxide
NHS	National health service
OHP	Older healthy population
OHV	Older healthy volunteers
PC-MRI	Phase contrast magnetic resonance imaging
PP	Pulse pressure
PPG	Peripheral pulse gating
PVD	Peripheral vascular disease
PWV	Pulse wave velocity
Q	Flow rate
RF	Radiofrequency
ROI	Region of interest
SA	Short axis
SBP	Systolic blood pressure
SD	Standard deviation
SMC	Smooth muscle cell
SNR	Signal to noise ratio
SSFP	Steady state free precesssion
SV	Stroke volume
T	Tesla
T1DM	Type-1 diabetes mellitus
T2DM	Type-2 diabetes mellitus

TE	Echo time
TIA	Transient ischaemic attack
TR	Repetition time
TrueFISP	Fast imaging with steady-state precession
TT	Transit time
TTF	Time to foot
TTP	Time to point
TTU	Time to upslope
$\bar{v}$	Average velocity
$\emptyset$	Vessel diameter
VENC	Velocity encoding
WSS	Wall shear stress
YHP	Young healthy population
YHV	Young healthy volunteers

ACKNOWLEDGEMENTS

Firstly, I would like to thank my supervisors Prof Graeme Houston, Dr Steve Gandy and Dr Faisel Khan for their high level of support and expertise. With their guidance, training and advice, they facilitated this opportunity to undertake my doctoral studies at the University of Dundee.

Additionally, I would like to thank the NHS Tayside MRI team for all their assistance and willingness to help over the past four years. To the Fuller lab and the Division of Cardiovascular and Diabetes Medicine, who provided a dynamic academic environment and many stimulating scientific discussions, for which I am grateful.

It goes without saying, the support from my fellow colleagues and friends has been very much appreciated. Also, to my flatmates who have endured many months of listening about this thesis. Their encouragement and support has not gone unnoticed.

Finally, and most importantly, I would to thank my parents and family for their support and love they have given me over the past few years, without which, none of this would be possible.

DECLARATION

I, Deirdre Cassidy, declare that this thesis is based on results obtained from investigations which I have personally carried out, and that the entire thesis is my own composition. Any work other than my own is clearly stated in the text and acknowledged with reference to any relevant investigators or contributors. For instance, in Chapter 4, to test inter-observer reproducibility, flow quantification analysis was kindly repeated by Dr Jonathan Weir-Mc Call (JWC). Also, left ventricular segmentation analysis in Chapter 5 and Chapter 7 was completed by experienced cardiac researchers, Dr Shona Matthew (SM) and Dr Suzanne Duce (SD). This thesis has never been presented previously, in whole or in part, for the award of any higher degree. I have consulted all the references cited within the text of this thesis.

Signed Deirdre Cassidy Date 30/09/14

SUPERVISOR STATEMENT

I, Professor Graeme Houston, confirm that Deirdre Cassidy has done this research under my supervision and that I have read this thesis. Also, the conditions of ordinance and relevant regulations of the University of Dundee have been fulfilled, thereby qualifying her to submit her thesis in the application for the degree of Doctor of Philosophy.

Signed……  …… Date ……23/9/14……

SUMMARY

Arterial stiffness has been demonstrated to predict cardiovascular morbidity above and beyond traditional risk factors and can be estimated from measurements such as pulse wave velocity (PWV). Aortic PWV can be estimated from the carotid and femoral sites (CF-PWV) by applanation tonometry and ultrasound. However, these methods only estimate a gross global burden, which may mitigate regional stiffness within the vasculature, and can be subjected to errors relating to uncertainties in estimating vessel length. Magnetic resonance imaging (MRI) is an established clinical cardiovascular imaging modality which like ultrasound, has the advantage of being non-invasive and non-ionising. Whilst not typically part of a clinical cardiovascular examination, MRI sequences can be implemented to provide localised aortic PWV measurements directly from aortic sites.

PWV derived by MRI (MR-PWV) is mostly confined to clinical research. It has been determined with high reproducibility and validated against invasive pressure measurements. MRI, as a technique, bears the potential to evaluate vascular anatomy and cardiac function in a single examination. For instance, it can provide aortic stiffness measure with a corresponding left ventricular assessment. Therefore, techniques such as MR-PWV warrants further investigation to see if it may prove beneficial in the detection of sub-clinical disease or as an imaging biomarker of cardiovascular disease (CVD).

In this research, MR-PWV was estimated using conventional methodology by determining the pulse wave transit time between two aortic sites, derived using MRI velocity encoded imaging of the aorta. When the technique was applied to a complicated diabetic population

with and without symptomatic CVD in chapter 5, PWV yielded an important distinction between the groups (CVD with T2DM: 8.7 ± 2.8 ms^{-1}, *n* =22, T2DM: 7.5 ± 2.3 ms^{-1}, *n* =28, CVD without T2DM: 8.9 ± 3.6 ms^{-1}, *n* =19 versus control 6.7 ± 1.8 ms^{-1}, *n* =19, ANOVA $P < 0.05$). However, it did not show significant differences in patients with T2DM before onset of symptomatic CVD.

This conventional method of PWV assessment was extended into a multi-site approach sampling several points along the aorta, with the hypothesis that aortic stiffness is a heterogeneous process that varies along the aortic length. This multi-site pulse wave velocity (MS-PWV) technique has been shown to increase the accuracy of PWV measures and was utilised in a subsequent study in chapter 6 and 7, involving healthy volunteers and patients with peripheral vascular disease (PVD) , (healthy volunteers under 40 years: 4.5 ± 0.7 ms^{-1}, n = 22, older healthy volunteers over 40 years: 6.5 ± 1.5 ms^{-1}, n=22 versus PVD patients 8.6 ± 3.1 ms^{-1}, n = 26, $P < 0.001$).

This thesis provides a novel insight into the process of arterial stiffening and subsequent cardiovascular health throughout different disease cohorts. It differs from current published work by examining MR-PWV in a heterogeneous diabetes and CVD population, while previous studies have solely examined either diabetic or CVD patients. Secondly, the use of MS-PWV has only been implemented in three previous studies to date; involving both a healthy population and cohort with Marfan syndrome. This research is the first to use this technique in PVD and the only study to derive MS-PWV in this population.

In summary, PWV was shown to change with both the extent and severity of atherosclerosis and CVD, which is agreement with previous studies. This demonstrates that MR-PWV may be a useful research tool within the area of cardiovascular MRI and further work is needed to clinically define the potential impact of PWV.

PREFACE

CVD is poised to become one of the most significant health problems worldwide. There is an inherent relationship between pathophysiology, biochemistry and structural remodelling with adverse cardiovascular outcomes. The research encompassed by this thesis involves the development and optimisation of cardiac imaging techniques in MRI and therefore detailed pathophysiology and biochemistry are outwit the scope of this thesis.

The research study participants involved in this thesis have been part of larger research studies within the department of Cardiovascular and Diabetes Medicine and the University of Dundee. The Clinical Research Centre facilitates MRI imaging (*Siemens Trio* 3.0 Tesla MRI scanner) and is utilised in many local, national and European studies. These studies often apply MRI to answer research questions at the forefront of neuroimaging, angiography to cardiac imaging.

Two substantial cardiovascular research studies carried out in the department include; The TASCFORCE Project: Tayside Screening for Risk of Cardiac Events and SUMMIT: Surrogate Markers for Micro- and Macro-vascular hard endpoints for Innovative diabetes Tools. Both projects have had assessments from both MRI and the Vascular and Inflammatory Unit. Simultaneously, a collection of other data has also been harvested from these studies including novel blood biomarkers and genomic screening.

One of the largest studies carried out in the department to date was the TASCFORCE study. All in all, over 1500 participants received a cardiac MRI scan as part of a larger screening program for to identify people with an increase risk of CVD. The participants were aged 40 and over, free from CVD and without an indication of preventative medication (e.g. statins). According to Adult Treatment Panel III (ATP III), they had less than a 20% 10 year risk of cardiovascular events. This cohort is referred to as 'older healthy volunteers' in Chapter 4 and Chapter 7.

The SUMMIT study was part of the IMI funded European SUMMIT project. As part of the imaging work package 3, University of Dundee investigated a population of patients with T2DM, with and without evidence of CVD and non-diabetic control patients with and without evidence of CVD. The aim of the SUMMIT consortium was to identify markers that can predict the risks of developing diabetic micro and macrovascular complications including diabetic nephropathy, diabetic retinopathy and CVD. For this sub-study, the objective was to evaluate different MRI imaging techniques such as aortic PWV, LV cardiac function and whole body angiography. These results are presented in Chapter 5.

This thesis is structured to provide an introduction to the cardiovascular system, with particular emphasis on the role of arterial stiffness and derivation of PWV using MRI techniques, followed by the project aims and hypothesis. The following chapter outlines the underlining theory of cardiac MRI and image formation. Subsequently, detailed descriptions of the equipment setup, image acquisition and analysis used will be discussed. The experimental chapters start from Chapter 4, where initial results for initial validation and optimisation of MR-PWV in this centre are presented. In Chapter 5, this MR-PWV

technique is evaluated as part of the MRI protocol for SUMMIT. Subsequently, a modification of the conventional MR-PWV technique into a multi-site aortic assessment is investigated in Chapter 6 and Chapter 7. Further details of the experimental cohorts are outlined in Table 1-5.

Part of the results presented in this thesis has also involved work from other fellow colleagues in the department. In Chapter 4, to test inter-observer reproducibility, flow quantification analysis was kindly repeated by Dr Jonathan Weir-Mc Call (JWC). Also, left ventricular segmentation analysis in Chapter 5 and Chapter 7 was completed by experienced cardiac researchers, Dr Shona Matthew (SM) and Dr Suzanne Duce (SD).

CHAPTER 1

Background and Literature Review

1.1 Development of the vascular network

The early vasculature is initiated from the first passage of fluid ejected from the immature heart in human embryogenesis. The remodelling of the vascular network is initiated by the first passage of blood flow which triggers a signal cascade based on physical cues including both shear stress and circumferential stress. This also allows the identification of arterial and venous systems, angiogenesis and the regulation of genes through mechanotransduction (Hahn & Schwartz 2009). These processes ensure the future stability of the mature vascular network. The walls of large vessels are composed of vascular smooth muscles cells (SMCs) which lineage tracking studies have shown that vascular SMCs in different vessels have distinct embryonically origins (Majesky 2007).

For instance, the largest conduct vessel, the aorta, begins its development during the third week of gestation (Kau et al. 2007) and shows heterogeneous embryonically differences along its length. The basal root is derived from secondary heart field, the arch and ascending aorta originates from the neural crest and the descending from the paraxial / somatic mesoderm (Cheung et al. 2012), illustrated in Figure 1-1. The regional diversity in SMC may in part contribute to susceptibility of site-localisation of vascular diseases such as vascular calcification, atherosclerosis or aortic aneurysms (Leroux-Berger et al. 2011; Haimovici 1991; Ruddy et al. 2008).

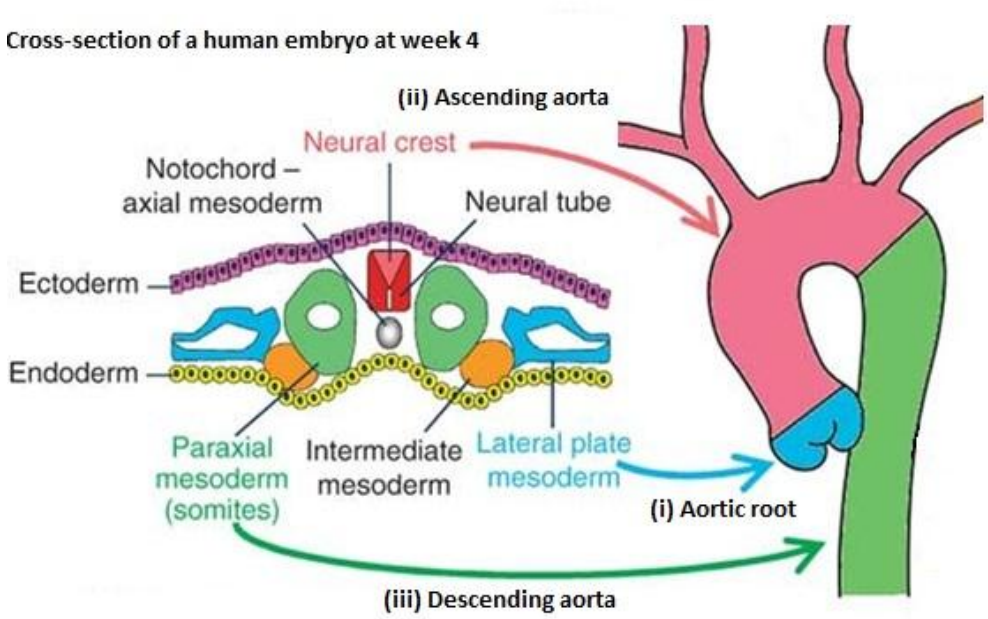

Figure 1-1 Embryological origins of the aortic smooth muscle cells (SMCs): The SMCs of the (i) aortic root originates from the lateral plate mesoderm, (ii) the ascending aorta is derived from the neural crest and (iii) the descending aorta originates from the paraxial mesoderm. (*Illustration adapted from Cheung et al., 2012)*

1.2 The Cardiovascular System

After maturation of the vascular network, the cardiovascular system is established as a fluid transport system which allows the circulation and transportation of blood throughout the body. Its primary function is the transport of oxygen, nutrients and metabolites throughout the body, while removing waste such as carbon dioxide. The muscular structure of the heart is core to the cardiovascular system. Its primary role is to impart energy to the blood in order to generate and sustain adequate perfusion of organs. The heart can be structurally divided into two pumps connected in series, divided by the septum. The left side of the heart is composed of the left atrium and left ventricle separated by the mitral valve. Contraction of the left ventricle ejects blood though the aorta and is responsible all systemic

blood flow to organs, except the lungs (Figure 1-2). On the opposing side of the heart, the right atria and the right ventricle are divided by the tricuspid value. They feed into the pulmonary system allowing gaseous exchange to occur. This newly oxygenated blood returns to the left side of the heart and is distributed to other organs as described.

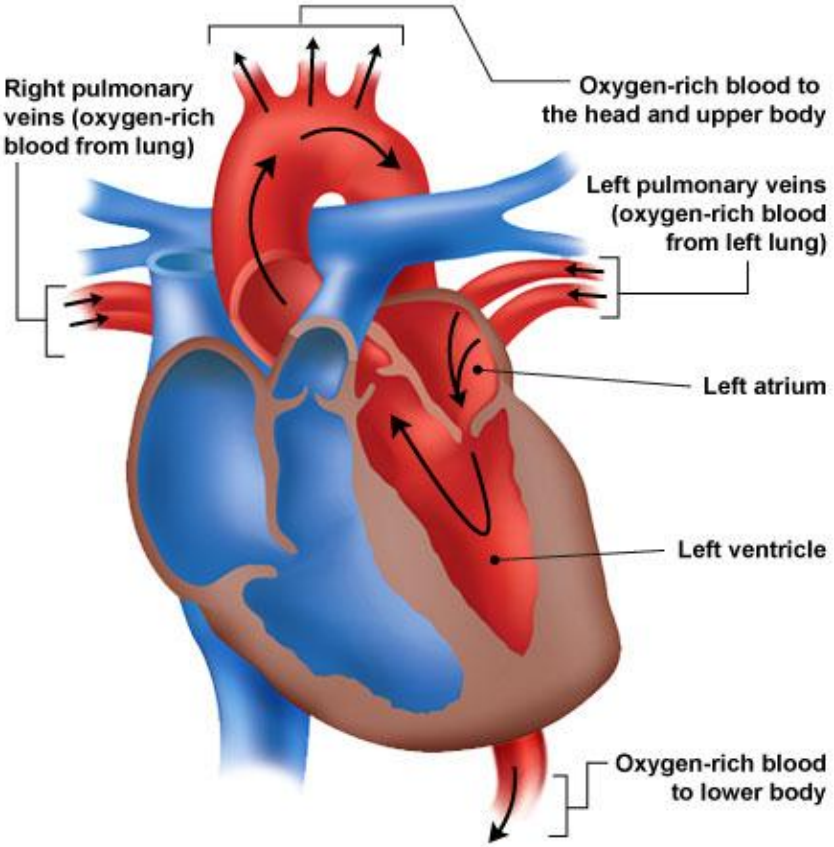

Figure 1-2 Blood flow through the left heart chambers: The left chambers of the heart are responsible for expelling oxygen rich blood to all systemic organs, except the lungs. Adapted from (*http://www.ceufast.com/).*

The heart's rhythmic beat is controlled electrically and there are two basic phases in the cardiac cycle, systole and diastole (Figure 1-3). In systole, the heart undergoes contraction with electrical activation. In contrast, the heart relaxes in its diastole phase when the cardiac

myocytes are at their resting electrical state. These electrical potentials can be recorded in an electrocardiogram (ECG).

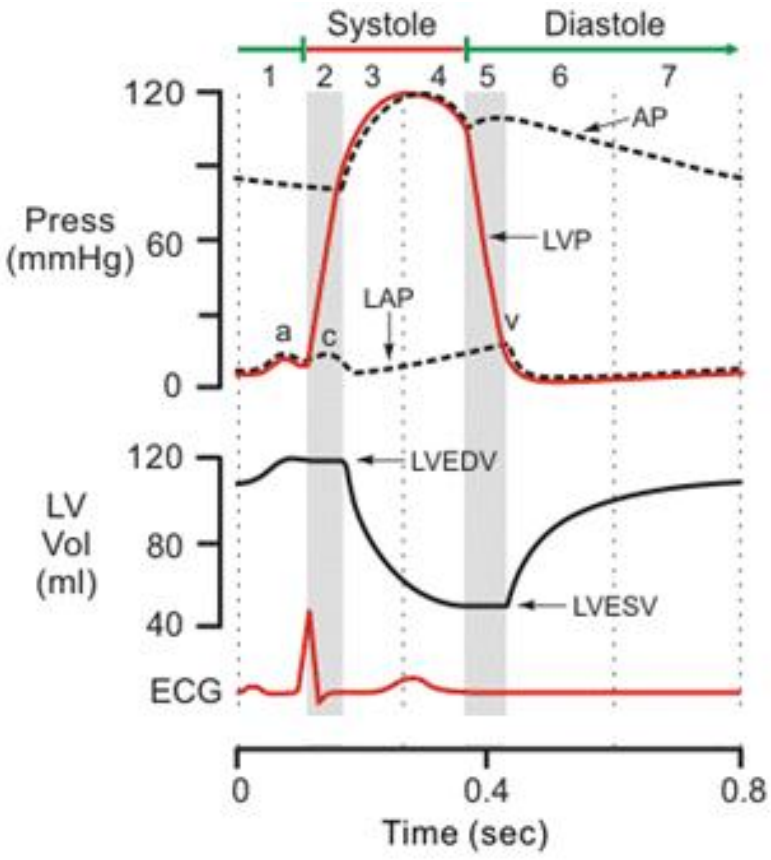

Figure 1-3 Systolic and diastolic phases of the heart cycle: Ventricular changes through systole and diastole with its related pressure, volume and ECG changes. Where AP is the aortic pressure, LVP is the left ventricle pressure, and QRS complex of ECG. LVESV left ventricular end systolic volume. Adapted from (*CVphysiology.com*).

Cardiac output can average approximately 4 to 6 litres of blood per minute at rest and is triggered by either intrinsic cardiac regulation in response to the volume flowing into the heart, or the control of heart rate and cardiac contractility by the autonomic nervous system.

1.2.1 Cardiac Indices

There are a number of cardiac indices to assess cardiac function. Systolic indices try to quantify how well the LV pumps blood; the diastolic indices quantify how well the LV is being filled. The indexes mainly focus on the left side of the heart (Lee *et al*. 2006).

- Stroke volume (SV) is the difference between the end diastolic volume (EDV) and end systolic volume (ESV) as shown in Equation 1-1.

$$SV = EDV - ESV \tag{1-1}$$

- Ejection fraction (EF) represents the percentage volumetric measure of blood ejected from the heart (%) given to Equation 1-2.

$$EF = \frac{EDV - ESV}{EDV}.100\% = \frac{SV}{EDV}.100\% \tag{1-2}$$

- The cardiac output (CO) is the net forward flow of blood per minute measured as millilitres per minute, calculated by Equation 1-3.

$$CO = SV.HR \tag{1-3}$$

1.3 Normal Haemodynamics of the Cardiovascular System

Homeostasis of haemodynamics involves the regulation of the blood circulation to provide adequate blood flow, maintaining optimal organ perfusion and tissue function. The circulatory system is composed of various structural components; the heart provides the key phasic pressure changes by the delivery of a bolus of blood into the aorta. The elastic characteristics of the aorta and large arteries allow for rapid expansion and recoil, pre and post ejection of the heart.

The ejected blood enters the arterial bed in systole and continues onwards during diastole under the 'Windlkessel effect', which refers to the compliance of the aorta with the arterial pressure wave. The systemic vascular resistance is determined by the small arterioles, pre-capillary arterioles and any changes in the viscosity of the blood. The post-capillary resistant vessels drain into the larger venules and veins which are termed the capacitance vessels. The dissipation of pressure between all these vessels is illustrated in Figure 1-4.

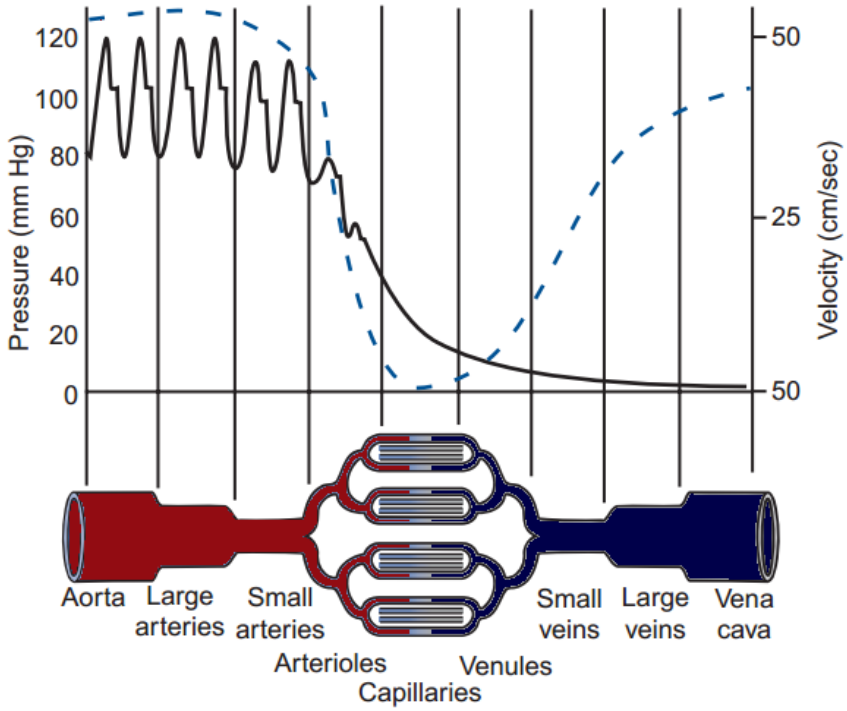

Figure 1-4 Pressure and flow velocity profile in the systemic circulation: The arterial part of the circulation is characterised by high pulsatile pressure and high flow velocity. This system changes to a low pressure and low velocity, filtering into the venous system. The lowest point is at the point with greatest vascular resistance in the capillaries beds. Adapted from (Bell *et al*., 2008).

Through different vascular beds, the system changes from a high to low pressure system. The dotted blue line in Figure 1-4 is the average velocity of the blood flow that is proportional to the pressure (P) difference along a vessel (Equation 1-4).

$$Q \propto \Delta P \qquad 1\text{-}4$$

The flow rate (Q) is determined by the average velocity ($\bar{v}$) (distance/time) of the blood by the cross area (A) of the vessel it is flowing through, where $A=\pi.r^2$, (Equation 1-5).

$$Q = \bar{v}.A \qquad 1\text{-}5$$

According to the principle of continuity, flow rate in equals the flow rate out, therefore as the velocity of a fluid increases, the area decreases proportionally. This is illustrated in Figure 1-5.

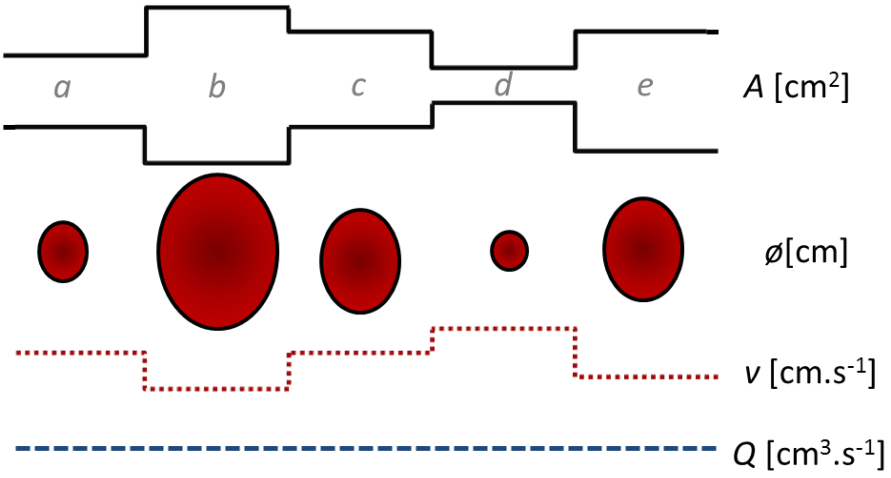

$$Q = A_a.\bar{v}_a = A_b.\bar{v}_b = A_c.\bar{v}_c = \cdots \ldots \ldots const$$

Figure 1-5 Principle of continuity of flow rate: Illustration of the principle of continuity: and the relationship between area (*A*), vessel diameter (*ø*) velocity (*v*) and flow rate (*Q*).

Normal aortic blood velocity has been shown to be independent of sex, body surface area (BSA) and blood pressure but it progressively decreases with age. In a study by Mowat *et al*. (1983), normal ranges of blood velocity was found to be between 52 and 152 $cm.s^{-1}$ in a healthy population (aged between 15 to 80 years), Figure 1-6. It shows an age dependant relationship, for example the mean peak velocity at age 70 has been shown to be 55% of that of age 20.

(In this thesis, flow rate has been used but it is equally acceptable to use average velocity or pressure for estimation of PWV.)

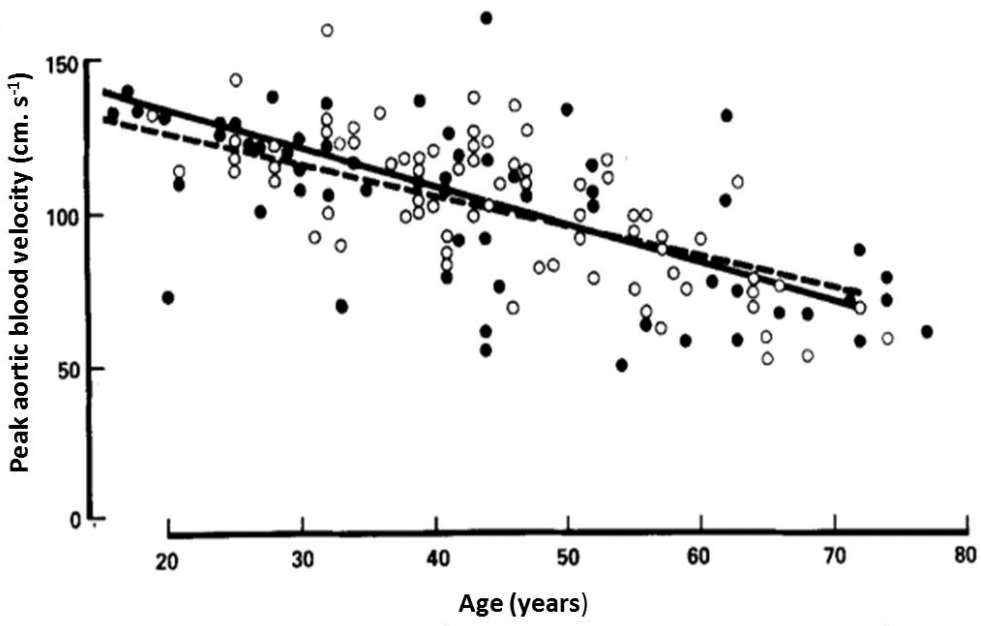

Figure 1-6 Relationship between aortic blood velocity and age in males and females: Mowat *et al* (1983) shows that peak aortic blood velocity falls progressively with increasing age (r = 0.7, $P < 0.005$), where the closed dots represent males (n = 61), and the open dots represents females (n = 79). Adapted from (Mowat *et al*. 1983).

1.3.1 Blood Pressure and Pulse Pressure

The arterial pressure of the systemic circulatory system has been used as an indicator of human health for over a century (Muller *et al*. 1989). Measurement of pressure can be divided into systolic blood pressure (SBP), diastolic blood pressure (DBP), mean arterial pressure (MAP) and pulse pressure (component of SBP and DBP). There is a well-established association between either SBP or DBP and the risk of CVD. Blood pressure is composed of both a pulsatile and a steady component. The pulsatile part, pulse pressure, represents the variation between SBP and DBP and is affected by left ventricular ejection fraction, large artery stiffness, heart rate and early pulse wave reflection. The steady component is represented by mean arterial pressure, and is a function of left ventricle contractility, heart rate, and vascular resistance (Franklin *et al*. 1997).

1.4 Pathophysiology of Cardiovascular Disease

Any disease or irregularity effecting normal function of the cardiovascular system is classified as CVD. It usually stems from vascular dysfunction and can manifest itself causing either structural abnormalities such as hypertrophy, cardiomyopathy, heart failure, ischaemic heart disease or vascular dysfunction. The causes of CVD are multi-factorial with risk factors being a combination of either behavioural, metabolic and other factors such as aging, gender and genetic polymorphism. In particular, high blood pressure, blood glucose, serum cholesterol and body mass index (BMI) have been identified as key mortality cardiometabolic risk factors in CVD, diabetes and chronic kidney disease (Lancet 2014).

The development of atherosclerosis, high blood pressure or thrombosis have been shown to be the principle causes of CVD events (Hackam & Anand 2003; Vasan *et al*. 2001). It is now recognised that CVD is part of a family of atherothrombotic diseases and patients who survive one major CVD event such as myocardial infarction or stroke are at a greater risk of subsequent adverse events and death (Adams *et al*. 2003).

In the past few decades, major improvements have been made in the treatment of certain types of CVD e.g. statin treatment and stent implantation in coronary and peripheral artery disease, resulting in a declining mortality rate (Smith *et al*. 2006). However, more treatment options are needed and improving diagnosis is crucial, particularly at the earlier stages of disease.

1.5 Epidemiology of Cardiovascular Disease

CVD is the leading cause of global mortality (17 million deaths, total 48% global burden, WHO, 2011), with diabetes contributing to an additional 1.3 million deaths. It has been projected that this will increase to 23.3 million by 2030 (WHO, 2011, Mathers 2006) and CVD is estimated to remain the single leading cause of death. Demonstrating the global need for identifying individuals at risk of developing cardiovascular complications early and providing therapeutic measures in order to prevent or reduce the incapacitating consequences associated with CVD.

1.6 Role of Risk Factors in Cardiovascular Disease

CVD has a long asymptomatic period which provides a possible opportunity for early preventive intervention. Risk factors for the development of atherosclerotic disease have been well established in evidence based medicine guidelines such as the American Heart Association (AHA) and the American College of Cardiology (ACC) (Greenland *et al*. 2010). Independent CVD risk factors include an unfavourable level of blood lipids, blood pressure, aging, body weight and body fat distribution and composition, smoking diabetes and genetic predisposition (Lloyd-Jones *et al*. 2006; Vinereanu 2006). Strategies for medical management revolve around identification, surveillance and management of risk factors, in particular modifiable factors (as shown in Table 1-1).

Table 1-1 Risk factors that effect CVD: Identification of key risk factors is important for CVD intervention.

Major modifiable risk factors	**Other modifiable risk factors**
○ High blood pressure ○ Abnormal blood lipids ○ Tobacco use ○ Physical inactivity ○ Obesity ○ Unhealthy diet ○ Diabetes mellitus	○ Low socioeconomic status ○ Mental ill health (depression) ○ Psychosocial stress ○ Heavy alcohol use ○ Use of certain medication ○ Apolipoproteins
Non-modifiable risk factors	**Novel risk factors**
○ Age ○ Heredity or family history ○ Gender ○ Ethnicity	○ Excess homocysteine ○ Inflammatory markers (e.g. C- reactive protein) ○ Abnormal blood coagulation (elevated blood levels of fibrinogen)

Preventive efforts target each risk factor, if left untreated these have the potential to develop into CVD. Risk factors are seldomly seen in isolation, and global risk assessment based on the summation of all major risk factors can be clinically useful. They can help with the identification of high risk patients, heighten motivation to adhere to risk reduction therapies and allow modification of the intensity of risk reduction efforts (Grundy *et al*. 1999). These multivariate risk functions have been derived from several large cohort studies and randomised controlled trials to form the basis of predictive function and risk scores. Many risk factors have been derived from the Framingham heart study, and have been subsequently adapted for assessing an individual absolute risk in primary care (Lloyd-Jones *et al*. 2004). These prevention methods have shown a significant impact on reducing CVD burden and can improve patient outcomes.

Although useful, the identification of traditional risk factors does not account for the entirety of CVD risk and there are many people that do not fit the traditional definition of "at risk". Risk models also are limited to showing either low risk or high risk individual, falling short on middle tier or intermediate risk. For instance, Futterman & Lemberg (1998) found that more than 50% of people diagnosed with chronic heart disease lack any of the conventional risk factors. To that end, there is still a need to identify new biomarkers in order to find ways of identifying those individuals at risk in an attempt to alter their prognostic outcomes (Montgomery & Brown 2013).

In pursuit of refining CVD risk prediction, recent studies have highlighted the potential identification of new novel biomarkers including carotid intima-media thickness

(cIMT)(Bots *et al*. 2014), Brain natriuretic peptide (BNP), C-reactive protein (C-RP) and a variety of genetic variants. Interesting to date, the majority of these markers add little to the existing risk prediction estimates such as that derived from Framingham Heart Study (Wang *et al*. 2006; Bots *et al*. 2014; Ben-Shlomo *et al*. 2014; Goff *et al*. 2014).

1.6.1 Age Related Changes in Vascular Function

The mechanistic explanation of aging in the cardiovascular system is believed to be a result of cumulative damage brought on by various physiological and physical insults. Ageing has been shown to contribute to major structural changes in large elastic arteries and increases in wall thickening are associated with age. As a consequence of this remodelling, there is a reduction of arterial compliance and vessel stiffness increases. Other factors such as increased collagen, reduced elastin and calcification further affect this process.

As large arteries become stiffer, changes in pressures within the cardiovascular system also occur. There is an increase in systolic arterial pressure, a decrease in diastolic pressure and a widening of pulse pressure (PP). This pattern of changes in the vasculature with respect to indices of pressure differs from what is seen with hypertension, for which there is a total increase of peripheral resistance (effecting both SBP and DBP equally).

Following this, data from population studies (Franklin & Wong 2013) have indicated that PP may be more important measure of large artery stiffness in ageing populations. The Framingham heart study found a progressive decrease in DBP and a rise in SBP with ageing causing a widening of PP, particularly in the elderly (Franklin *et al*. 1999). Other

elastic indexes (as further described in Table 1-1) have the ability to reflect vascular stiffening as it is determined by a stress strain relationship of the vascular wall.

A portion of the arterial stiffening that happens with ageing can be attributed to a reduction in endothelial cell function, which normally opposes contraction of the underlying vascular smooth muscle. It has been shown with ageing, there is a reduction of nitric oxide (NO) produced by the endothelial cells. NO is produced from the oxidation of L-arginine by endothelial nitric oxide synthase (eNOS). A full mechanistic breakdown of this process is outside the scope of this thesis, however Davignon & Ganz (2004) provides a summary of the process.

1.6.2 Endothelial Dysfunction and Atherosclerosis

When endothelial cells become dysfunctional, vascular smooth muscle cells (SMC) relaxation is impaired and its phenotype is shifted to a synthetic form that promotes growth, pro-inflammatory responses and thrombosis. Eventually these functional defects result in structural changes to the arterial wall with SMC proliferation. This then leads to favourable conditions for platelet and leukocyte activation and adhesion as well as cytokines that increase permeability to oxidised lipoproteins and inflammatory mediators. Hence, endothelial dysfunction is pivotal to early stages of atherogenesis as shown in Figure 1-7 and has been linked to levels of vascular disease risk factors (Della Rocca & Pepine 2010).

In later stages of atherosclerosis, fatty fibrous lesions or plaques are evident within the vessel walls. Atherosclerosis is a chronic inflammatory disorder and is associated with CVD and is exacerbated by risk factors such as central abdominal obesity, insulin

resistance, hypertension and type 2 diabetes mellitus (Burnett 2004). The balance between atherosclerotic plaque stability and instability determines plaque fate and risk of adverse clinical events. In recent years, a significant improvement of outcomes have stemmed from therapies that reduce the level of circulating cholesterol (Scott 2004).

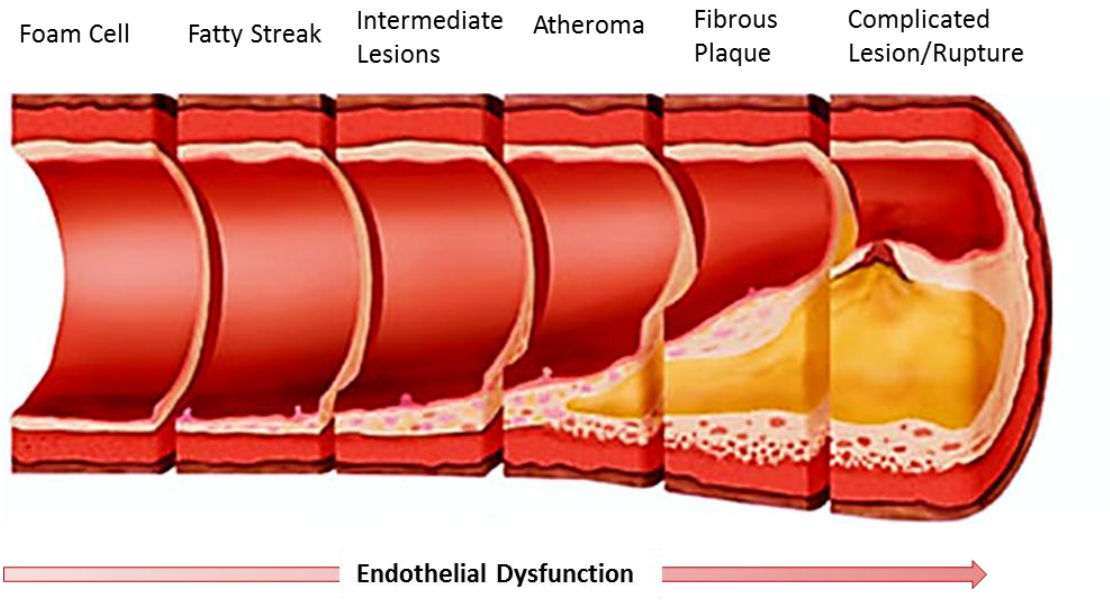

Figure 1-7 Atherosclerosis timeline: The underlying role of endothelial dysfunction is shown in the progression of atherosclerosis from initial lesion to complicated lesion. Adapted from (Pepine *et al*. 1998).

1.6.3 Diabetes Mellitus

CVD is the major risk factor and cause of morbidity and mortality for patients with diabetes being first described as a major risk factor by Haffner *et al*. (1998), (Figure 1-8). Compared to the general population, patients with diabetes have a four times greater incidence of CHD and a two to four fold higher risk of cardiovascular event.

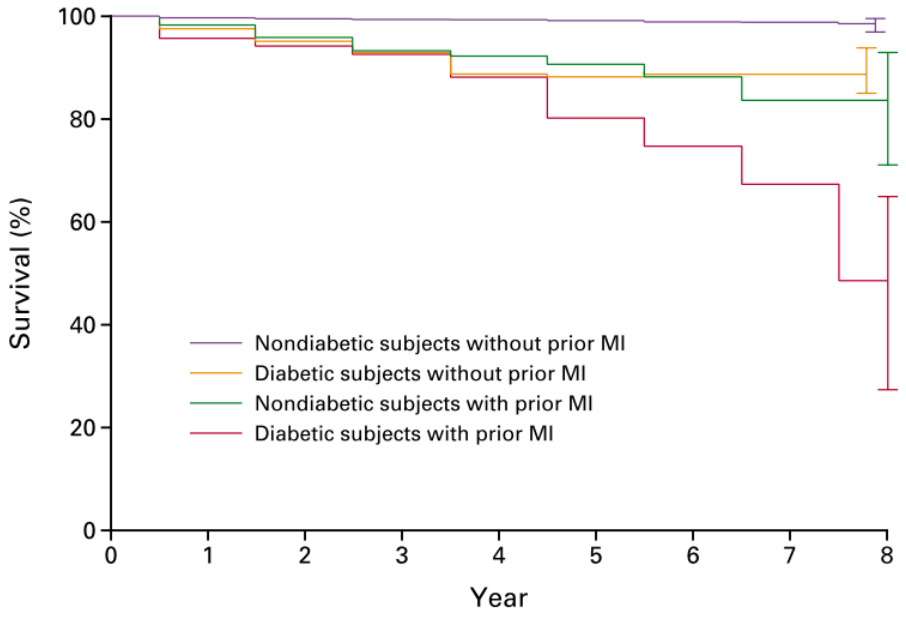

Figure 1-8 Kaplan–Meier estimates of the probability of death from coronary heart disease: Percentage survival in the Haftner study for 1059 subjects with diabetes and 1378 non-diabetic subjects with and without prior history of myocardial infarction. Adapted from *(*Haftner *et al*, 1998*)*.

The American Diabetes Association (ADA) have classified diabetes into four subgroups (ADA 2008); Type-1 diabetes mellitus (T1DM) which results from the β-cell destruction, usually leading to the absolute insulin deficiency, Type-2 diabetes mellitus (T2DM) is developed from a progressive insulin secretory defect on the background of insulin resistance, gestational diabetes mellitus where diabetes is diagnosed during pregnancy and other specific types of diabetes due to other causes such as genetic defects in insulin action or defects from β-cell function, diseases of the exocrine pancreas e.g. cystic fibrosis and drug or chemical induced e.g. treatment of acquired immunodeficiency syndrome or after organ transplantation.

In this thesis, patients with T2DM with and without cardiovascular complications, the other classifications of diabetes have not been detailed and are outside the scope of this thesis. Both T2DM and CVD share similar characteristics as the occurrence increases with age, obesity, both have an adverse lipid profile and both can be reduced by lifestyle modification. In recent years, there has also been new focus on measurement of 'non-traditional' risk factors such as inflammatory markers, advanced glycosylation end products (AGEs), cardiac autonomic neuropathy and polymorphic genes to investigate if they may provide novel insights into mechanisms linking diabetes and CVD.

1.6.4 Hypertension

Hypertension is defined as a chronic increase of arterial blood pressure and is associated with adverse outcomes. It is a physical symptom that increases the after load on the heart and stresses the coronary arteries which progresses to an increased mean arterial pressures and increase in arterial diameter and stiffness. Initially, at low pressures the elastin components of the vessel wall is able to endure the increased stress. However, as the pressure increases, the arterial wall recruits mores collagen fibres to compensate for changes in wall stress and thus resulting in larger, stiffer arteries. Over a period of time, hypertension accelerates arterial degeneration in the arterial wall. It has been shown to be associated with increased risk of CHD, heart failure, and other CVD complication. Overall the prevalence of hypertension appears to be around 30–45% of the general population, with a linear increase with ageing (Mancia *et al*. 2014).

1.6.5 Coronary Heart Disease

Coronary heart disease (CHD) is the most common type of cardiovascular complications and is responsible for one out of every five deaths (Chilton 2004). CHD is characterised by atherosclerosis in the epicardial coronary arteries. The atherosclerotic plaques progressively narrow the coronary artery lumen and cause impairment of antegrade myocardial blood flow (Libby & Theroux 2005). Epidemiological studies and long term outcome trials have established a link between plasma lipids and CHD, with lowering low density lipoprotein (LDL) significantly reducing major coronary events (Nissen *et al*. 2004).

1.6.6 Cerebrovascular Disease

Cerebrovascular disease is associated with associated with vascular disease and is caused by an impaired supply of blood to the brain resulting in loss of brain function. The severity of stroke can be classified as major stroke, minor stroke and transient ischaemic attack (TIA), also referred to as a mini stroke. Following a period of cerebral ischemia or haemorrhage, long-term or permanent neurological symptoms may arise and result in disability. Minor stroke refers shorter term effects, usually lasting less than 24 hours and the symptoms are considered mild and non-disabling (Slark & Sharma 2009).

1.6.7 Peripheral Vascular Disease

Peripheral vascular disease (PVD) is a disease of the lower extremities as a result of atherosclerotic occlusive disease. It has been recently linked as an independent risk factor for myocardial infarction and cerebrovascular disease with the incidence of PVD in the general population from 3- 10% in under 70 years, to 15- 20% in people above 70 years. Typical presentation of PVD is intermittent claudication, however this has been shown to

only reflect 10% of patients and approximately 40% of patients are asymptomatic (Schirmang *et al*. 2009; Hennion & Siano 2013).

1.7 Arterial Stiffness

Arterial stiffness has been shown to be a strong predictor of cardiovascular morbidity and mortality. It is a reflection of the degree of arterial ageing and can be defined as the ability of the artery to expand and contact during cardiac pulsation and relaxation (Kawasaki *et al*. 1987). Arterial stiffness is a dynamic parameter that can be regulated by changes in the structural components of the vessel wall such as collagen, elastin and endothelial cells, but also by vascular smooth muscle tone and circulatory factors including NO and endothelin-1 (Wilkinson & McEniery 2004).

As previously mention, there is a dependent relationship between elasticity and pressure of the arterial system. Linking of these factors was first described by Bramwell and Hill (1922) in Proceedings of the Royal Society of London;

> "The amount of energy expended by the heart … is … proportional to the pressure developed; hence the amount of energy which the heart has to expend per beat, other things being equal, varies … with the elasticity of the arterial system"

Bramwell and Hill used their observation of haemodynamic measures to provide alternative measures of arterial stiffness, which will be described later in 1.8.1.

These observations have been refined into several elastic indexes, incorporate pressure, distance and diameter change to estimate arterial compliance and distensibility. They are often used to describe arterial stiffness and are further detailed in Table 1-2. Arterial compliance can be defined as the change in the vessel diameter in response to blood pressure and has an effect on contractility, blood flow dynamics and perfusion. Distensibility is the arterial compliance relative to the inner diameter of the artery, providing normalisation for vessels of different sizes.

Table 1-2 Indices of arterial stiffness.

Term	Definition	Formula	Units	Methods of measurement
Elastic modulus	The pressure change required for theoretical 100% stretch from resting diameter	$(\Delta P \text{xD})/\Delta D$	mmHg	Ultrasound MRI
Young's modulus	Elastic modulus per unit area	$(\Delta P \text{ x } D)/(\Delta D \text{xh})$	mmHg/cm	Ultrasound MRI
Arterial Distensibility	Relative change in diameter (or area) for a given pressure change; inverse of elastic modulus	$\Delta D/(\Delta P \text{x} D)$	$mmHg^{-1}$	Ultrasound MRI
Arterial Compliance	Absolute diameter (or area) change for a given pressure step	DD/DP	cm2/mmHg or cm/mmHg	Ultrasound MRI
Pulse Wave Velocity	Velocity of travel of the pulse along a length of artery	Distance/Δt	cm/s	Pressure waveform Volume waveform Ultrasound MRI
Augmentation Index	The difference between the second and first systolic peaks as a percentage of pulse pressure			Pressure Waveform
Stiffness Index (β)	Ratio of ln (systolic/diastolic pressures) to (relative change in diameter)	$\beta = \frac{\ln(P_s - P_d)}{(D_s - D_d)/D_d}$		Ultrasound
Capacitative Compliance	Relationship between pressure change and volume change in the arteries during the exponential component of diastolic pressure decay	$\Delta V/\Delta P$	cm^3 /mmHg	Pressure waveform
Oscillatory Compliance	Relationship between oscillating pressure change and oscillating volume change around the exponential pressure decay during diastole	$\Delta V/\Delta P$	cm^3 /mmHg	Pressure waveform

Abbreviations: *P*: pressure, *D*: diameter, *V*: volume, *h*: wall thickness, *t*: time, *v*: velocity.

The haemodynamic wall shear stress (WSS) is a result of innermost intima vessel layer is exposed to both wall stress caused by pulsating blood pressure and WSS caused by pulsatile blood flow (Qian *et al*. 2014). In clinical practice, these changes of blood flow dynamics have been used to diagnosis target and an important issue in the development of CVD. Studies have also shown that although ageing is the strongest predictor of arterial stiffness, the degree of stiffness can be accelerated by various risk factors such as hypertension, smoking, high salt intake, dyslipidemia, diabetes mellitus and biomarkers such as high sensitivity CRP (hs-CRP) (Laurent, Cockcroft, Bortel, *et al*. 2006).

1.8 Pulse Wave Velocity

Aortic PWV represents the speed at which the pulse wave propagates through the arterial system to the peripheral vasculature. The rate of propagation reflects on the viscoelastic properties of the artery with PWV being an index of regional arterial stiffness (Laurent, Cockcroft, Bortel, *et al*. 2006). Increased arterial stiffness has been shown to be cardiovascular risk factor independent of classical risk factors and has been included in the European society of hypertension guidelines (Mancia *et al*. 2007). It has been generally agreed that many cardiovascular disorders are associated with the rigidity of the arterial wall due to atherosclerosis. PWV has been shown to provide CVD risk predication independently of standard risk factors such as pulse pressure, blood pressures and glycaemic control (Cardoso *et al*. 2013). This predicative power of CVD mortality of aortic PWV and pulse pressure is shown in Figure 1-9.

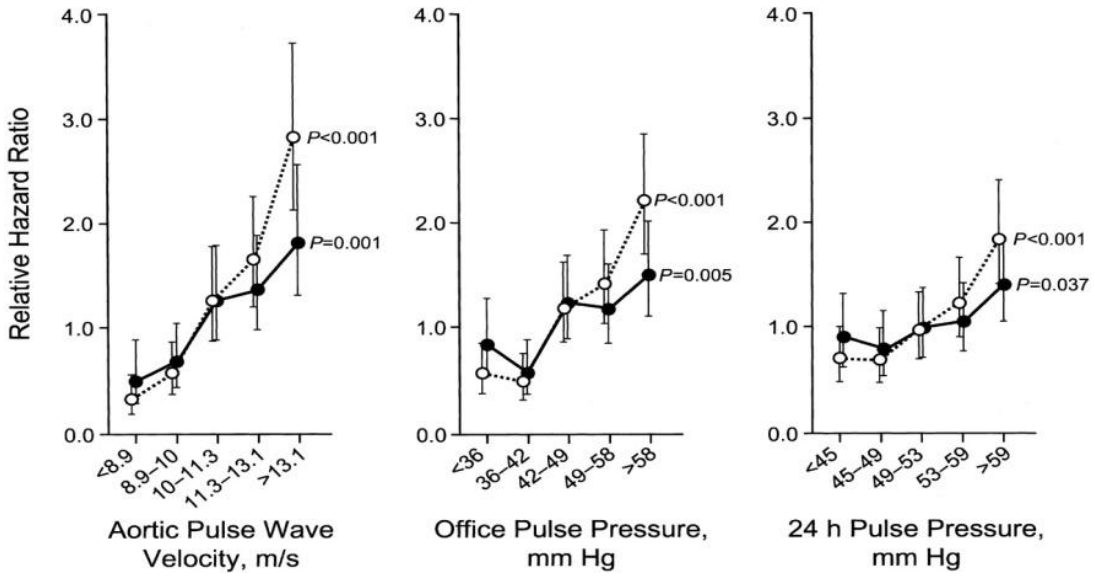

Figure 1-9 Relative hazard ratios for aortic PWV, office PP and 24h PP: Hanson T *et al* (2006) shows the composite cardiovascular end point of aortic PWV, office pulse pressure, and 24 hour pulse pressure with white circles indicating unadjusted, and black circle adjusted for age and sex. Reproduced from (Hansen *et al*. 2006).

It has also been found adding PWV, just like pulse pressure and number of carotid or femoral atherosclerotic plaques, to the Framingham risk score improves the accuracy of the risk prediction model in apparently healthy subjects (Bérard *et al*. 2013)

1.8.1 Theoretical Model: Derivation of PWV

Elastic and hydraulic theory was first established by early physicists such as Young (1808), Poisuille (1840), Moens and Korteweg (1878). Pulse transit time (PTT) is the time it takes the pulse waveform to propagate through the length of the arterial tree. The pulse pressure waveform forms the ejection of blood from the left ventricle and moves with velocity much greater than the forward movement of blood.

The first principles of the velocity of the pulse wave through the arterial tree is derived from Newton's second law of motion (Young 1808). Later, the relationship between the pulse wave and the elasticity of a thin walled elastic tube filled with an incompressible fluid is expressed by Moens-Korteweg Equation 1-6. This directly relates PWV and arterial wall stiffness, where *E*: Young's modulus of arterial wall, *h*: arterial wall thickness, *r*: arterial radius at end diastole and *ρ:* blood density.

$$PWV = \sqrt{\frac{E.h}{2r\rho}} \qquad 1\text{-}6$$

The assumptions being; there is no or insignificant change in vessel area or wall thickness and that *dv* (dr^{-1}) *dx*. *dt* is small to the point of insignificant. From this equation we can see that PWV is related to the square root of Young's modulus of elasticity (*E*). Therefore measuring PWV leads to an estimation of stiffness of the tube. Higher velocities correspond to higher arterial stiffness. The blood density of a person should stay fairly constant. The other two parameters *h* and *r* may be estimated with imaging techniques. In the progression of atherosclerosis, as the vessel wall thickness (*h)* increases, the vessel radius decreases (*r*) and therefore will be indicated by an increase PWV.

1.8.2 Measurement of PWV

The mechanical behaviour of large arteries caused some difficulties to the technical and theoretical aspects. Firstly, arteries have marked anisotropy and exhibit non-linear viscoelastic properties. Secondly, no single arterial segment has identical viscoelastic properties and has a powerful adaptive capability (Nichols WW 2011). Adaptions to the

Windkessel Model or the arterial wave propagation, has allowed the clinical application of aortic PWV (Safar 2006)

The first method that can estimate PWV is by using the velocity of the forward travelling wave. The PWV is defined as the velocity of an arterial wall disturbance towards the periphery and rate of contraction of the ventricle. It can be determined by measuring the time delay of the flow or pressure waveforms, Δt, between two sites of a known distance Δx, Equation 1-7 .

$$PWV\ (ms^{-1}) = \frac{\Delta x}{\Delta t} \qquad \textbf{1-7}$$

This definition holds true under the assumptions that no wave reflections occur as the transmission for the pressure pulse as a sum of incident and reflected waves does not represents true PWV. The wave speed is measured from the wave characteristics such as the foot of the wave, upslope of the wave or the mid-point of each wave at two locations. Equation 1-7 used in this thesis as MRI can provide a direct measure of blood velocity ejected out at different aortic sites.

The second method of estimating PWV is by two simultaneously measured pressure waves. This method utilises the feature of the arterial waveform that occurs during late diastole and early systole, where there is none or minimal interference of the incident pressure wave by the pressure wave (Bramwell & Hill 1922). The time difference between these two waves is

generally estimated by the foot-foot method, under the implicit assumption that the foot of the wave is free of reflections. This measurement can be obtained using invasive pressure catheters or non-invasively by pressure tonometers placed on the skin, where the sites have a known distance apart.

PWV can also be estimated in terms of pressure and flow by the Bramhill & Hill model (Bramwell & Hill 1922) derived from Moens-Kortweg equation, where the wave speed is in terms of *dV*/*VdP*. The Bramhill &Hill equation for pressure and flow in Equation 1-8.

$$PWV = \sqrt{\frac{dP.V}{\rho.dV}} \qquad 1\text{-}8$$

This alternative method can be estimated where pressure can be measured and flow and arterial dimensions measured with A or M-mode ultrasound or Doppler measurement of flow.

1.8.3 Gold Standard, Clinical Standard and MR Derived PWV

As previously mentioned, there are several methods and devices that can measure PWV both regionally and locally. Although not common, gold standard PWV derivation is the invasive pressure wire method. While this method can give highly accurate measurements of PWV, the invasiveness involved restricts its use to animal studies or patients undergoing cardiac catherisation.

The most common and widespread methodology is the non-invasive carotid-femoral tomography or ultrasound method. Due to its low cost and non-invasiveness, it is thought to be a clinically viable method. However these methods only provide a gross global PWV from the carotid and femoral arteries and may mitigate regional stiffness within the vasculature.

MR-PWV can also be used with the advantage that a local aortic measure can be made and there is no geometric assumptions needed, and additionally it can be added to a standard cardiac examination. However, it is still confounded to research studies and has limitations such as expense and is unsuitable for patients with contraindications (e.g. implants, pacemakers or claustrophobia). Nonetheless, there is still a need to determine if it can add more prognostic value than the regional CF-PWV method, particularly as an early surrogate marker of macrovascular changes and CVD.

1.8.4 Carotid-Femoral PWV

In CF-PWV, a tonometer device is placed on the skin over both the carotid and femoral arteries. A pressure waveform is recorded at both locations and the temporal shift is estimated between the carotid and the femoral pressure wave times as transit time, which predominantly the time to foot method. The distance measuring between these two sites are calculated with a tape measure by either two methods. Either by measuring the direct distance between the carotid and femoral arteries or by taking the difference between the distance from the sternal notch to the femoral artery and the sternal notch to the carotid artery. This distance is divided by the transit time to compute PWV.

A major source of error in this setup configuration is the accuracy of the distance measurement and has been reported to cause errors up to 30% (Vermeersch *et al*. 2010; Salvi *et al*. 2008), particularly in patients with large BMI (> 35 $kg.m^2$) (Joly *et al*. 2009) However, there has equations proposed to correct for inaccuracies in these distance measurements (Huybrechts *et al*. 2011; Vermeersch *et al*. 2009).

1.8.5 MRI and PWV

The measurement of MR-PWV using conventional phase contrast (PC) MRI is recognised as a standard technique to assess arterial stiffness by measuring the arrival times of blood velocity waveforms. Conventional PC-MRI requires the acquisition of two sets of complex images with different velocity sensitivities or encodings.

The aortic PWV is commonly calculated in MRI as the ratio between the distance separating two locations of the aorta and the transit time needed for the flow wave to cover this distance. Although the estimation of the distance can be quite easily calculated from an abdominal image of the aorta, the determination of the transit time is somewhat more difficult. Indeed, due to the wave reflections and damping by aortic wall, the profile of the velocity waves extracted from PC-MRI data can change and bias the transit time measurement. Several studies described different methods for the aortic PWV estimation using MRI. However, the main difference between the proposed methods was the determination of the transit time, and even if the foot-to-foot method is commonly used to calculate the transit time there is no standardised method for the PWV determination.

1.8.6 Predicative Power of Carotid-Femoral PWV

A range of reference values for CF-PWV have been reported in the literature. A large multi-centre study measured CF-PWV with tonometry and reported a normal range of 6 ms^{-1} in healthy individuals under 30 years and up to 10ms^{-1} in individuals > 70 years of age, independent of blood pressure. As part of a Framingham heart study, Mitchell *et al*. 2010 investigated the prognostic value of CF-PWV in CVD; the results are shown in Figure 1-10.

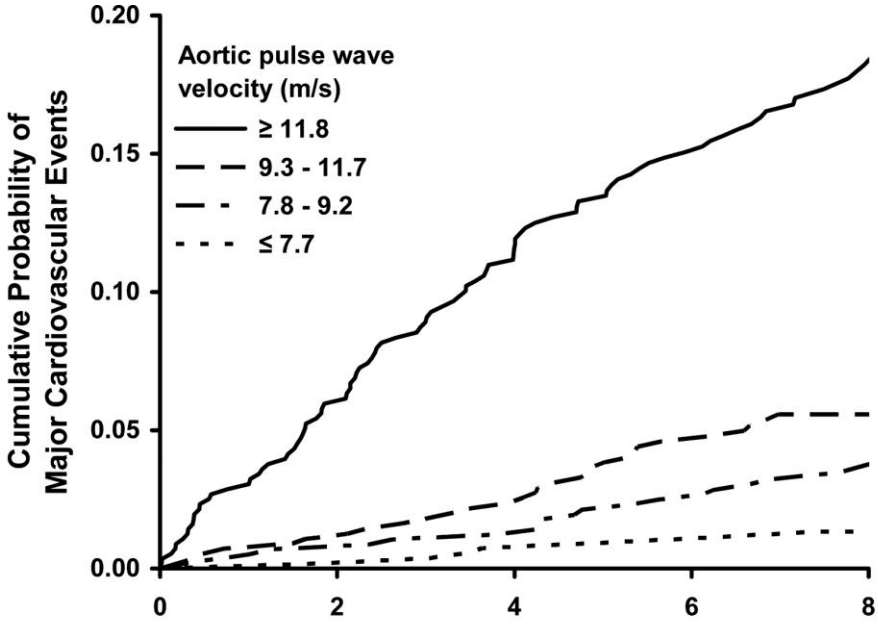

Number at risk: Aortic pulse wave velocity (m/s)					
≥ 11.8	560	513	462	424	161
9.3 - 11.7	555	542	529	502	246
7.8 - 9.2	573	561	551	537	278
≤ 7.7	544	541	535	531	275

Figure 1-10 Kaplan–Meier plot of cumulative probability of a first major CVD event: Participants from the Framingham heart study were grouped according to quartiles of CF-PWV to investigate its prognostic value for CVD events. Reproduced from (Mitchell *et al*. 2010).

Until recently, CF-PWV has been confined to research studies, however it is gaining increasing recognition of its potential prognostic value through large population and longitudinal studies (Vlachopoulos 2010). A recent meta-analysis of 17,635 subjects by Ben-Shlomo *et al*. (2014), has shown with consideration of CF-PWV that include standard risk factors, it can better identify high-risk CVD populations. Collectively, these studies can provide a strong evidence base for a potential risk stratification reference ranges.

Unfortunately, there is a discrepancy between CF-PWV and phase contrast MR-PWV value ranges so they are not directly comparable. In general, CF-PWV are higher (~2 ms^{-1}) than MR derived values. The reason for this is likely to be multifactorial. The difference could be caused by the lower temporal resolution of MR and or the more focal nature of the MR based measurements of the aorta compared to the more global nature of the carotid and femoral vascular beds. Furthermore, one of the key differences between these techniques is the accuracy of the distance which may another contributing factor. The initial study that used MRI to detect early arterial disease via PWV was discussed by Mohiaddin (Mohiaddin & Longmore 1989). However, renewed interest in MR-PWV occurred in later years when faster and more robust MR sequences became commercially available.

1.8.7 Aortic PWV in MRI studies

MRI derived PWV has shown good agreement with invasive intra-aortic pressure measurements (Grotenhuis *et al*. 2009) and has been shown to correlate well with the 'gold-standard' CF-PWV (via tomography method) (Joly *et al*. 2009). However, the 'normal ranges' of PWV have been found to be higher in CF-PWV estimation methods than in MR-PWV. To date, the majority of MR-PWV studies have been single centre with small sample cohorts, but in general normal ranges for a healthy population is of the range of 4 – 6 ms^{-1} (Wentland *et al*. 2014). To date, there has been no systematic review or meta-analysis generated on a collective view of normal ranges in MR publications. In order to provide baseline PWV comparison for later result chapters, a table of all MR studies (last updated search Pubmed July 2014) has been compiled.

Using the Preferred Reporting Items of Systematic reviews and Meta-Analyses (PRISMA) method (Liberati *et al*. 2009), 422 articles were identified and screened by abstract. Seventy-two articles were further analysed by full paper, leaving a remainder of 23 applicable studies with comparable PWV techniques. A summary of all the studies is shown in Figure 1-11.

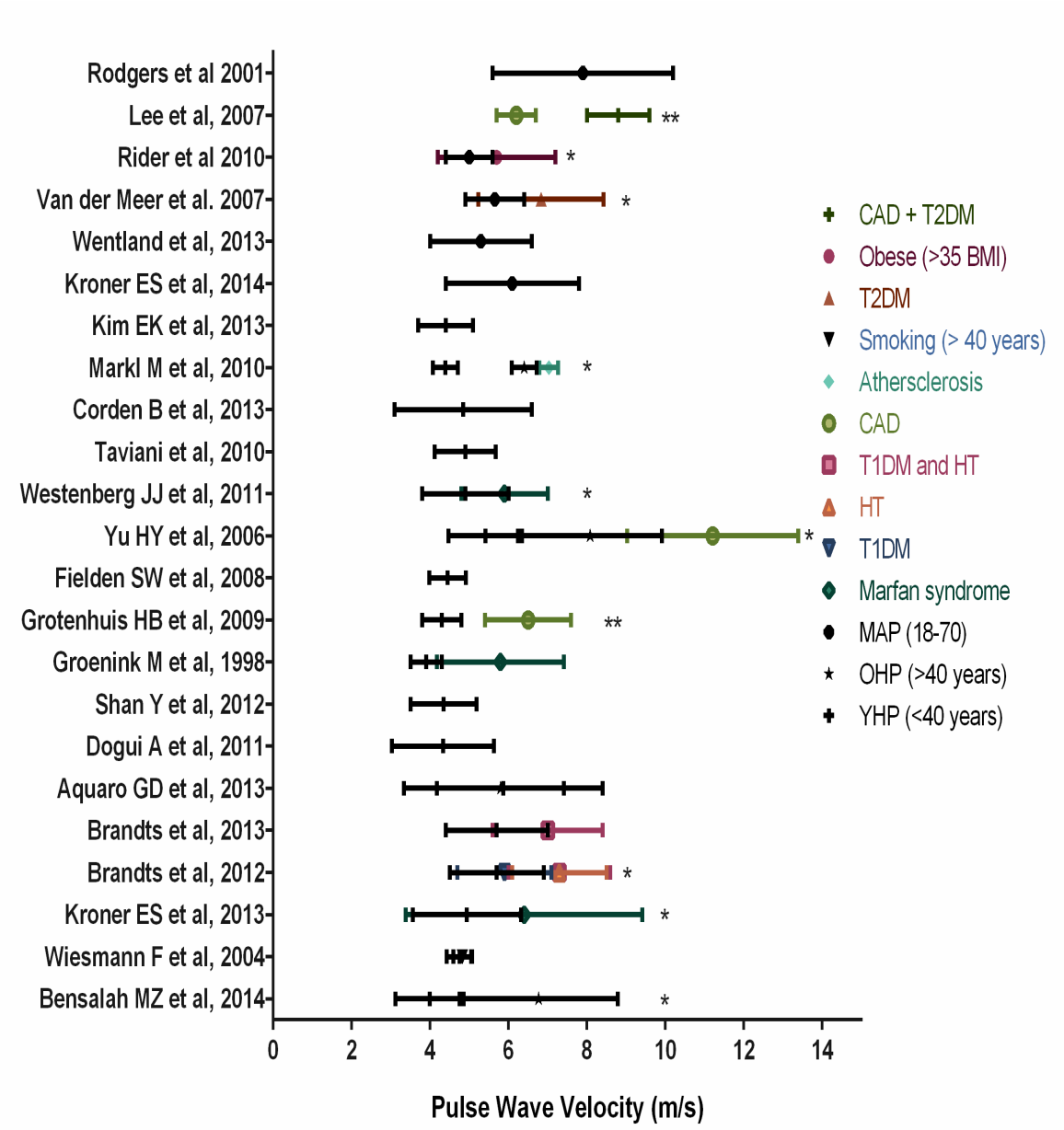

Figure 1-11 Summary of comparable MR-PWV studies (*n* = 23): Most studies have used a healthy population as a comparator to a patient group. Abbreviations: *CHD*: Coronary Heart Disease, T1DM: Type-1 Diabetes Mellitus T2DM: Type-2 Diabetes Mellitus, HT: Hypertension, YHP: Young Healthy Population, OHP: Older Healthy Population and MAP: Mixed Age Population.

1.8.8 Healthy Range for MR-PWV

To obtain ranges for healthy participants, data was extracted from the 22 out of the 23 selected MR-PWV papers. They were further divided into the following subheadings; under 40 years (participants were between 15 to 39 years, weighted average of 29 years), over 40 years (range between 40 and 76 years, weighted average of 54 years) and a mixed age group (MAP) (range between 18 to 70 years), where it was not possible to break down values.

The results of the described analysis are displayed in Table 1-3 for the entire aorta and graphically displayed in Figure 1-12.

Table 1-3 Summary of MR-PWV ranges for healthy population: Average PWV values are given for young healthy population (YHP, < 40 years), older healthy population (OHP, > 40 years) and a mixed aged population (MAP, 18 to 70 years old) from 26 studies.

Type of participants	No of Studies	Av no of participants per study	Total number of patients	Age Range	Average PWV (ms^{-1})
YHP	17	37 ± 40	633	< 40 years	4.7 ± 0.6
OHP	4	24 ± 20	98	> 40 years	6.8 ± 0.9
MAP	5	23 ± 10	117	18 – 70 years	5.9 ± 1.3

1.8.9 Patient Ranges for MR-PWV

To obtain ranges for different patient population, data was extracted from the 13 out of the 25 selected MR-PWV papers (15 different cohorts of patients). The results are displayed in Table 1-1 and Figure 1-13 for the PWV of the entire aorta. From out analysis of the patient cohorts, there has been three studies that have included CVD patients (*CHD*) (Grotenhuis *et al*. 2009; Yu *et al*. 2006; Lee *et al*. 2007a) and one study with T2DM and CHD (Lee *et al*. 2007a) with T2DM (van der Meer *et al*. 2007).

Table 1-4 MR-PWV ranges for patient populations: PWV values as collated from previous studies.

Type of participants	Total number of patients	Age Range (years)	No of Studies	Av no of participants per study	Average PWV (ms^{-1})
Atherosclerosis (with prior evidence of stoke)	25	66 ± 8	1	25	7.0 ± 0.24
CHD	42	63 ± 7	3	14	8.0 ± 2.8
CHD + T2DM	17	65 ± 2	1	17	8.8 ± 0.8
Hypertension	31	49 ± 14	1	31	7.3 ± 1.2
Hypertension + T1DM	28	50 ± 6	1	28	7.3 ± 1.3
Marfan Syndrome	52	36 ± 15	3	17	6.2 ± 1.5
Obese (>35 BMI)	50	43 ± 9	1	50	5.7 ± 1.5
Young smokers	22	31 ± 2	1	22	5.2 ± 0.3
T1DM	20	48 ± 6	1	20	5.9 ± 1.2
T2DM	14	55 ± 8	1	14	6.8 ± 1.6

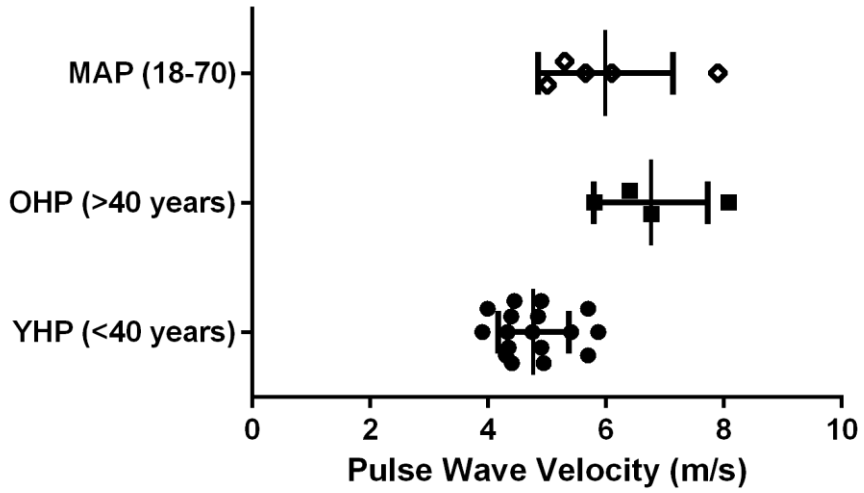

Figure 1-12 Dot and box plot of the mean PWV in healthy populations: A summary of mean PWV values of MRI studies for young healthy population (YHP), older healthy population (OHP) and mixed age population (MAP).

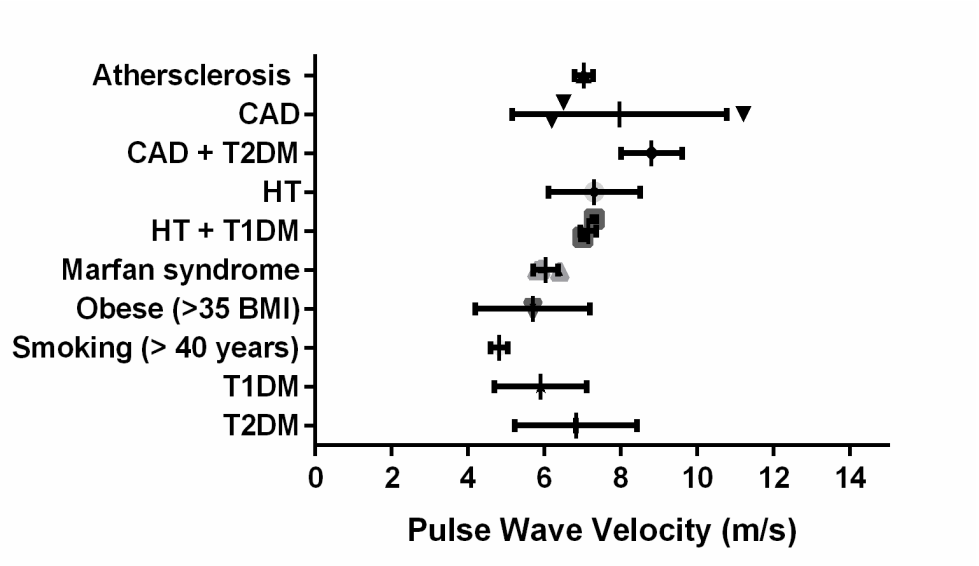

Figure 1-13 Dot and box plot of the mean PWV in each of patient populations A summary of mean PWV values of MRI studies for atherosclerosis, coronary heart disease (CHD), type-2 diabetes mellitus (T2DM), hypertension (HT), marfan syndrome, obese population and smoking.

1.9 Chapter Summary

This chapter highlights the asymptomatic period of CVD provides an opportunity for early prevention and intervention. Established risk prediction models can identify patients at high risk but studies have also shown this may only be effective in 50% of CHD patients. Thus the search for other predictive markers is therefore needed. The scope of this research is to investigate whether PWV, as derived by MRI, can show an independent statistical association with disease risk. A major limitation was uncovered while reviewing literature, highlighting the need of MR-PWV reference ranges. In order to provide a reference base for the subsequent chapters in this thesis, a systematic review of the MR-PWV studies was collated for healthy participants in Table 1-3 and for various patient groups in Table 1-4, allowing comparison of previous published ranges.

1.10 Aim of thesis

The purpose of this thesis is to examine the use of MR-PWV (i) to investigate whether PWV can be used as a surrogate MRI marker of macrovascular disease in a heterogeneous population with and without CVD, and (ii) whether these markers can provide greater risk prediction of CVD risk compared to established MRI parameters of cardiac function such as left ventricular mass.

1.11 Specific Objectives of Thesis

The specific objectives are:

i. To implement and validate aortic PWV measurements as derived from 3.0T MRI velocity encoded images of the aorta in a healthy population.

ii. To examine whether aortic PWV can be used as an imaging marker in high risk CVD patients with complications such as T2DM, hypertension and/or evidence of CVD complications such as CHD, stroke and PVD.

iii. To extend the MR-PWV two slice assessment into a multi- site aortic assessment and to investigate its inter-scan repeatability in a cohort of young healthy volunteers (< 40 years of age).

iv. To apply the multi-site aortic PWV technique to a cohort of healthy population and patients with PVD, to investigate if aortic stiffness varies at different sites along the aorta (aortic arch, distal and proximal aorta).

1.12 Outline of Thesis

The structure of the thesis is as follows:

Chapter 1 Thesis aims and design.

Chapter 2 Introduction and literature review, covering a background to the haemodynamics of cardiovascular system, the prevalence of CVD and associated risk factors, and measurements of arterial stiffness using MRI.

Chapter 3 MRI physics overview and description of the cardiac imaging sequences.

Chapter 4 A description of the MRI hardware for image acquisition protocols and image analysis methods used throughout the thesis.

Chapter 5 Two slice MR-PWV validation: method development, implementation and optimisation of the 'standard' MR-PWV protocol.

Chapter 6 Clinical study I: Application of the MR-PWV 'standard' protocol to assess arterial stiffness in a heterogeneous complicated T2DM population with and without symptomatic CVD.

Chapter 7 Multi-site MR-PWV validation: further development and application of a multi-slice PWV method, compared to conventional two slice approach, in a young healthy population.

Chapter 8 Clinical study II: Application of multi-slice PWV method in a cohort of healthy volunteers and patients with PVD.

1.13 Overview of MRI Experiments and Patient Groups

See Table 1-5 below for summary.

Table 1-5 Summary of experimental chapters discussed in thesis.

Chpt.	Test hypothesis	Cohort size (n)	Cohort description	Techniques tested
CH 5	To test if PWV measurements can be derived from MRI and to compare with standard values from previously published studies and the effect of different methods	3 cohorts of (n =10)	OHV (> 40 years)	HR-PWV LR- PWV Pre/post contrast Different transit time methods of estimating PWV Intra/inter PWV reproducibility
CH 6	To assess if PWV can distinguish arterial stiffness in a heterogeneous complicated T2DM population with and without symptomatic CVD	Total cohort n=88, G1: n = 23 G2: n = 29 G3: n = 19 G4: n = 19	G1: T2DM+ CVD G2: T2DM G3: CVD G4: Non CVD/ T2DM controls	LV analysis Aortic MR-PWV
CH 7	To validate a multi-site PWV technique and compare with the 2-site conventional PWV technique	Total cohort of n = 22	YHV (< 40 years)	LV analysis Standard MR-PWV Multi-site PWV Repeat scan of multi slice PWV
CH 8	To apply the multi-site PWV technique to patient population with PVD	Total cohort, n = 70 YHV: n = 22 OHV: n = 22 PVD: n = 26	YHV (< 40 years) OHV (> 40 years) and patients with PVD	LV analysis Multi-site PWV

Abbreviations: G: Groups, OHV: Older Healthy Volunteers, YHV: Young Healthy Volunteers, T2DM: Type-2 Diabetes Mellitus, CVD: Cardiovascular Disease, PVD: Peripheral Vascular Disease, PWV: Pulse Wave Velocity, HR: High Resolution, LR: Low Resolution, LV: Left Ventricle.

CHAPTER 2

Physics of Cardiac MRI

2.1 Introduction

The aim of this chapter is to cover the basic physical principles underlying the most commonly used cardiovascular magnetic resonance (CMR) techniques. The chapter starts with a review of hardware, the basic principles of nuclear magnetic resonance signal generation and image formation and subsequently includes a technical review of CMR with a particular emphasis on the phase contrast imaging technique for PWV measurement in this thesis.

2.1 Magnetic Resonance Imaging

2.1.1 Hardware

The hardware components of a MRI scanner include the magnet, gradient coils, radiofrequency (RF) coils (for transmitting and receiving), all supported by the system software which controls sequence parameters, timing and safety measures. All MR imaging in this study was performed on a 3.0 Tesla (T) MRI system (*Magnetom Trio, Siemens,* Erlangen, Germany).

2.1.2 The Magnet

The magnet is the core of the system and generates the static magnetic field for nuclear polarisation. The main magnetic field is homogeneous but contains inherent non-uniformities which are minimised by system shimming. Magnet types include permanent

(~0.064 T - 0.3 T), resistive (up to 0.3 T) and superconducting (high field strengths up to 12.0 T). The most common MRI systems in clinical practice utilise superconducting magnets with static fields of 1.5 T, however systems with greater field strengths of 3.0 T and 7.0 T are increasingly being used (Wood *et al*. 2012). The advantages of higher field imaging is a significant improvement in signal to noise ratio (SNR) due to increased polarisation of spins which can either improve spatial or temporal resolution or decrease imaging time.

Cardiac imaging at higher field strengths can be problematic due to differences in tissue relaxation times, increased susceptibility artefacts and RF homogeneity issues. However, cine cardiac imaging at 3.0 T demonstrates high SNR, good blood-myocardium contrast to noise (CNR), high resolution and image quality (Nayak *et al*. 2004).

2.1.3 The Gradient Coils

An MR system has gradient coils in the *x*, *y* and *z* direction which enables it to image a slice in any plane of the body. To produce an image, gradient coils are used to spatially encode the position of protons by varying the magnetic field across the imaging volume. Application of different gradients and RF-excitation signals in a particular sequence and frequency, an image can be formed with faster and stronger gradients allowing for higher image resolution and faster image acquisition.

2.1.4 Radiofrequency Coils

RF coils are needed to transmit and receive radiofrequency waves used in image formation and receive only coils are generally specific to each body region. There are two types of RF coils; volume coils (e.g. head coils) and surface coils (e.g. spine coil). Most volume coils

are quadrature coils or circularly polarised and contain two loops of wire allowing more signal than single loop coils. However, they are closed coils so they are not practical for all applications.

Surface coils have high SNR but have a limited sensitive area. To overcome this limitation, multiple surface coils can be combined and are known as phased array coils.

The integration of the different MR components is illustrated in Figure 2-1.

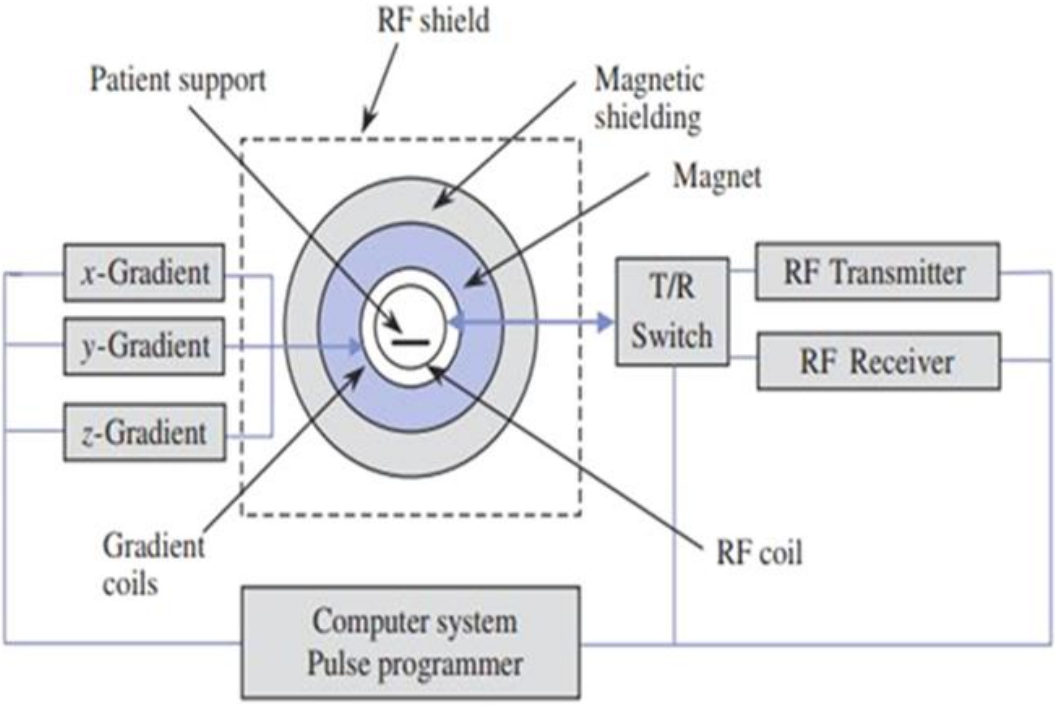

Figure 2-1 Basic components and hardware of an MR system: T/R: Transmit/ Receive. Adapted from (Mc Robbie *et al*, 2004).

2.2 Basic Principles of MRI

2.2.1 Nuclear Magnetic Resonance Theory

The basic unit of mater, the atom, hosts a dense central nucleus containing a mix of positively charged protons and electrically neutral neutrons. The protons and neutrons spin in motion at the same rate, but in opposite directions. If the number of neutrons and protons are equal, the net spin of the nucleus is zero. In the case of an unequal amount of protons and neutrons, the nucleus possesses a net spin. This intrinsic magnetic momentum is a key feature for MR. Commonly used nuclei includes hydrogen (H^{1}), carbon (C^{13}), sodium (Na^{23}) and phosphorous (P^{31}) (Balter 1987).

Hydrogen is abundant in water and fat tissues in the body making it ideal for MRI. By virtue of this property of nuclear spin, the hydrogen nuclei in human tissue produce an electromagnetic field known as a magnetic dipole moment. When an external magnetic field is applied, the individual magnetic dipole moments align either high or low energy states, parallel or anti-parallel to the field, depending on the thermal energy of the spins. Under thermal equilibrium, a very small excess of low energy spins produces a net magnetic moment or equilibrium bulk magnetisation which is used to form the MR signal.

When a nucleus interacts with an external magnetic field, the spins precess with a specific frequency, the Larmor frequency. The larger the field strength, the higher the precessional frequency, this relationship is described by the Equation 2-1.

$$\omega_0 = \gamma B_0 \qquad \textbf{2-1}$$

Where ω_o is the angular precessional frequency or Larmor frequency of spins, γ is the gyromagnetic ratio i.e. a constant that equals to 42.6 MHz/T for hydrogen nuclei, and B_o is the static magnetic field strength.

When a radiofrequency (RF) pulse is applied, whose frequency matches the Larmor frequency, resonance occurs. Resonance results in the RF pulse transferring energy to the protons. During this process, some of the spins absorb a discrete amount of energy from the RF that causes a transition of spins from low to high energy state, resulting in the bulk magnetisation moving of alignment from equilibrium (B_0). The angle between these vectors is known as the flip angle. When a flip angle of 90^0 is applied, then all magnetisations move into the transverse plane, perpendicular to B_0, where it rotates around at Larmor frequency. A flip angle less than 90^0 allows only a portion of the magnetisation to be tipped over. The main purpose the RF pulse is to flip the longitudinal magnetisation (Hashemi *et al*. 2012; Weishaupt *et al*. 2003).

2.2.2 The Bloch Equation

The Bloch equations can be used to model spin systems and these describe the time dependent behaviour of the magnetisation as it reverts back to the equilibrium state.

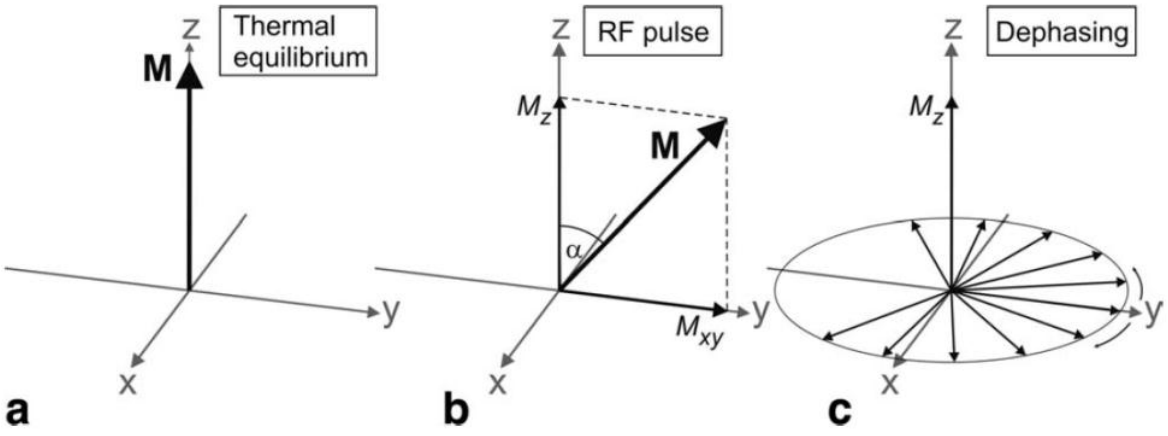

Figure 2-2 Spin magnetisation during thermal equilibrium: (a) after RF excitation, (b) and following dephasing of the transverse magnetisation M_{xy} (C). Adapted from (Markl & Leupold 2012).

The different states of spin magnetisation are shown in Figure 2-2. Initially, the net magnetisation precesses along B_o at the Larmor frequency (Equation 2-2)

$$\frac{d\boldsymbol{M}(t)}{dt} = \gamma \boldsymbol{M}(t).\boldsymbol{B}(t) \qquad \textbf{2-2}$$

Where $\boldsymbol{M}$ the net magnetisation vector in the *x*, *y* and *z* direction, $\boldsymbol{B}$ is the net magnetic field and γ is the gyromagnetic ratio.

The application of an RF pulse at Larmor frequency causes the net magnetisation to be tipped towards the transverse plane at a particular flip angle, which is dependent upon the strength and duration of the RF pulse. Eventually, the net magnetisation will return back to its equilibrium value M_o due to spin-lattice interactions. (McRobbie 2007).

2.2.3 Nuclear Spin; T_1 and T_2 Relaxation

The Bloch equations describe the recovery of the nuclear spin system as it returns to equilibrium (M_o). There are two types of relaxation processes; longitudinal and transverse relaxation. The first incorporates the return of net magnetisation into alignment with the main magnetic field and is known as longitudinal or T_1 (spin-lattice) relaxation. This return to equilibrium is described by Equation 2-3 and takes the form of an exponential recovery characterised by time constant T_1. This is an energetic process and involves the exchange of energy between the spin system and the tissue lattice via thermal mechanisms.

$$M_Z(t) = M_0(1 - e^{-\frac{t}{T1}}) \qquad \textbf{2-3}$$

where M_z is the longitudinal component of magnetisation, M_o is the magnetisation at equilibrium, and T_1 is the relaxation time.

The second relaxation process occurs due to the loss of phase coherence (without the loss of energy) between spins known as transversal or T_2 (spin-spin) relaxation, following the RF pulse. The transversal magnetisation (M_{xy}) decays at a rate characterised by time constant T_2 (Equation 2-4).

$$M_{XY}(t) = M_0 e^{-\frac{t}{T2}} \qquad \textbf{2-4}$$

Where M_{xy} is the transverse component of magnetisation , and T_2 is the decay time.

The decay rates of T_1 and T_2 are different since they can be considered as simultaneous but independent processes. The T_2 decay occurs more rapidly due to dephasing of spins from both intrinsic and external factors. The time constant T_2 depends purely on spin-spin interactions and only considers the loss of phase coherence due to spin interaction, which is

an irreversible process. However, magnetic field inhomogeneities and susceptibility effects result in additional dephasing known as T_2*. The T_2* decay results in a faster loss of signal than T_2 and is described by Equation 2-5.

$$\frac{1}{T_2*} = \frac{1}{T_2} + \frac{1}{2}\gamma\Delta B \qquad \textbf{2-5}$$

Where γ is the gyromagnetic ratio, and ΔB is the variation in the magnetic field.

The T_1 and T_2 relaxation times are dependent on the tissue properties. Additionally, T_1 values can vary corresponding to the strength of the main magnetic field, while T_2 tend to show less dependency. Schematic exponential curves T_1, T_2 and T_2* are shown in Figure 2-3.

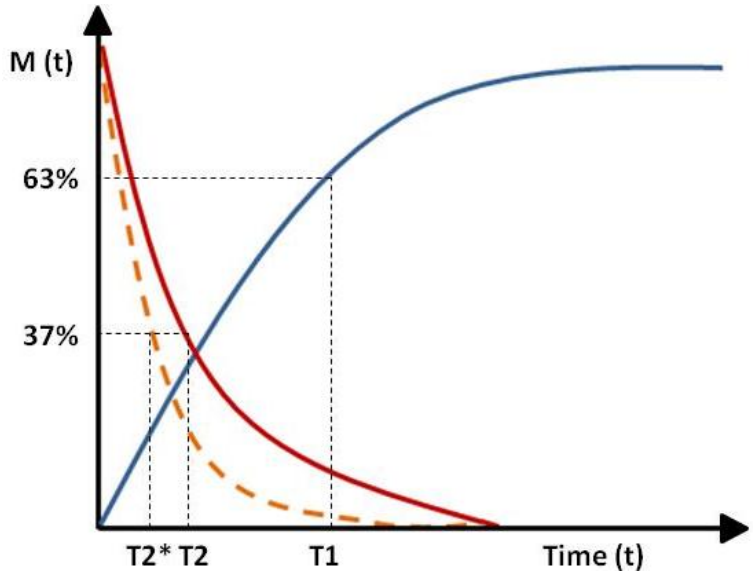

Figure 2-3 T_1, T_2 and T_2* relaxation: T_1 curve: recovers to 63% of equilibrium ($1-e^{-1}$), and T_2, spin-spin decays back to 37% (e^{-1}).

For MR imaging, the recovery or decay curve defines some of the intrinsic effects of tissue relaxation (T_1, T_2) needed for image contrast (Table 2-1). Other factors that also alter contrast include flow, perfusion and diffusion. In combination to these effects, MR generated extrinsic factors such as relaxation time (TR), time to echo (TE), time to inversion (T_I) and flip angle can manipulate image contrast weighting and also provide spatial information for the image formation (Hashemi *et al*. 2012; McRobbie 2007).

Table 2-1 Example of T_1 and T_2 relaxation times: T_1 and T_2 approximate values for liver, cartilage, heart and blood at 3.0 T (Stanisz *et al*. 2005).

Tissue	T_1 [ms]	T_2 [ms]
Liver	812 ± 64	43 ± 3
Heart	1471 ± 31	47 ± 11
Blood	1932 ± 85	275 ± 50

2.2.4 Spatial encoding in MR

In order to construct an image of the excited region of interest, spatial localisation of the signal needs to be determined. The received signal is defined by its frequency and phase as well as its intensity. Different gradients referred to such as the slice-select gradient, the frequency-encoding gradient and the phase encoding gradient are applied in three directions, G_z, G_x and G_y to obtain spatial information. This provides a spatial encoding scheme in which an accurate position of the MR signal can be defined as illustrated in Figure 2-4.

Magnetic field gradients are produced and vary linearly over the area of interest or field of view (FOV). The gradients are bipolar with a positive component (added to B_o) and a negative (subtracted from B_o).

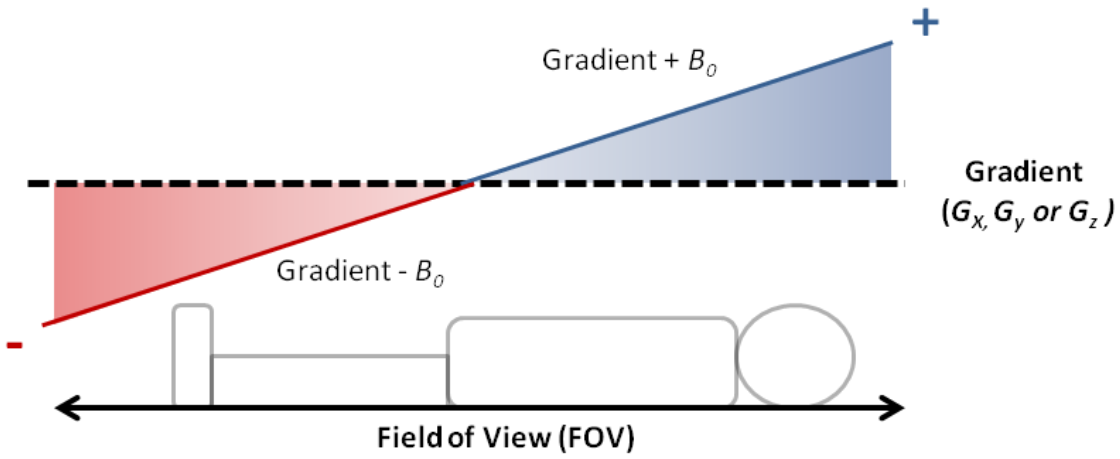

Figure 2-4 Application of a magnetic gradient: Illustration of gradient that varies linearly over the field of view.

The gradient field induces a linear change to the spin's precessional frequency. The negative gradient results in a lower magnetic field and causes the spins to precess at a frequency lower than the Lamour frequency and the positive gradient results in higher magnetic field and increased precession rates. For example, the application of the G_z causes the precessional frequencies to be a function of *z*, Equation 2-6.

$$\omega_z = G_Z z \qquad \textbf{2-6}$$

A standard pulse sequence is usually started by applying the slice selection gradient (G_z) in the presence of an RF pulse to localise spins. The G_z alters the precessional frequencies of spins located along the *z*-direction (along the magnetic field gradient) dependent upon their position in the direction of the gradient. The slice thickness can be controlled by altering the strength of the slice select gradient or by altering the bandwidth of the RF excitation pulse.

Following slice selection the next step is usually to apply a phase encoding gradient in the *y*-direction. This induces a phase change between proton spins by virtue of their position along the gradient. When the gradient is switched off the protons resume precession at the Larmor frequency but the phase information is retained. In a simple pulse sequence the phase encoding gradient needs to be applied at different strengths (increments) in step-wise fashion for successive RF pulses in order to fully encode the data. This has an impact on the scan time such that the time taken for a simple sequence is equal to the TR multiplied by the number of phase encode steps. Finally, frequency encoding is applied along the *x*-direction in order to readout the signal. This gradient allows spatial localisation due to protons precessing at a slightly higher frequency where the field is stronger, and slightly lower frequency at lower field. It does not affect the time of the scan but the sampling time may have an effect on the number of slices that are possible. The echo is sampled during frequency encoding, where the individual frequencies comprising of the total signal are each identified via Fourier mathematics. These steps are later shown in pulse sequence timing diagrams (Figure 2-6).

2.2.5 K-Space

Each repetition of the phase-encoding step generates a signal echo that can be digitised and stored in a data matrix known as k-space. Data points in k-space represent the spatial frequencies content of an MRI as illustrated in Figure 2-5.

Every point in the raw data matrix contains information for the entire image. The outer rows of the raw data matrix contain high spatial frequencies and provide information regarding the details of the structure. The centre of the data space contains information on

the general contrast of the image. In order to convert the final image from k-space, Fourier transform is applied.

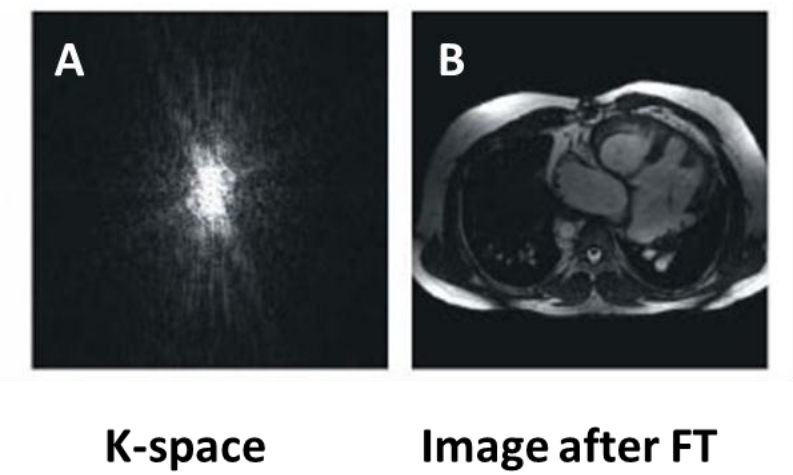

Figure 2-5 K-Space in MRI acquisition: (A) K-space and(B) its associate image after Fourier transform. Adapted from (Moratal 2008).

2.3 MR Pulse Sequences

A pulse sequence is an ordered combination of RF and gradients applied to the object- usually shown as a timing diagram. As previously described, the different gradients are utilised in a particular arrangement to produce an image and these are categorised generally into either spin echo (SE) or gradient echo (GE) sequences. This thesis will deal with only GE sequences since these are by far the most common sequences for CMR.

The time between the RF pulse and the centre of the echo is defined as the echo time (TE). This is the time at which the spins produce a maximum signal. The repetition time (TR) is the time between successive of RF excitation pulses. The pulse sequence is directly related to the filling of k-space by the application of magnetic field gradients to a premeditated

scheme, and when this is completed the image can be formed via Fourier transform. For example, if each TR interval contains one phase encoding step per slice, each of these signals fills one row of k-space corresponding to the G_y and is repeated N_y times to fill the entire k-space (McRobbie 2007).

2.4 Gradient Echo Sequences

The GE sequence starts off with a slice selection RF pulse (typically less than 90°) in combination with a slice selection gradient (G_z) and uses opposite gradient polarities during frequency encoding (G_x) to form an echo. The spins are initially dephased and then re-phrased by an opposite gradient. A peak signal is formed when the bipolar gradient (gradient with equal strength, but opposite polarity) in G_x (shaded regions in Figure 2-6) is implemented.

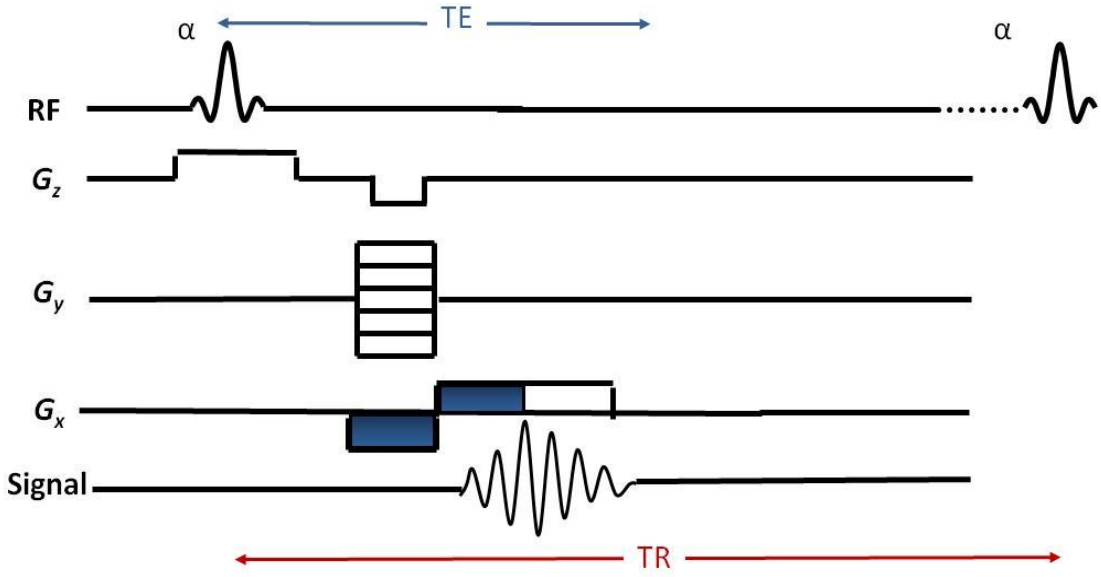

Figure 2-6 Gradient echo pulse sequence: Basic gradient echo timing diagram, where RF is the radiofrequency, TE is echo time; TR is the time of repetition time and α is the flip angle.

GE sequences are generally bright blood techniques. They also have faster imaging speeds than SE sequences as their flip angle can be less than 90°, and they do not require the use of a 180^{o} refocusing pulse. This helps to shorten the length of the time for T_1 recovery, meaning that shorter repetition times can be used.

The optimal flip angle for a particular tissue is known as the Ernst angle and is calculated from the TR and T1 values.

$$cos\alpha_E = \exp\left(-\frac{\mathrm{TR}}{\mathrm{T1}}\right) \qquad \textbf{2-7}$$

Where the α_E is Ernst angle, TR and T1 is recovered.

2.4.1 Fast Gradient Echo Imaging

Fast GE sequences use shorter TR times such that a steady state of the magnetisation has built up during acquisition time (Markl & Leupold 2012). They generally exist in two main categories – spoiled GE and balanced 'steady state' free precession (bSSFP) GE. For spoiled GE, the free induction decay signal is sampled during frequency encoding and any residual magnetisation is then destroyed (or 'spoiled') by the use of RF pulses or strong 'crusher' gradients prior to the next TR. For balanced GE (bSSFP) the gradients are arranged such that the net gradient area over one TR is zero along each axis, and this results in an efficient recycling of all available magnetisation s for MR signal generation (i.e. residual transverse magnetisation in the form of a stimulated echo is subsequently included in the signal along with the FID) (Markl & Leupold 2012). Steady state GE sequences such as True fast imaging with steady state precession (TrueFISP) are commonly used in CMR since they generate T2/T1 contrast that highlights the blood pool as hyperintense relative to the myocardial structures. They offer good signal-to-noise but are prone to off-resonance artefacts if not correctly balanced. Fast GE techniques have many applications such as dynamic (CINE) cardiac imaging, MR angiography, assessment of tissue perfusion and viability.

2.5 Additional Contrast

In addition to the traditional T1, T2, T2* and proton density images, the use of contrast agents, mainly based on chelates of the gadolinium ion (Gd^{3+}) can be used in MRI (Strijkers *et al*. 2007). They predominantly used to shorten the T1 relaxation time and have been shown to provide a diagnostic role in coronary, myocardial perfusion and injury, peripheral and angiography (Saeed *et al*. 2000).

2.6 Cardiac MRI

2.6.1 Challenges of Cardiac Imaging

Cardiac MRI has become a routinely used modality in the investigation of patients with suspected cardiac disease and is considered to be the clinical gold standard for assessment of myocardial viability and cardiac function (Wieben *et al*. 2008). Compared to other anatomical regions, heart specific difficulties include cardiac and respiratory motion and flow phenomena which can lead to image artefacts. To overcome these difficulties, cardiac sequences need to be adjusted or acquired by specialist methods using synchronisation with the ECG trace, prospective or retrospective gating of data acquisition, and acquisition of data during respiratory gating or breath-holding, and utilisation of faster imaging sequences.

i. Synchronisation with ECG

The quality of cardiac MRI is highly dependent on consistent ECG triggering. Therefore using the electrical activity of the heart, MRI data can be acquired and synchronised to the corresponding mechanical event. To record this, MRI- compatible ECG leads are attached to the anterior chest of the participant to gate the examination. However these may be subjected to artefacts caused by the magnetohydrodynamic effect. Peripheral pulse gating (PPG) can also be used in this case via a pulse oximeter.

ii. Prospective Triggering and Retrospective Gating

The ECG can be used in different ways to facilitate image acquisition. One method is to use prospective gating where the presenting R-wave acts as a trigger to acquire information

during an R-R interval or cardiac cycle as shown in Figure 2-7. This can be adapted for either single segments for morphology imaging or a series of segments for multiphase imaging.

The alternative method is to acquire the data continuously and to retrospectively match this to the ECG tracing. This is illustrated in Figure 2-7 and results in a cine study with a number of equally spaced temporal phases throughout the cardiac cycle. These multi-cardiac phases are used for investigating the dynamic contraction and relaxation of the ventricles.

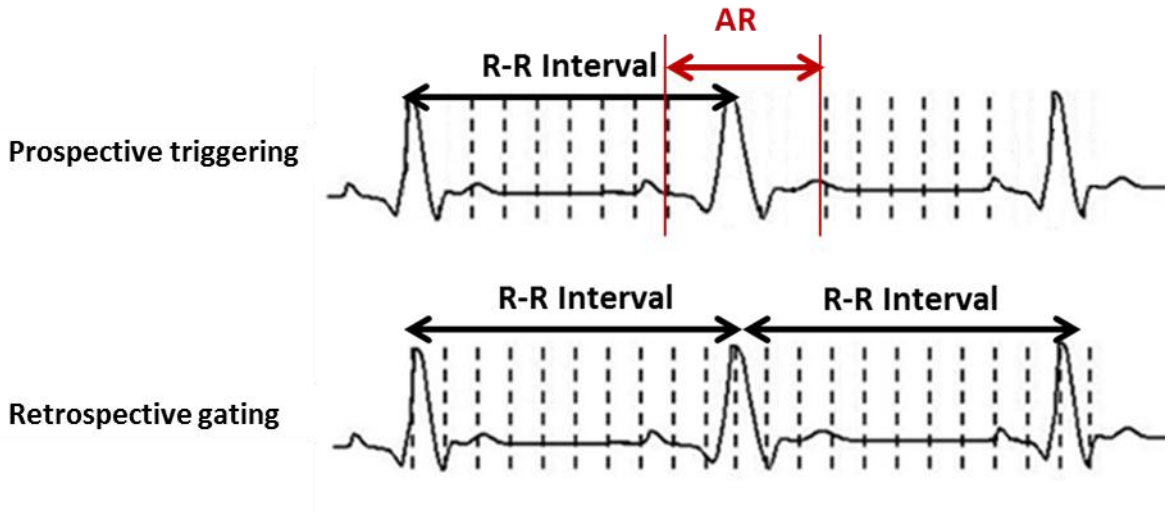

Figure 2-7 Prospective triggering and retrospective gating of an ECG: The difference between prospective and retrospective is arrhythmia rejection (AR) period and retrospective is acquired throughout the R-R interval.

ii. Faster Imaging

Parallel imaging is used to accelerate the image acquisition in MRI data. It works by acquiring a reduced amount of k-space data with an array of receiver coils. The theoretical description of which is beyond the scope of this thesis. In a clinical setting, parallel imaging

results in faster image acquisition, which in turn can shorten breath-hold and reduce motion artefacts and is utilised in fast gradient echo imaging.

2.7 Cardiac Imaging Sequences

Image quality has significantly improved in cardiac imaging since the development of segmented data acquisition. Other developmental improvements have allowed high temporal and spatial resolution to be achieved in cine MRI sequences. Using SSFP sequences and parallel imaging, a full set of cine images can be obtained in 5 - 10 breath-holds of approximately ten seconds. Nevertheless, cardiac arrhythmias and patients that struggle with long breath-holds can still affect image quality. A brief summary of Fast Low Angle SHot (FLASH), TrueFISP and PC imaging will be provided as they are used in this thesis.

2.7.1 (i) TrueFISP and FLASH

As previously mentioned, both trueFISP and FLASH are commercial *Siemens* fast gradient echo sequences commonly used in cardiac MRI. Differences between solid structures such as the myocardium and flow can be achieved in both cine trueFISP and FLASH and mainly differ in the way they deal with residual magnetisation. TrueFISP steady state signal is determined by T2 to T1 ratio and provides excellent blood-myocardium contrast and ability to identify cardiac morphology.

FLASH generally relies on inflow enhancement to generate the blood-myocardial enhancement. Figure 2-8 shows an example of both a trueFISP and FLASH image of 25-year old male with aortic regurgitation. In this case, the trueFISP (A) provides a clearer image of the regurgitation and the myocardial boundaries than the FLASH image (B).

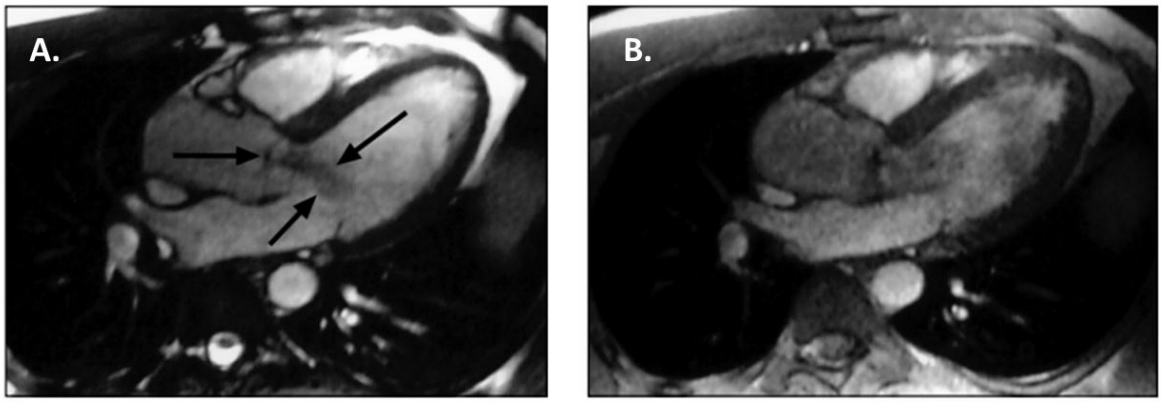

Figure 2-8 Comparison of TrueFisp and FLASH: Image of aortic regurgitation at located pointed by arrows where (A) is an axial trueFISP image (TR/TE 3.0/1.6) and (B) is an axial FLASH (8.0/4.0) (1.5 T *Siemens Magnetom scanner,* Pereles *et al*. 2001).

Limitations of TrueFISP is its sensitivity to magnetic field non-uniformity and metal objects such as sternal wires can often result in inhomogeneity in the magnetic field resulting in image artefacts. In addition, phase cancelation artefacts are can be seen as dark etched outline at the interface between major structure interfaces such as fat and water. However, these artefacts are easily recognisable and generally not in the field of interest and with adequate shimming allow cine series to be of diagnostic quality for most patients. Saturation of signal in the blood pool can cause artefacts in FLASH images. Also due to its slightly longer acquisition time, cardiac gating and breathing motion artefacts can be more of an issue than the shorter trueFISP sequence (Pereles *et al*. 2001).

2.7.1 (ii) Phase Contrast MRI

Phase contrast MRI (PC-MRI) is a technique based on the principle that moving spins acquire a phase shift in the presence of a magnetic field gradient. The phase shifts can be related to blood velocity by applying bipolar gradients. A bipolar gradient has two parts, each with equal area and opposite polarity. It provides velocity profiles at any point of the cardiac cycle and is used clinically to measure flow in difficult regions and has superior spatial accuracy in comparison to other methods (Jung *et al*. 2004; Kilner *et al*. 2010). It has shown diagnostic application in cardiac function, heart valves, congenital heart diseases, major blood vessels, coronary arteries and myocardial wall velocity (Gatehouse *et al*. 2005). In this thesis, the traditional 2D PC-MRI sequence was used to estimate blood velocity in the aorta.

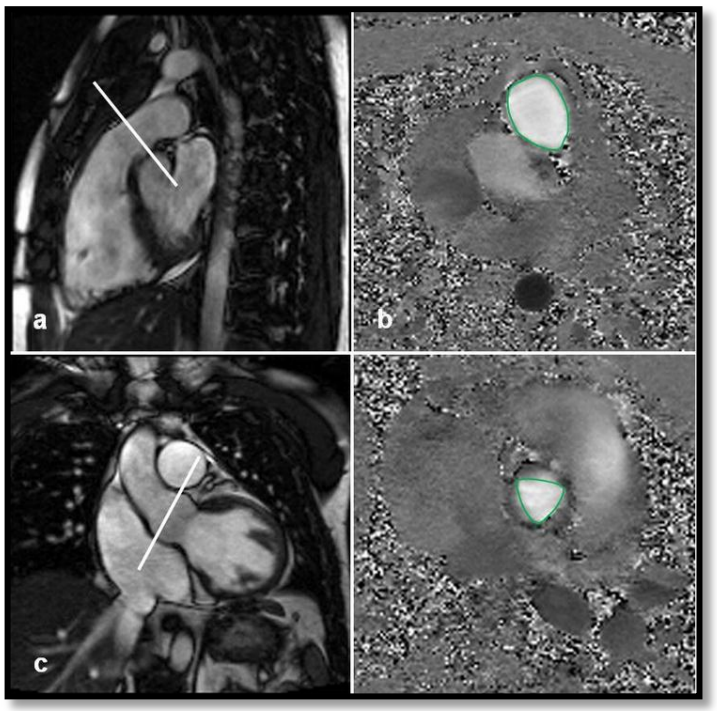

Figure 2-9 Application of phase contrast: Sample planning and PC image for RV outflow track plane (a and b) and aortic flow quantification. Reference Selyavko *et al*, (2009).

Phase Contrast and Velocity Encoding

The dynamic range of the measureable phase shift is limited to ± 180°. Therefore, the operator tunes the pulse sequence such that the peak velocity in the vessels corresponds to a phase shift of 180 or less. Velocity encoding (VENC) and has units of velocity- centimetres per second (cms^{-1}) and the relationship between velocity and VENC is given below, where $\varphi = [-\pi, \pi]$.

$$v = VENC\ \frac{\varphi}{\pi} \qquad \textbf{2-8}$$

The VENC should be selected close to the peak velocity of the vessel, however if too low of VENC is selected, then aliasing will occur. If the VENC is too high, there will be an increase of noise and a loss of sensitivity of the output.

Chapter Summary

This chapter has provided an overview of hardware needed for cardiac applications. The back-ground of cardiac sequences was reviewed such as trueFISP and FLASH and PC-MRI. The set-up and methods will be further discussed in Chapter 4.

CHAPTER 3

Materials and Methods

3.1 Introduction

The principal technique used for the work carried out in this thesis was cardiovascular magnetic resonance imaging (CMR) as described in Chapter 3. All volunteers involved in these research studies were scanned at the Clinical Research Centre (Ninewells Hospital, Dundee) on a 3.0 T Magnetom Trio MRI scanner (*Siemens*, Erlangen, Germany). This section provides an overview of the general MRI scanning procedure and scan set-up for both clinical study participants (SUMMIT and TASCFORCE) and healthy participants.

3.2 Study Ethics

For research participants from both TASCFORCE and SUMMIT studies, the imaging protocols were reviewed and approved by the East of Scotland Research Ethics Committee. The study was conducted at Ninewells Hospital and Medical School, Dundee, UK in accordance with the Declaration of Helsinki. All volunteers provided written informed consent to participate in this study.

Permission to scan healthy volunteers using 3.0 T Trio machine was covered by an existing agreement allowing scanning of consenting volunteers for validation and developmental work, equipment testing and generation of images for teaching purposes.

3.1 MRI Studies Protocols

Participants in TASCFORCE and SUMMIT studies underwent an extensive MRI study protocol, designed to assess cardiac and aortic function and evaluate whole body atheroma burden. In total, the scan time for each participant ranged from 50-70 minutes. The imaging protocols are discussed in the following sections and details of the specific scan protocols are outlined in Appendix A.

3.1.1 Patient Eligibility

The eligible study participants were safety screened before consenting to the MRI research study. MR specific exclusions include claustrophobia and the presence of metallic implants or devices such as surgical clips, pacemakers, artificial heart valves, metal joints or nerve stimulator *in-situ*.

In the two clinical studies, a paramagnetic gadolinium based contrast agent was administered as per clinical protocol; therefore patients with impaired estimated glomerular filtration rate (eGFR) of < 30 ml/min /1.73 m^2 were also excluded.

3.1.2 Patient Positioning

Patients were positioned head first and supine in the magnet bore, with surface coils used to cover the entire body namely the head matrix, neck matrix, spine matrix, two body matrix coils and a peripheral angiography coil as shown in Figure 3-1. Breath hold instructions were relayed via headphones and music played if desired. Coils covering the whole body were set-up on the participants from both clinical studies (SUMMIT and TASCFORCE).

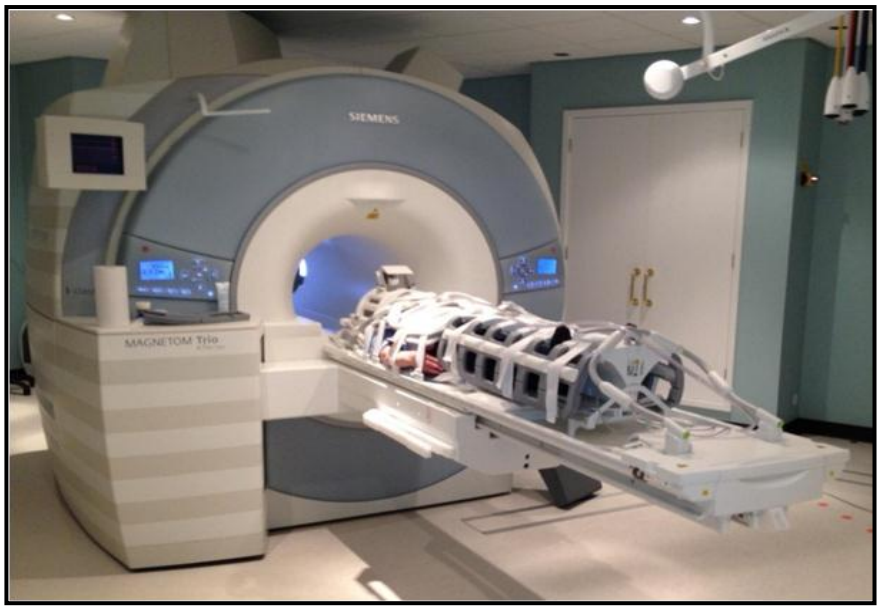

Figure 3-1 *Siemens* 3.0 T Trio Scanner: CRC scanner set-up with typical whole body imaging coil set-up as used in both the TASCFORCE and SUMMIT studies.

For the healthy volunteer validation study, only the body matrix coils were used as no contrast was administered to acquire whole body angiographic images. Healthy volunteers underwent cardiac function and aortic flow quantification (as described in 3.2, i and iii)

3.2 Image Acquisition Protocol

The protocol was split into three sections:

1. Acquisition of the cine images acquired in 2 and 4 chamber orientations and a stack of cine images acquired in the short axis from base to apex to assess cardiac function.
2. Dual injection of contrast and images acquired before and after these injections to image the whole body vasculature.
3. Aortic flow quantification for the calculation of PWV.

3.2.1 (i) Localisers and 2-Chamber and 4-Chamber Views

The cardiac protocol starts with reference images to accurately localise the heart. These low resolution slices (turbo FLASH) are acquired rapidly (~1 sec) in 3 planes (axial, coronal and sagittal planes) (Figure 3-2(a)) and are followed by localiser images acquired in the 2-chamber, 4-chamber and short axis (SA) views. The frequency scout, 4-chamber cine, 2-chamber cine and short axis cine are acquired using trueFISP. From these views, clinical qualitative assessment of myocardial function can be assessed.

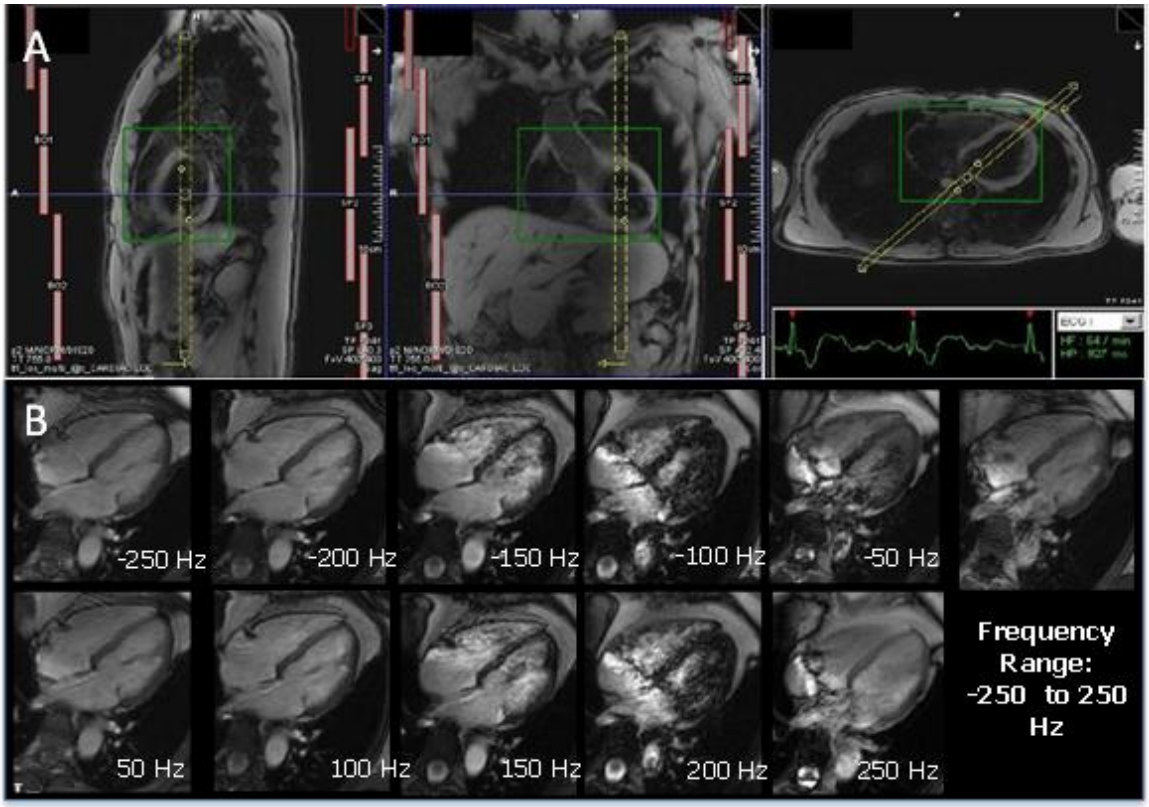

Figure 3-2 Different cardiac localiser orientations and the frequency scout: A. Localiser for cine 4-chamber, 2-chamber and SA views, shimming box (green box) over the selected volume, B. Frequency scout, range (-250 Hz to 250 Hz). Frequency scouts are utilised at 3.0 T to determine the optimal resonance and minimise banding artefacts.

3.2.1 (ii) Left Ventricular Cardiac Function

The SA images are used for quantitative analysis of the left ventricle. To evaluate systolic and diastolic LV functional parameters, ECG gated cine images were acquired through the LV using a multiple short-axis cine sequences from the mitral valve to the apex. Slices are acquired sequentially at 1 cm intervals through the entire left ventricle (slice thickness of 6 mm and an inter-slice gap of 4 mm). Further details of this method used are described by Gandy *et al*. 2008.

Table 3-1 Sequence parameters for LV assessment: Short-axis stacks of CINE TrueFISP images of the LV acquired from the base of the mitral valve to the apex.

Parameter	**3.0T (*Siemens*)**
Repetition Time (ms)	86.6
Echo Time (ms)	1.47
Field of View (mm)	320 x 420
Matrix	256 x 256
GRAPPA factor	2
Flip angle	50 - 60°
Slice thickness (mm)	6
Inter-slice gap (mm)	4

3.2.2 Whole Body Magnetic Resonance Angiography Protocol

For localisation, four low resolution images were acquired from head to foot in the coronal orientation using gradient echo fast FLASH sequence. Whole body magnetic resonance angiography (WB-MRA) images involved the acquisition of 4 overlapping 3D data sets as shown in Figure 3-3.

Four anatomically distinct stations were divided into head and thorax (station 1), thorax and abdomen (station 2), abdomen and upper legs (stations 3) and lower legs (station 4).

Table 3-2 Sequence parameters for WBA imaging: The parameters for pre and post contrast 3D FLASH sequence used at 1 station. WBA involves the acquisition of 4 overlapping 3D data sets.

Parameter	**3.0T (*Siemens*)**
Repetition Time (ms)	2.68
Echo Time (ms)	1.10
Field of View (mm)	500 x 360
Flip angle	19°
Number of slice	96
Voxel size (mm^2)	1.0 x 0.8 x 1.1
Slice thickness (mm)	1.1

Anatomical paired images were acquired pre- and post-contrast. Gadoteric acid contrast agent (Dotarem, Guerbet, Villepinte, France) was administered by intravenous injection into antecubital fossa using a Spectris Solaris power injector (MedRad, Pittsburgh, USA) at a rate of 1.5 ml/sec, followed by a 20 ml bolus of saline. Further details of this methods used in this centre (Waugh *et al*. 2009) and

results for the WBA (not included in this thesis) are presented in Weir-McCall *et al* (under review).

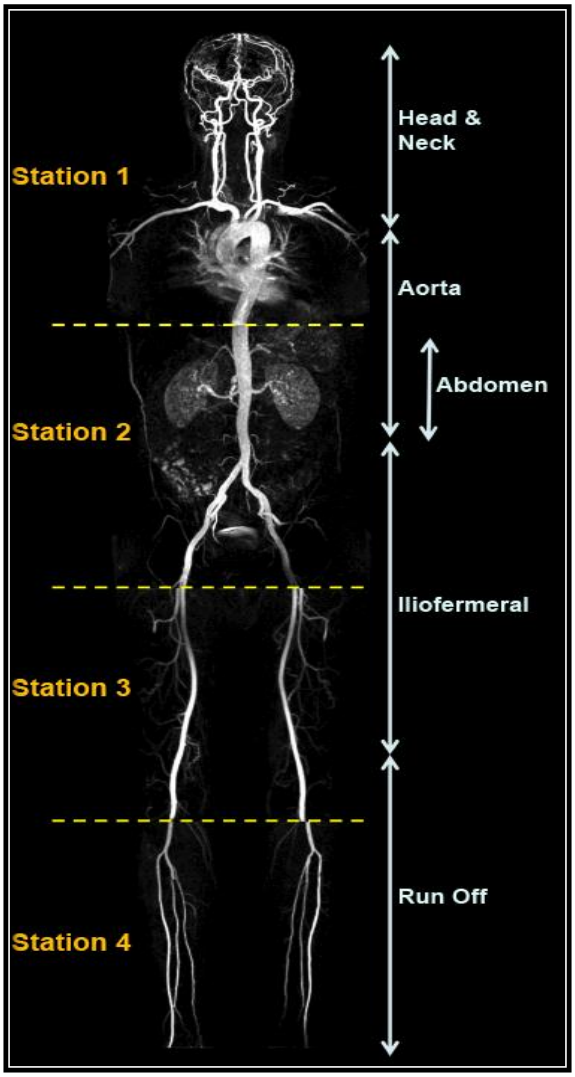

Figure 3-3 Whole body magnetic resonance angiogram: WBA is made up of four imaging stations 1 to 4, head and neck, aorta and abdominal, illiofemoral and the run off peripheral vessels. Adapted from Weir-McCall (under review).

3.2.3 (i) Phase Contrast Imaging of Aortic Flow

To generate flow and mean velocity waves, PC-MRI sequences were acquired at the level of the bifurcation of the pulmonary trunk, perpendicular to both ascending and descending aorta and the second slice was placed axial through the descending aorta immediately proximal to the renal arteries. The PC-MRI data was acquired continuously using a retrospectively, ECG-gated breath-hold gradient echo sequence with a velocity encoding gradient in the through plane direction, which provides phase related pairs of modulus and velocity encoded image as shown in Figure 3-4. Retrospective gating was employed in order to avoid an end diastolic gap in data acquisition. The image acquisition details are described in Table 3-3.

Table 3-3 Sequence parameters for PC-MRI imaging: PC-MRI gradient echo sequences were acquired at the aortic arch.

Parameter	**3.0T (*Siemens*)**
Repetition Time (ms)	14
Echo Time (ms)	4.83
Field of View (mm)	350
Flip angle	20°
Slice thickness (mm)	8
Resolution	256 x 256
Number of phases	128
VENC ($cm.sec^{-1}$)	150
Average Scan Time	4 - 6 mins

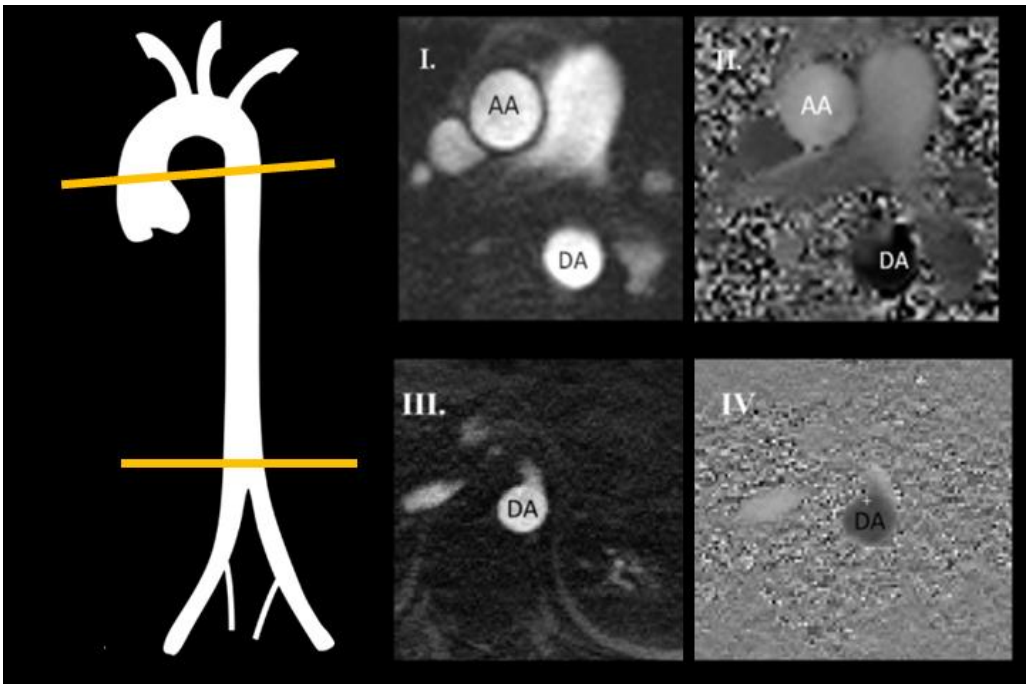

Figure 3-4 Through-plane cine PC-MRI mapping: (i) magnitude and (ii) phase at the aortic arch, and (iii) magnitude and (iv) phase above the renal bifurcation. Abbreviations: AA: ascending aorta, DA: descending aorta**.**

3.2.3 (ii) Aortic Distance Measurement

To determine the distance between the two aortic slices, a 2D GE FLASH was acquired of the aorta in a 'candy stick' double-oblique orientation (Figure 3-5 (A)). The scan parameters are detailed in the Table 3-4.

Table 3-4 Pulse sequence parameters for 2D FLASH: 2D FLASH of the aorta is used to measure the distance between imaging sites.

Parameter	3.0T (*Siemens*)
Repetition Time (ms)	40
Echo Time (ms)	1.2
Field of View (mm)	350
Flip angle	15°
Slice thickness (mm)	8
Resolution	256 x 256
No of phases	23
Average scan time (s)	9

The data in this thesis used the FLASH 'candy cane' image for distance measurements; however the aortic path can also be visualised by a multi-planar reconstruction (MPR) from the angiographic images as shown in Figure 3-5 (B).

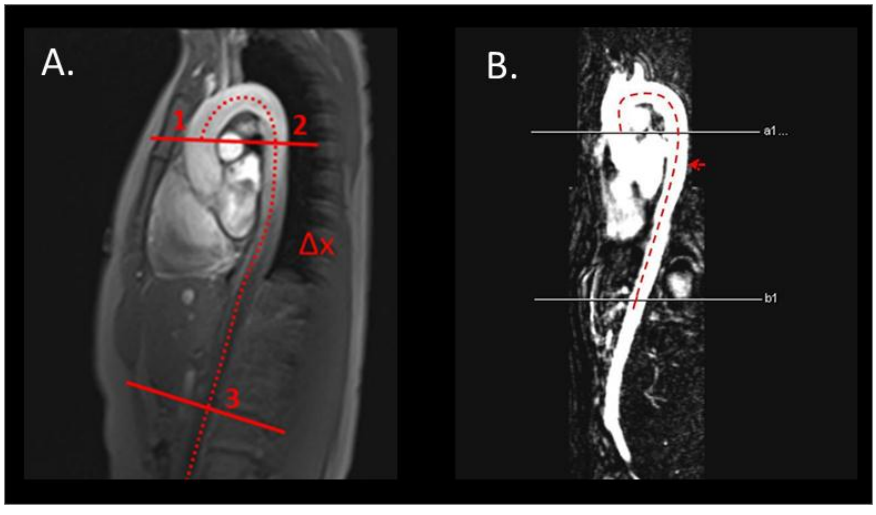

Figure 3-5 Aortic distance measurement: A. FLASH 'candy-cane' view of the aorta B. MPR reconstruction of the aorta.

3.3 Post Processing of Cardiac Images

3.3.1 Left Ventricle Assessment

CMR is considered ‘gold standard for measuring cardiac volumetric and mass; however there are different methods for cavity delineation to deal with the inclusion and exclusion of trabeculae and papillary muscles (Papavassiliu et al. 2005). For this study, the LV segmentation followed an in-house optimised protocol, previously described by Gandy *et al*. (2008). Semi-automated contours were placed on the endocardial and epicardial myocardial borders at end-diastolic and end-systolic phases from the basal to the apical slice. These were then manually adjusted to ensure that the contours precisely matched the anatomic detail. Papillary muscles and trabeculae were included in the LV mass when they were indistinguishable from the endocardial border, but otherwise assigned to the LV blood pool volume. All images were acquired during 10-15 second breath-hold and were post-processed by two experienced segmenters using dedicated Argus software (VB15, *Siemens*), Figure 3-6.

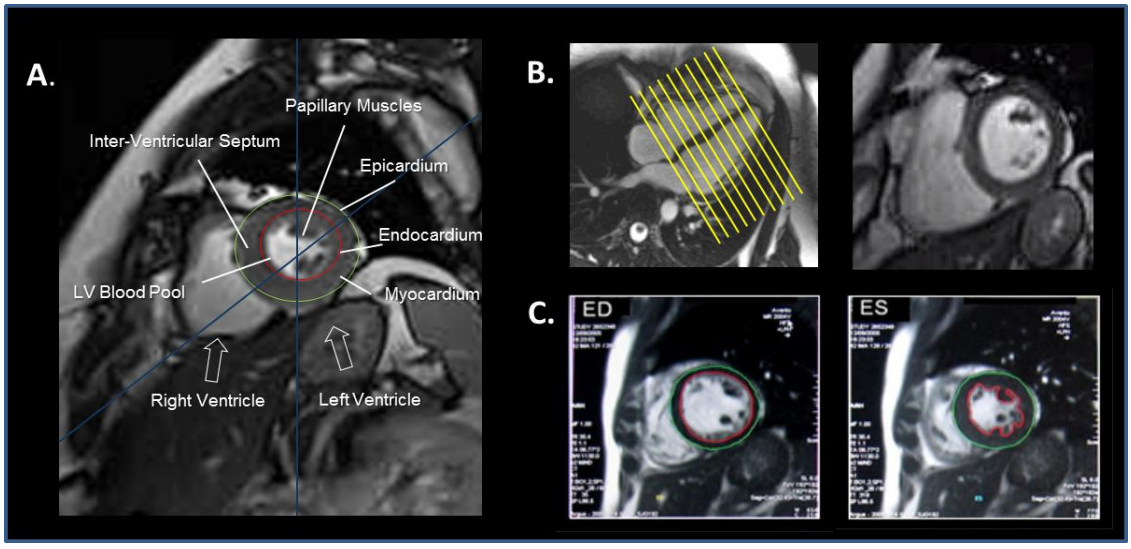

Figure 3-6 Post processing of short axis LV images: A. Descriptive of short axis (SA) image. Left ventricle volume planned from the 4-chamber view, B. to get the SA image, C. The endocardial and epicardial boundaries are manually segmented using Argus at end diastolic (ED) and end systolic (ES) phase to derive quantitative measures of LV function

Parameters such as EF, EDV, ESV, SV, CO or CI and left ventricular mass (LVM) were automatically calculated by the software using Simpson's rule. These parameters were normalised to body surface area. Cardiac output and index are derived from SV and heart rate and although they are an output of analysis they are rarely used. This is due to the intrinsic fluctuations in heart rate that frequently result in a high variability in the measure. Therefore, these measures were excluded from the statistical analyses in this work.

3.3.2 (i) Aortic Flow Analysis

Flow analysis was derived using the 'flow analysis' module on the freely available open source software package *Segment version 1.9 R10* (Heiberg *et al*. 2010a). Contours were placed on the ascending and descending aorta for all 128 phases throughout the cardiac cycle using a semi-automated process as shown in Figure 3-7.

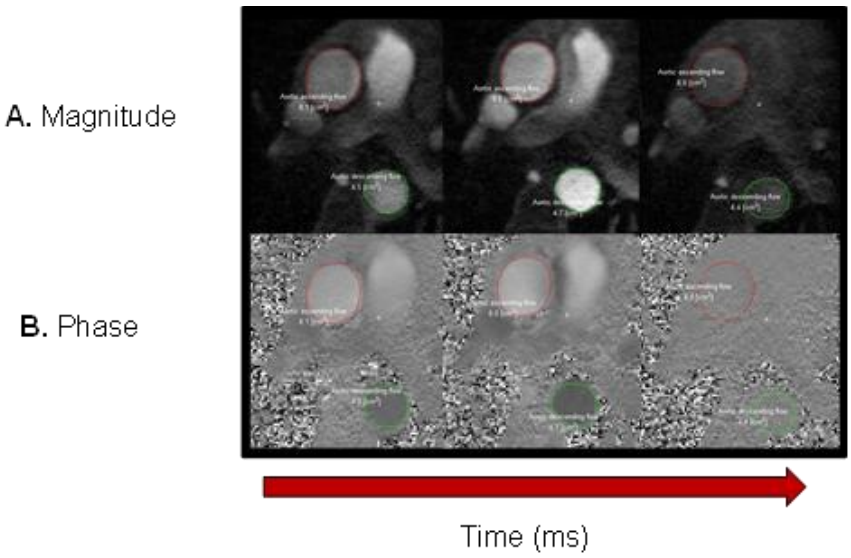

Figure 3-7 Phase contrast MRI: A. Magnitude and B. PC-MRI images acquired over a R-R cycle over 128 phases

From these contours, the software calculated volume flow curves, positive and negative flows, mean velocity curves and vessel area curves. It can also provide a 3D profile of flow, which allows a visual examination of skewness of flow profiles (Heiberg *et al*. 2010b) as shown in Figure 3-8.

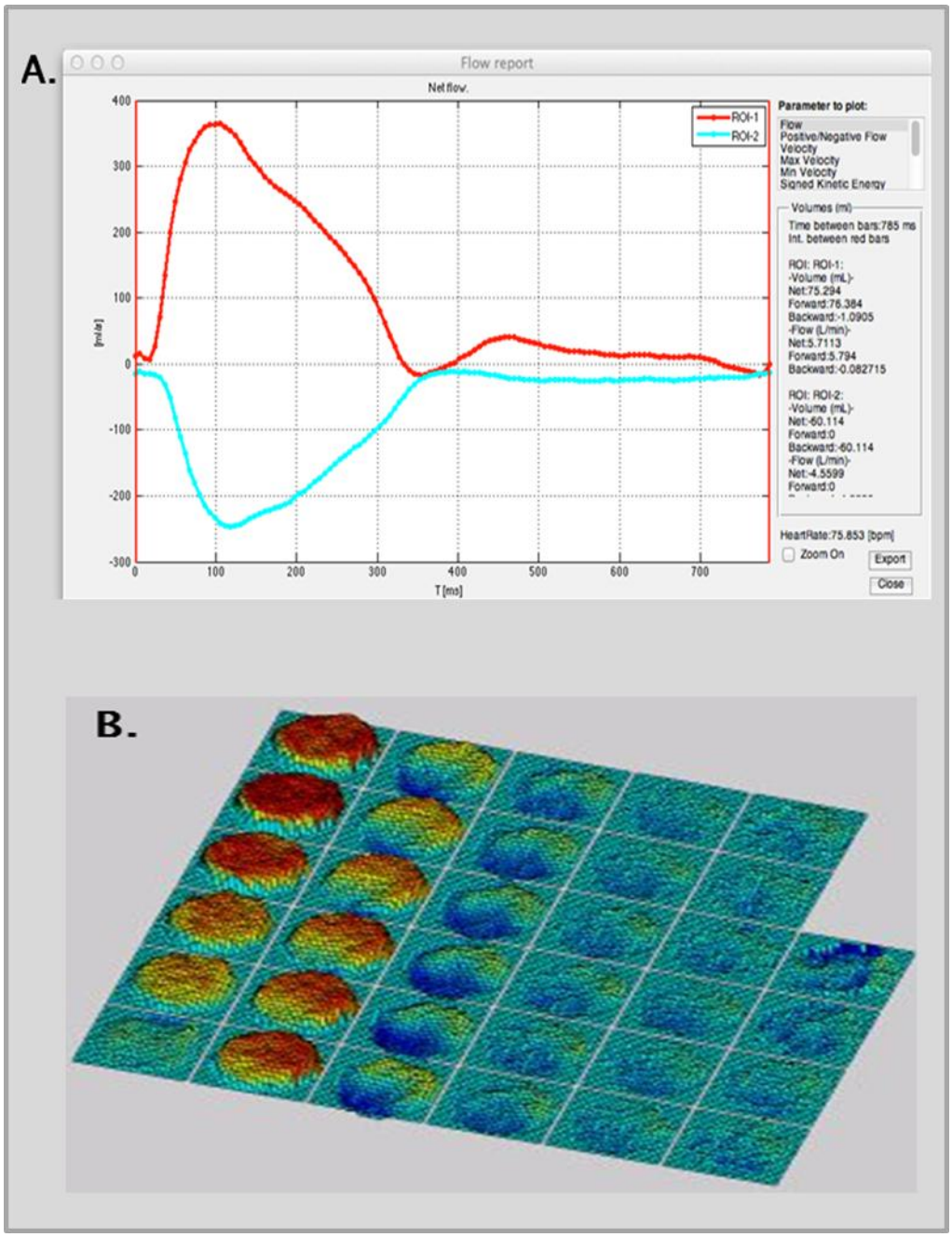

Figure 3-8 Flow analysis software: Segment flow analysis software with ascending (red) and descending (blue) flow curves. (B) 3D flow map the ascending flow ROI

(ii) Aortic Distance Measurement

The aortic path length between the imaging sites was measured using the software package *Argus (Siemens Medical Systems, Germany),* visualising the course of the thoracic aorta (as shown in Figure 3-5). This was repeated 3 times and a mean distance was used to calculate PWV as mentioned previously in Equation 1-3 (Brandts *et al*. 2012).

3.3.3 Statistical Analysis

Statistical assessments in this thesis were performed using Statistical Package for the Social Science (*SPSS), Version 21.0* for *Windows (IBM Corporation, Armonk, New York)* and significance was assumed at $P < 0.05$. Means were shown with standard deviation (SD). Bland-Altman analysis was used to assess agreement and performed with 95% confidence intervals by *Graphpad Version 6.0* (*Windows, GraphPad Software, La Jolla California USA*). Further specifications of specific statistical tests used are outlined in each experimental chapter.

3.4 Summary

This chapter summarises general methods and tests used throughout Chapter 4 to 7. In particular, a general set-up and protocol has been described for cardiac imaging, whole body angiography and assessment of aortic flow as well as relevant imaging processing tools. As this thesis investigates the development and validation of PWV, there is further commentary on the utilised PWV protocol in Chapter 4.

CHAPTER 4

Validation of MRI Derived Pulse Wave Velocity

4.1 Introduction

Aortic stiffness has been shown to be an important diagnostic and prognostic factor of CVD, as well as an estimate of overall cardiovascular health (Ben-Shlomo *et al*. 2014). Surrogate markers such as aortic PWV and distensibility have been validated as indicators of aortic stiffness and aortic elasticity index. To quantify aortic PWV and distensibility from MRI, an imaging protocol and diverse segmentation tasks need to be applied.

Firstly, to design a study protocol several imaging parameters, sequence selection and setup orientations need to be determined. A review of recent studies protocols provides guidance in this process, although further in-house optimisation is needed to correct for different vendors (*Philips*, *Siemens* or *General Electrics*), field strength (1.5 T versus 3.0 T) or variation in commercially available sequences. Other in-house decisions for PC-MRI acquisition include; what range of velocity encoding (VENC) needs to be applied, do the images need to be of high resolution, length of scan time, should the acquisition be before or after administration of a contrast agent and how many time-points are needed along the R-R cycle. In MR imaging, there are well known trade-off between resolution, SNR and acquisition time. A compromise between the different factors is made in order to have an output with sufficient

information for the image analysis process e.g. high temporal resolution may be more important than spatial resolution.

Following image acquisition, three outputs are needed to derive PWV such as segmentation of different aortic regions on the velocity encoding image, the analysis of the pulse waveform and extraction of the aortic centre line between the different slices. For each of these steps, different software, methodologies and analysis need to be performed. The overall purpose of this chapter was to evaluate the performance and repeatability of the use of PC-MRI in order to calculate PWV through a pilot investigation. Preliminary investigation included healthy participants with no previous evidence of CVD. Different methods of calculating PWV by transit-time (TT) were examined to evaluate which method was the most robust for studies within this thesis. The anticipated outcome of this chapter was an optimised PWV protocol that could be implemented as part of a research study protocol (Chapter 5, SUMMIT study).

4.2 Study Aims

The aims of this chapter were:

i. To provide in-house validation for estimating aortic PWV via from a small cohort of healthy participants (n = 10) without prior history of CVD

ii. To optimise sequence parameters such as in-plane resolution, velocity encoding settings

iii. To determine if PC-MRI images are affected by MR-contrast in order to determine if the sequence should be placed either pre or post contrast in a scanning protocol

iv. Comparison of different transit time segmentation techniques that can estimate aortic PWV (transit time, foot to foot method and upstroke) and to verify their intra- and inter-observer reproducibility.

4.3 Methods

4.3.1 Demographics and Baseline Characteristics

For this study, three groups (n = 10, in total n = 30) of an older (above 40 years) healthy population were recruited. None of the volunteers had a previous history of adverse cardiovascular events or hypertension. All MR examinations were performed with setup as described in Chapter 3.

A summary of the groups demographics are displayed in Table 4-1. All participants underwent a standard cardiac protocol, after which each group of n = 10 underwent one of the three experimental protocols of PC-MRI.

Group 1: High resolution PC-MRI, at both the aortic arch and the descending aorta, proximal to the renal bifurcation. Inter and intra-operator image analysis was performed on this group, comparing this in each of the different methods of PWV calculation (time to upstroke, time to foot and time to point).

Group 2: Two PC-MRI acquisitions at the aorta arch, a high resolution (256 X 256 matrix) with a scan time of approximately 6 minutes), and the second of lower resolution acquisition (192 x 192 matrix, scan time approximately 4 minutes).

Group 3: A high resolution acquisition of the aortic arch was performed pre-contrast injection early in the scan, and post-contrast administration (after a dual bolus injection). Images were compared to assess the effects of contrast media on the PWV calculation.

Table 4-1 Demographics for groups: Older healthy volunteers (OHV) scanned with different PC-MRI parameters (group 1-3) to evaluate if there was an impact on PWV estimation

Descriptive	Group 1	Group 2	Group 3
Age (years)	60 ± 9	52 ± 8	51 ± 7
Gender	5M:5F	3M:7F	3M:7F
Sample size (*n*)	10	10	10

4.3.2 Image Acquisition and Analysis

To extract flow and mean velocity waves, PC-MRI sequences were acquired using protocol as described in Methods and Materials (3.2.3) and distance between slices was measured from a 'candy stick' 2D FLASH aortic image as shown in Figure 3-5.

4.3.3 Comparison of PWV Transit-time Techniques

Several mathematical algorithms have been proposed for calculating transit-time calculation (Butlin *et al*. 2008; Dogui *et al*. 2011). The three most commonly used methods are; time to upstroke, time to foot and time to point. The intra and inter-observer reproducibility of each of these techniques was tested in estimating PWV.

- The time to upslope (TTU) method, calculates the arrival time of the pulse wave from the intersection of the systolic up-slope of the velocity curve and the baseline velocity. The systolic upslope is defined as the line connecting the points at the 20% and 80% of the maximum velocity in the waveforms.
- The second technique used the time to foot (TTF) method of the wave and provides the time changes between the foot of the velocity curves of the ascending and descending aorta. This type of estimation is commonly used in tonometric CF-PWV studies (Laurent, Cockcroft, Van Bortel, *et al*. 2006). The foot of the curve was defined as the intersection between the horizontal line passing through the baseline and the linear regression is modelled between the initial 10% and 30% of the systolic upslope.
- The time to point (TTP) method uses a single point at the half maximum point of the wave.

An example of these three transit-time methods is illustrated in Figure 4-1. Analysis and calculation of the PWV was measured twice by a single observer (DC) and once by a second experienced observer (JWC) to determine intra and inter-operator repeatability.

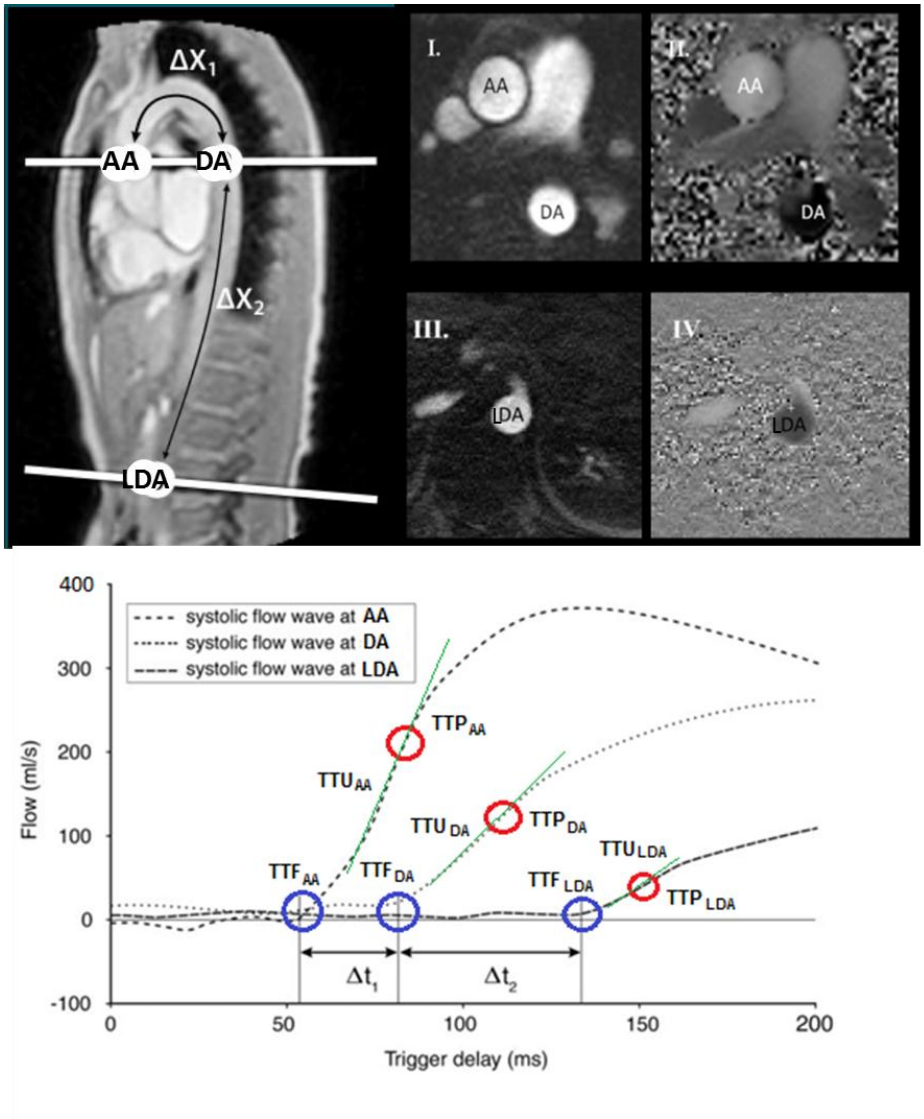

Figure 4-1 PWV Transit-time calculation: (Top) Aortic sites used for convention 2-slice PWV method where AA: ascending aorta, DA: descending aorta and LDA: lower descending aorta. (Bottom) Graph of flow waveform from each of the aortic sites after analysis for each of the transit time methods: TTU, TTF and TTP.

For each of these methods, the time interval at each site was determined and plotted against its corresponding distance along the aorta (AA, DA OR LDA). This relationship was modelled using a linear regression, and the inverse of this slope used to elicit the mean aortic PWV value.

4.3.4 Statistical Analysis

The different measurements (TTU, TTF, and TTP) were compared to each using a paired and unpaired t-test, with $P < 0.05$ considered statistically significant. Regression analyses were used to test the relationship between techniques. Percentage co-variance (CoV) was calculated as SD over mean PWV of the group. Inter-observer reproducibility was tested using Bland-Altman (difference vs. average method), with upper and lower confidence intervals of 95% (Bland & Altman 1999).

4.4 Results

4.4.1 Transit-time Estimation of PWV

Using a sample (n = 10) healthy volunteers, different transit-time estimators were tested to see which method provided a more repeatable result. The average co-variance was lowest in the TTU (9.4%) and higher in both TTF and TTP method (22.4%, 25.6%). For the TTU and TTF method, good agreement was found between observers (r^2 = 0.90, 0.94), however a lower correlation between observers was found with the TTP method (r^2 = 0.64), (Table 4-2).

Table 4-2 Comparison of different transit-time estimators.

	PWV measurement (ms^{-1})	Repeated PWV measurement (ms^{-1})	Repeated by different operator (ms^{-1})	Regression Analysis between observers (r^2)	Av. Cov %
TT-Upslope (TTU)	5.67 ± 0.9	6.16 ± 0.5	6.10 ± 0.5	0.90	9.4%
TT-Foot (TTF)	6.32 ± 2.1	6.69 ± 1.6	6.63 ± 1.5	0.94	22.4%
TT- Point (TTP)	6.89 ± 2.8	6.70 ± 2.6	7.35 ± 1.8	0.64	25.6%

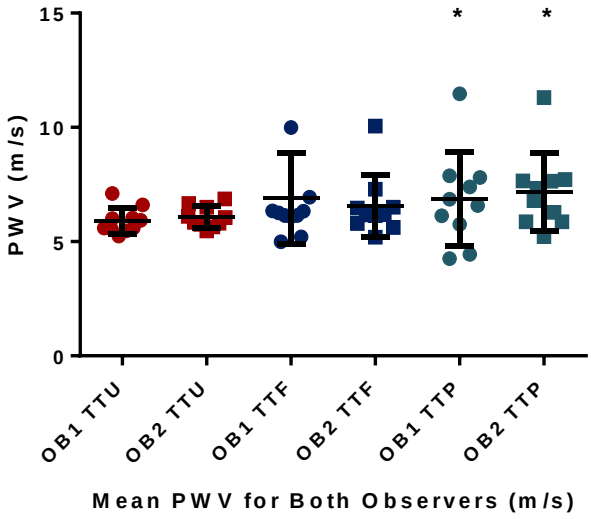

Figure 4-2 Transit-time PWV methods: Dot and scatter plot of the mean PWV for each of the transit-time techniques (TTU: Transit Time Upslope, TTF: Transit Time Foot: TTP: Transit Time Point) for two observers (OB1 and OB2). A difference in mean PWV was found with TTP method in comparison of TTU and TTF (paired t-test, *P <0.05).

Means between the techniques were tested using paired t-test. TTU and TTF did not show significant difference between techniques (P = 0.23), however TTP showed significant with both TTU (P = 0.04) and TTF (P = 0.02).

Bland-Altman plots were performed by calculating the difference (A - B) vs. average with confidence intervals of 95% in Figure 4-3.

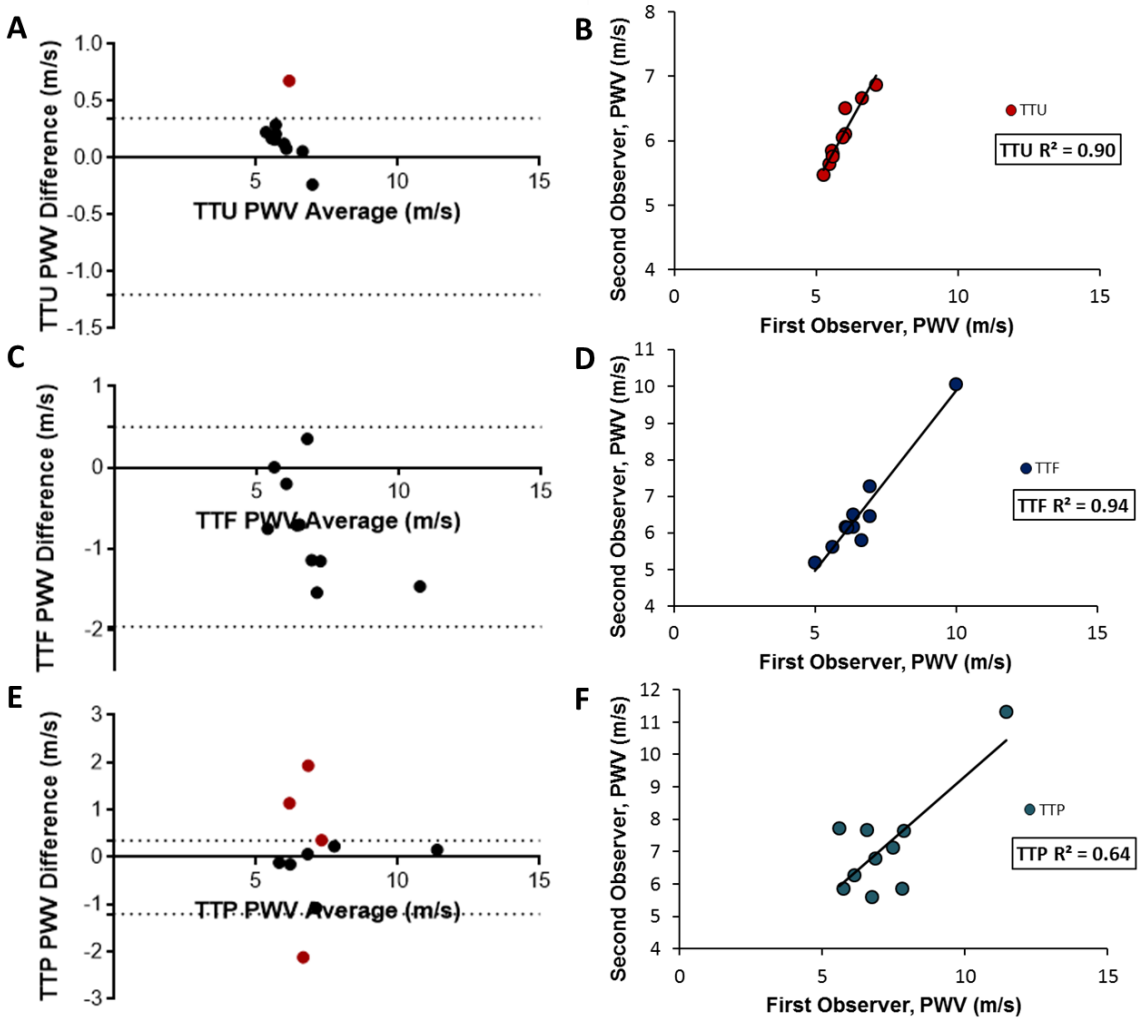

Figure 4-3 Bland-Altman (left) and regression correlation (right) for Transit-time methods: Where A. upslope (TTU) - A, B; TT-foot (TTF)- C, D and TT-Point (TTP)-E, F.

4.4.2 Optimisation of Imaging Protocol

(i) Effect of In-plane Resolution

Different in-plane resolution was applied. The results of both high (256 x 256) and low (192 x 192) in plane spatial resolution PC-MRI images are displayed in Table 4-3.

Table 4-3 Results from using different in-plane resolutions.

In-Plane Resolution	PWV measurement (ms^{-1})	Repeated PWV measurement (ms^{-1})	Average Acquisition Time (min)
PWV High Resolution	5.79 ± 0.8	5.88 ± 0.9	06:12 ± 0:45
PWV Low Resolution	7.89 ± 2.5	6.85 ± 2.1	04:25 ± 0:30

From these results, PWV values with higher in-plane resolution were seen to be more reproducible and showed less variance when repeated**.**

(ii) Effect of MR Contrast on PWV

A single slice high resolution PC-MRI was analysed pre and post-contrast. No significant difference was found between the mean PWV pre and post contrast (paired t-test, $P > 0.05$) (Table 4-4).

Table 4-4 Results of effect acquiring PWV pre and post-contrast

Acquisition time	PWV (ms^{-1})	Average Acquisition Time (mins)	% CoV	Regression Analysis (r^2)
Pre-contrast	6.14 ± 1.4	06:12 ± 0:45	18.2%	0.84
Post-contrast	5.62 ± 1.3	06:12 ± 0:45	19.2%	0.82

An example of a flow waveform for a partipiant pre and post the bolus injection of contrast is displayed in

Figure 4-4.

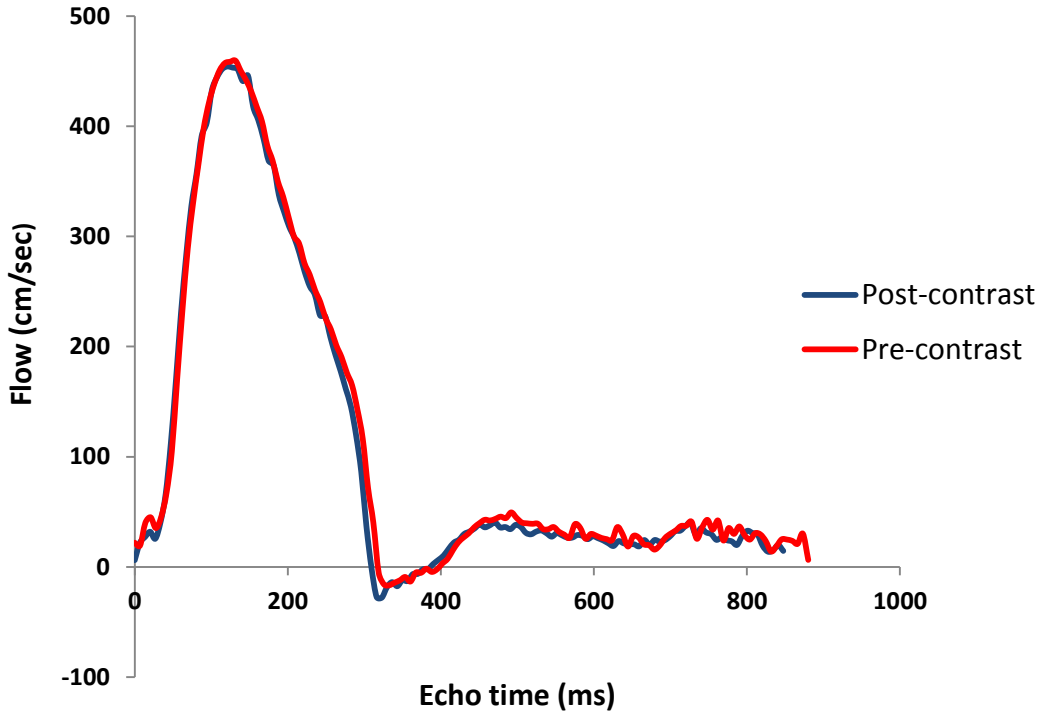

Figure 4-4 Flow waveform pre and post contrast: A flow analysis of pre (red) and post (blue) contrast at the ascending aorta for a healthy volunteer (n = 1). The administration of MR-contrast had no significant effect on determining PWV (paired t-test, $P > 0.05$).

Table 4-5 Summary of key results: Validation of MR derived PWV

Investigation	Results
I. Transit time methods of estimating PWV	
Which transit time method had the lowest variance between a healthy cohort?	• The average covariance was lowest in the TTU (9.4%) and higher in both TTF and TTP method (22.4%, 25.6%). However statistical significance was only seen in both TTU, TTF versus TTP ($P < 0.05$).
Which transit time method showed the best inter and intra reproducibility?	• For the TT-upslope and TT-Foot method, good agreement was found between observers (r^2 = 0.90, 0.94), however a lower correlation between observers was found with the TT- Point method ($r^2 = 0.64$)
Recommendation	• The TT-upslope showed the best co-variance and repeatability between observers
II. Optimisation of imaging protocol	
Does high and low resolution PC-MRI imaging effect PWV result?	• Reducing resolution shortens the scan time by 2 minutes. • Contour boundaries were more defined in higher resolution images, making segmentation easier with resultant improved reproducibility.
Recommendation:	• Use high resolution velocity encoding imaging for higher reproducibility.
Does the administration of contrast provide any additional value to PC-MRI imaging?	• No significant change was seen pre or post contrast on single slice acquisition
Recommendation	• PC-MRI images for MR-PWV can be placed either before or after contrast without any significant effect with PWV

4.5 Discussion

Several studies have previously evaluated MR-based measurements of PWV with intravascular pressure measurements (Grotenhuis *et al*. 2009) and applanation tonometry as a reference standard (Rogers *et al*. 2001; Suever *et al*. 2011). This chapter provides preliminary results of our in-house initial testing of PC-MRI MR-PWV methods such as technique reproducibility and the effect of scanner variables. The aim of this chapter was to provide experimental results in order to optimise the protocol for a clinical study (Chapter 5). A summary of the key findings are shown in table below.

Transit Time Analysis Methods for Estimating PWV

The temporal shift between the two waveforms at different sites through the vasculature gives an indication of the stiffness the vessel. The shorter the temporal shift, the greater the vessel stiffness resulting in higher PWV value. The computation of transit time for PWV depends on various waveform characteristics and can be computed by the TTU, TTF or the distance between the mid-point of the curve (TTP). In this validation work, all these methods were assessed and tested for repeatability and covariance distribution of the small sample cohort of ten healthy volunteers. Our results in this study showed that the average co-variance was lowest in the TTU (9.4%) and higher in both TTF and TTP method (22.4%, 25.6%). When reproducibility was tested between two observers, the TTU and TTF method showed good agreement between observers (r^2 = 0.90, 0.94), however a lower correlation between observers was found with the TTP method (r^2 = 0.64). From this preliminary analysis, we can see that the upstroke method shows more robustness and better

reproducibility than the other methods so it will be used for any further PWV analysis in this thesis.

Image Acquisition: In-Plane Resolution

After a review of current literature (1.8.7), it is evident that there is no standard approach. PWV studies have used both through-plane and in-plane aortic orientations, and different PC-MRI parameters, such as in-plane resolution. To experimentally test the effect of changing in-plane resolution, a small cohort of ten healthy participants received both a high and low spatial resolution PC-MRI at the aortic arch and analysed to determine the PWV. The purpose behind trying to reduce the in-plane resolution was an attempt to reduce scan protocol time for the clinical study with the heterogeneous diabetic and cardiovascular population. The results from this study showed that reducing the high resolution image matrix from (256 x 256) to a lower resolution (192 x 192), showed a reduction of 2 minutes in scan acquisition time. However, the lower resolution images shows higher variance than the high resolution acquisition and proved to have poorer intra-operator reproducibility too. This may be due to a poorer SNR of the lower resolution images, making image segmentation and boundary definition more difficult and hence affecting the PWV measurement. As the aim of the clinical study was to investigate if we could see early arterial stiffness in T2DM patients, the high resolution acquisition was selected for final protocol.

Image Acquisition: Pre and Post Contrast

The patients in the clinical study received contrast as part of a whole body angiogram acquisition. It was therefore questioned if the administration of contrast would affect the velocity encoding imaging and thus effect the placement of the acquisition in the

protocol i.e. pre and post-bolus of contrast. Some studies have suggested in the case of 4D flow acquisition, contrast can improve the SNR slightly and thus improve image quality (Bock *et al*. 2010). However, no effect was seen in our study, so it was therefore decided that the PWV acquisition could be performed towards the end of the scan.

In conclusion, this study has highlighted that adapting a high resolution in plane acquisition and using TT-upstroke estimation method would provide an optimal PWV acquisition protocol. We have also demonstrated that the effect of image acquisition pre or post bolus injection of contrast will not affect our results and it has been therefore decided that PWV will be placed at the end of the scanning protocol of the clinical study. These experiments have provided preliminary data to assist in the protocol design and acquisition.

Study Limitations

These experiments recruited participants in an opportunist nature, with small groups of 10 patients sequentially selected to test each of the experiments. The aim of this study was to gather preliminary data to test and optimise the PWV acquisition to be later implemented into the clinical study protocol. For the TT methods experiment, a group of patients received two-slice PWV ‘standard’ set-up as described in papers (van der Meer *et al*. 2007; Ibrahim *et al*. 2010). However the results obtained in this experiment are not comparable to the in-plane resolution or pre and post contrast study as they only had a single slice PWV acquisition due to scan time restrictions and were demonstrated on different cohorts of volunteers.

4.6 Summary

This preliminary work aimed to test the effect of various MR acquisition setups such as image resolution and the effect of contrast on the calculation of PWV. Different methodologies for estimation of transit-times were also examined for both intra and inter-observer variation. The final results of this validation have been used for optimising the PWV of the clinical study protocol as shown in the following Chapter 5.

CHAPTER 5

Aortic Stiffening in Type-2 Diabetes and Cardiovascular Disease

5.1 Introduction

Type 2 diabetes mellitus (T2DM) is a chronic metabolic disease resulting in an inability to control glucose homeostasis due to insulin resistance. In many countries, T2DM is reaching epidemic proportions due to an ageing population, with an increasing prevalence of obesity and sedentary lifestyles. The disease is associated with high morbidity and mortality due to cardiovascular macro and micro-vascular disorders such as stroke, CHD and PVD, as well as nephropathy and retinopathy. Such complications can impose a significant burden on the quality of life of diabetic patients. As a consequence, there is a need for methods to detect cardiovascular degeneration in diabetic patients at an early stage of disease development before these conditions emerge as an adverse event. Increased aortic stiffness, as measured by PWV, may provide an important marker of disease development, linking T2DM with CVD. Indeed, a study by Van der Meer *et al* (2007) utilised MR-PWV in the assessment of aortic and cardiac function in uncomplicated T2DM patients. It was uncovered that patients with T2DM had increased PWV, lower aortic distensibility and compromised LV diastolic function, compared to age matched controls, showing coherency to the other studies on metabolic syndrome (Cruickshank 2002; Roes *et al*. 2008; Lee *et al*. 2007b).

As previously reviewed in Chapter 1, MR-PWV can be derived from flow analysis at different aortic locations using PC-MRI and has shown good reproducibility with the gold standard invasive pressure measurements (Westenberg *et al*., 2011, Grotenhuis *et al*., 2009). The aim of this study was to evaluate MR-PWV in a complicated diabetic population with and without symptomatic CVD, and to interrogate if it bares an impact on LV function.

5.2 Study Aims

The aims of the research presented in this chapter were:

i. To implement a validated MR-PWV technique on four cohorts of patients covering early uncomplicated T2DM, through to later stages (0 - 24 years duration) with clinical evidence of CVD (CHD, stroke and/or PVD);
ii. To investigate if there are any correlations between LV function and aortic PWV
iii. To determine if aortic PWV can discern any difference on aortic stiffness between T2DM patients and patients without T2DM.

5.3 Methods

5.3.1 Study Participants

The participants in this study were recruited as part of the SUMMIT project (as described in *Preface*), to which 156 participants underwent an MRI as part of imaging work-package 4. Study participants were recruited from multiple sources across local and national networks such as the Health Informatics Centre (HIC), Scottish Primary Care Research Network (SPCRN), Scottish Diabetes Research Network (SDRN), local advertising and from the Secondary Care Diabetes Clinics (SCI-DC). All participants were over 40 years of age and after initial evaluation, they were assigned into one of the following cohorts in Table 5-1. These grouping will be referred to for the rest of the chapter.

Table 5-1 SUMMIT Groups: Classification of each of the four groups with and without T2DM and with and without CVD. *The sample sizes of each of the groups was based on intended MRI recruitment for the study.

No.	Description of cohort	Sample size
Group 1	Participants with T2DM with CVD	n = 50*
Group 2	Participants with T2DM without CVD	n = 50*
Group 3	Participants without T2DM and with CVD	n = 25*
Group 4	Participants without T2DM and without CVD	n = 25*

5.3.2 Eligibility Criteria

(i) Screening Interview

Each participant underwent a screening interview with research nurses (Scottish Diabetes Research Network) in which medical history, anthropometric measurements, venous blood, and urine collection was taken as outlined by SUMMIT case report form (CRF), which is included in Appendix A. For medical history; diabetes history (age at diagnosis, presentation, treatment and complications), document of other co-morbidities including cardiovascular status, significant past medical history, concomitant medication and smoking status was recorded. Participants' height, weight, hip and waist circumference were measured, their body mass index ($kg.m^{-2}$) and hip to waist ratio were calculated from these values. Resting blood pressure was measured three times with participants in the supine position with Omron M6 (OMRON Healthcare, Europe, Hoofddorp, The Netherlands).

Informed consent was obtained from all subjects with ethical approval from the local ethics commission, East of Scotland Research Ethics Service. SUMMIT receives support from the Innovative Medicines Initiative (IMI) Joint, undertaking under the grant agreement n° [115006], resources of which are composed of financial contribution from the European Union's Seventh Framework Programme (FP7/2007-2013) and EFPIA companies' in kind contribution.

(ii) MRI Participants

Additional MR specific exclusions were applied as outlined in Chapter 3.1.1. A total of 156 eligible volunteers participated in the MRI section of the SUMMIT study; however 6 opted out before the scan.

A final total of 146 participants underwent cardiovascular MRI protocol with all participants having WBA, n = 144, having LV assessment and 90 participants continuing to have an aortic assessment for PWV measurement. A detailed breakdown of target recruitment and final MR participants is outlined in Figure 5-1. As this study is focused on PWV, the rest of the results will only include participants that had both PWV and LV assessment (n = 90).

Figure 5-1 SUMMIT recruitment flow diagram for MRI cardiac assessment and aortic flow quantification: Final recruitment for LV assessment was *n* = 144 and for aortic flow quantification was *n* = 88. *The first 23 scans were under an older protocol and excluded for this study. # Extreme outliers at 3 SD. over the mean

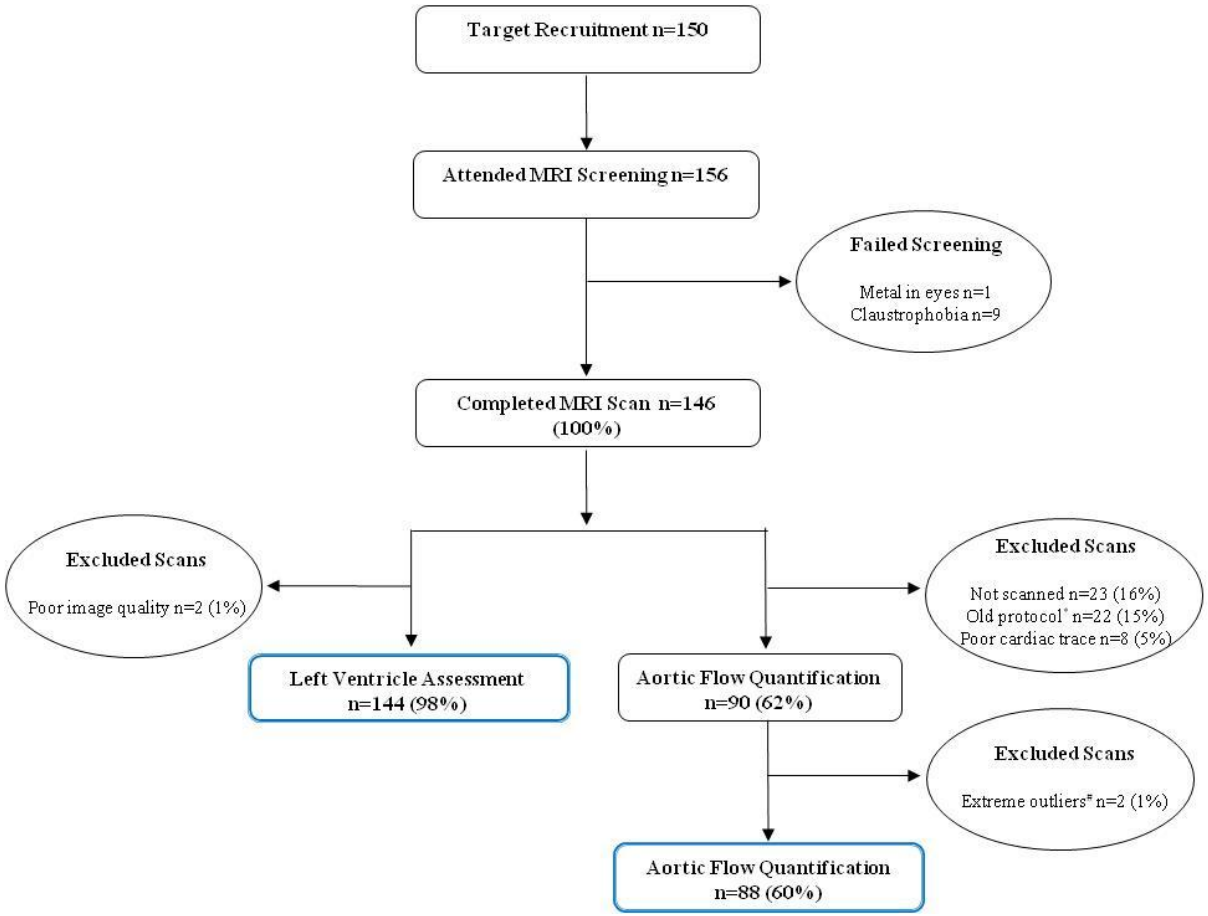

(iii) Type 2-Diabetes Participants

The inclusion criteria for G1 and G2 included diagnosis of T2DM after the age of 35 and not on insulin for the first 12 months of disease. The non-diabetic criteria status of those in G3 and G4 were confirmed by haemoglobin A1C (HbA1C) levels (< 5.7% and < 39 mmol/mol). Patients with diabetes were on a range of treatments with the majority on oral agents (72%). Otherwise, treatments include diet only (12%), insulin and oral agents (8%), insulin only (2%), GLP-1 and insulin (2%), no treatment (2%) and other (2%).

(iv) Cardiovascular Participants

For Group1 and 3, clinical evidence of CVD had to be a minimum of one of the following: CHD, stroke and/or PVD. Further description and criteria can be seen in Table 5-2. A breakdown is for CVD groups G1 and G3 are shown in Table 5-3.

The majority of patients had a CHD event (75-79%) with a minority having stroke and PVD (> 20%) as a cardiovascular complication. From both groups, patients mostly had single cardiac event (93%, n = 37) with 8% (n = 3) of CVD patients having two complications. The majority of the study populations had underlying hypertension (85%, n = 34). Further breakdown is shown in Table 5-3.

Table 5-2 Cardiovascular inclusion criteria for SUMMIT participants: G1 and G3 were required to have clinical evidence of at least one of the following (I-III) to satisfy CVD criteria

	Cardiovascular Inclusion Criteria	Description
I	**Coronary Heart Disease (CHD)**	Non-fatal acute myocardial infarction, hospitalised acute coronary syndrome, resuscitated cardiac arrest, coronary artery bypass graft (CABG) or any coronary revascularisation procedure
II	**Stroke**	Non-fatal stroke and transient ischaemic attack (TIA) confirmed by specialist (excluding TIA not confirmed by specialist, haemorrhagic stroke, and stroke associated with a primary haematological disease e.g leukaemia, polycythaemia, blood disease, tumour, trauma, or surgical procedures)
III	**Peripheral Vascular Disease (PVD)**	Ankle-brachial index (ABI) < 0.9 with intermittent claudication, or abnormal toe systolic pressure, pulse volume recordings, transcutaneous oxygen measurements or vascular imaging or prior corrective surgery, angioplasty or above ankle amputation

.

Table 5-3 Type of CVD diagnosis in patients: A breakdown of the diagnosed CVD participants from Groups 1 and 3. Data presented as % (*n*) of total participants.

Cohorts with CVD	Group 1 (CVD and T2DM)	Group 3 (CVD only)
CHD	74% (17)	79% (15)
PVD	17% (4)	10% (2)
Stroke	19% (5)	16% (3)
Acute MI	48% (11)	68% (13)
CABG	18% (4)	16% (3)
Cardiac Arrest	8% (2)	16% (3)
Hypertension	78% (18)	84% (16)
PCI	22% (5)	42% (8)
TIA	0% (0)	13% (1)
Unstable Angina	26% (6)	31%(6)
T2DM	100% (23)	0% (0)

Abbreviations: CHD: Chronic Heart Disease, PVD: Peripheral Vascular Disease, Acute MI: Acute Myocardial Infarction, CABG: Coronary Artery Bypass Surgery, PCI: Percutaneous Coronary Intervention, TIA: Transient Ischaemic Attack.

5.3.3 MR Clinical Protocol for SUMMIT

MRI study protocol was designed to assess cardiac and aortic function with whole body imaging. Full details of the setup are described in full in Methods and Materials (3.2) and full MRI SUMMIT protocol can be found in Appendix A. Full LV analysis was completed for these patients by experienced MRI segmenters (SM, SD) and aortic flow quantification was completed using the optimised transit-time methods as described in Chapter 3 (DC).

5.3.4 Statistical Analysis

Descriptive statistics was used for the analysis of the demographic and clinical features of the cohorts with data expressed as mean ± SD. All data was tested for equality of variance by using Levene's test of homogeneity, where $P > 0.05$ indicated normal parametric data. An outlier labelling rule was applied to data returning an extreme outlier ($> 3\sigma$).

Between group differences were calculated using an ANOVA test, and a Fisher's LSD post-hoc adjustment was applied for multi-comparisons with both PWV and LV function.

Pearson's correlations were used to assess independent associations with PWV and LV function with population risk factors. In these analysis, dummy variables were used for gender (female = 0, male = 1) and smoking (0 = non-smoker, 1 = ex-smoker, 2 = smoker) and significance was assumed at $P < 0.05$.

5.4 Results

5.4.1 Demographics and Baseline Characteristics

Baseline characteristics are shown in Table 5-4. There was no significant difference regarding age, body weight, BMI, SBP or DBP across the groups. However gender, BSA, waist circumference and hypertension were found to differ significantly ($P < 0.05$). BMI and BSA were found to be marginally higher in the T2DM groups (G1 and G2) and hypertension and males were more predominant in the CVD groups (G1 and G3).

Table 5-4 Anthropometric data for participants: Data presented as mean value ± SD for each Groups 1 - 4.

	Group 1 CVD & T2DM	**Group 2 T2DM**	**Group 3 CVD**	**Group 4 Controls**
Age	65 ± 7	61 ± 9	66 ± 8	63 ± 8
Gender	19M:4F	17M:12F	14M:5F	6M:13F
Sample size	23	29	19	19
Body weight (kg)	90.3 ± 13.4	88.1 ± 17.7	83.4 ± 14.3	78.0 ± 14.9
BMI (m^2)	31.3 ± 4.5	30.5 ± 5.3	29.8 ± 3.9	28.4 ± 3.8
BSA (kg/m^2)	2.0 ±0.2	2.0 ± 0.3	1.85 ± 0.1	1.9 ± 0.3
Systolic blood pressure (mmHg)	136 ± 12	136 ± 14	136 ± 19	129 ± 9
Diastolic blood pressure (mmHg)	75 ± 8	78 ± 8	76 ± 8	77 ± 9
Pulse Pressure	67 ± 14	68 ± 12	65 ± 9	54 ± 9
Hypertension	78% (18)	48% (14)	84% (16)	26% (5)
T2DM Duration (years)	9.3 ± 4.9	7.7 ± 5.8	0	0

Abbreviations: T2DM: Type-2 Diabetes Mellitus, BMI: Body Mass Index: body weight (kg)/ $height^2$ (m), BSA: Body Surface Area Dubois and Dubois formula

5.4.2 Cardiac MR Assessment

Of the original 146 recruited into the MRI study, 23 participants opted not to continue with PWV scanning or retiring the scan before completion (Figure 5-1). In addition, the first 22 patients studied were subsequently excluded due to change of protocol and a further 8 scans were judged uninterpretable, due to cardiac triggering errors, poor traces or unacceptable image quality. This resulted in a final total of 90 participants (65%) to undergo PWV assessment.

5.4.3 Aortic PWV in SUMMIT Groups

An outlier labelling rule was applied to the data returning an extreme outlier (> 3 σ) in G2. Before removal of outliers, G2 mean PWV was 8.4 ± 4.8 ms^{-1} with n = 29 subjects. Levene's test verified the equality of variances in the samples, $P > 0.05$, thus the data is of normal distribution. One other patient was excluded from G1 (leaving n = 22) as the LV data was of poor image quality. The PWV results for the final 88 participants are shown in the table below.

Table 5-5 Aortic PWV means ± SD for each group: The mean PWV was found to be significantly different between groups

CMR data	Group 1 CVD & T2DM	Group 2 T2DM	Group 3 CVD	Group 4 Controls	ANOVA Sig.
PWV (ms^{-1})	8.7 ± 2.8, n =22	7.5 ± 2.3, n =28	8.9 ± 3.6, n =19	6.7 ± 1.8, n =19	*P = 0.04

Statistical Analysis of Aortic PWV between Groups

The means and SD of aortic PWV are presented in Table 5-5, in which a significant difference was found between groups (ANOVA, $P = 0.04$).

Post-hoc LSD test revealed that groups with diagnosed CVD (G1 and G3) were significantly greater than controls, G4 ($P = 0.02$, $P = 0.02$ respectively). No difference in PWV was found between T2DM (G2) or control groups (Figure 5-2) or between either the CVD groups (G1 vs. G3), ($P > 0.05$).

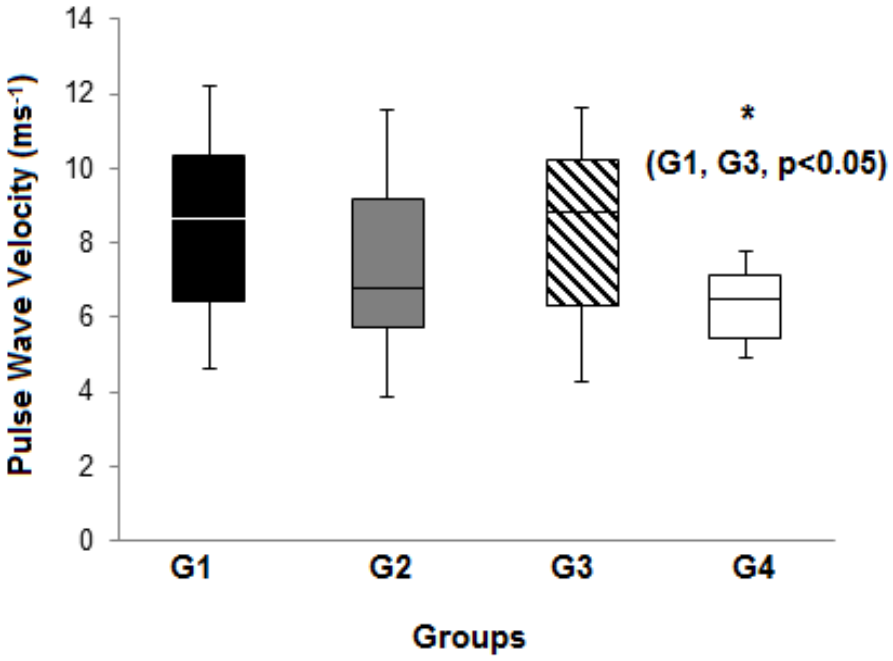

Figure 5-2 Box Plot of mean aortic PWV across groups: The mean PWV was found to be significantly higher in CVD groups (G1, G3) than controls (G1), (ANOVA, $P < 0.05$).

5.4.4 Left Ventricle Function in SUMMIT Groups

The LV parameters were calculated for each of the groups and tested for equality of variances (Levene's test, $P > 0.05$). Due to poor image quality, one participant was excluded from G1. The results for the final 88 participants are displayed in Table 5-6. A combination of both absolute (also referred to as indexed) values for LV function (EF, LVM-A) and LV function normalised to BSA were analysed (EDV-N, ESV-N, SV-N and LVM-N).

Table 5-6 Box Plot of mean LV parameters across groups: The mean PWV was found to be significantly higher in CVD groups (G1, G3) than controls (G1), *(ANOVA, $P < 0.05$)

CMR data	Group 1 CVD & T2DM	Group 2 T2DM	Group 3 CVD	Group 4 Controls	ANOVA Sig.
EF (%)	63.4 ± 9.8	65.1 ± 8.4	64.1 ± 12.0	65.3 ± 7.9	NS, $P = 0.91$
EDV-N (ml)	72.5 ± 11.5	69.32 ± 13.9	76.1 ± 23.6	68.78 ± 9.1	NS, $P = 0.40$
ESV-N (ml)	27.0 ±9.9	24.6 ± 9.7	28.9 ± 19.0	24.1 ± 7.0	NS, $P = 0.55$
SV-N (ml)	45.5 ± 8.0	44.7 ± 8.4	47.2 ± 9.3	44.7 ± 6.9	NS, $P = 0.73$
LVM-N (gm^{-2})	62.5 ± 10.4	56.8 ±12.0	61.5 ± 10.9	51.5 ± 5.3	*$P = 0.004$
LVM-A (g)	125.4 ± 24.2	114.1 ± 32.1	117.5 ± 23.2	95.9 ± 18.22	*$P = 0.005$

Abbreviations: EDV-N: Normalised End Diastolic Volume, ESV-N: Normalised End Systolic Volume, SV-N: Normalised Stroke Volume, LVM-N: Normalised Left Ventricular Mass, LVM-N: Absolute Left Ventricular Mass.

Statistical analysis of LV function between groups

There was no significant difference was seen between EF, EDV, ESV, SV between the 4 groups, (ANOVA, $P > 0.05$).

LVM was found to be different across the groups; LVM-N, (ANOVA, $P = 0.004$) and LVM-A, (ANOVA, $P = 0.005$). Post-hoc LSD comparisons revealed that G1 and G3 (CVD and with or without T2DM) had significantly higher LVM-N than controls, G4 ($P = 0.001$, $P = 0.003$, respectively). Similarly to PWV, T2DM participants (G2) did not differ significantly from the control group (G4), (ANOVA, $P = 0.08$) and the CVD groups (G1, G3) did not differ from each other (Figure 5-3).

In the case of LVM-A, all patient groups (G1, G2 and G3) were found to have significantly higher LVM than control group, (post-hoc LSD, $P < 0.05$) (Figure 5-4). However, there no significant difference between patient groups (G1, G2 and G3), (post-hoc LSD, $P > 0.05$).

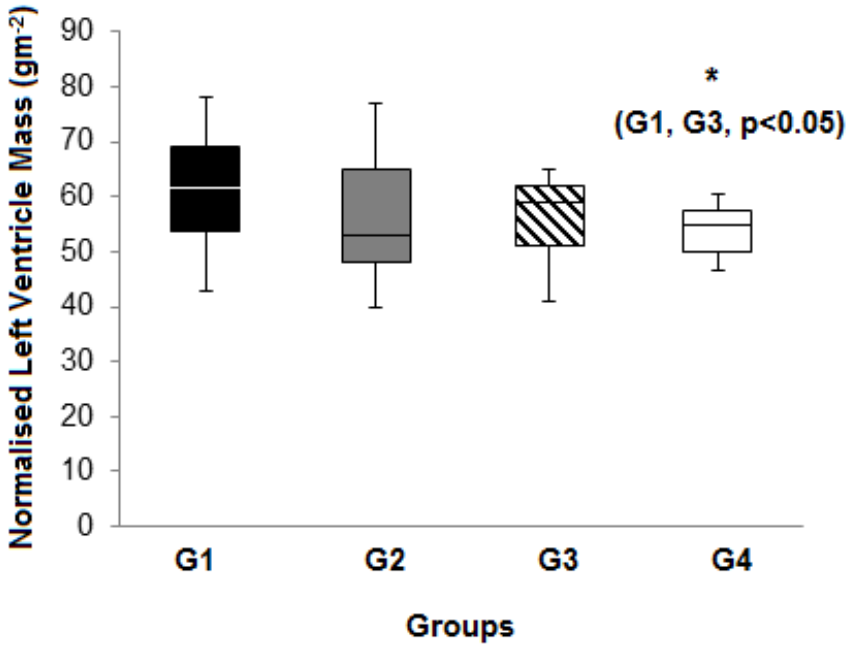

Figure 5-3 Box-plot of normalised LVM across groups: The mean LVM-N was found to be significantly higher in CVD groups (G1, G3) than controls (G1), (ANOVA, $P < 0.05$).

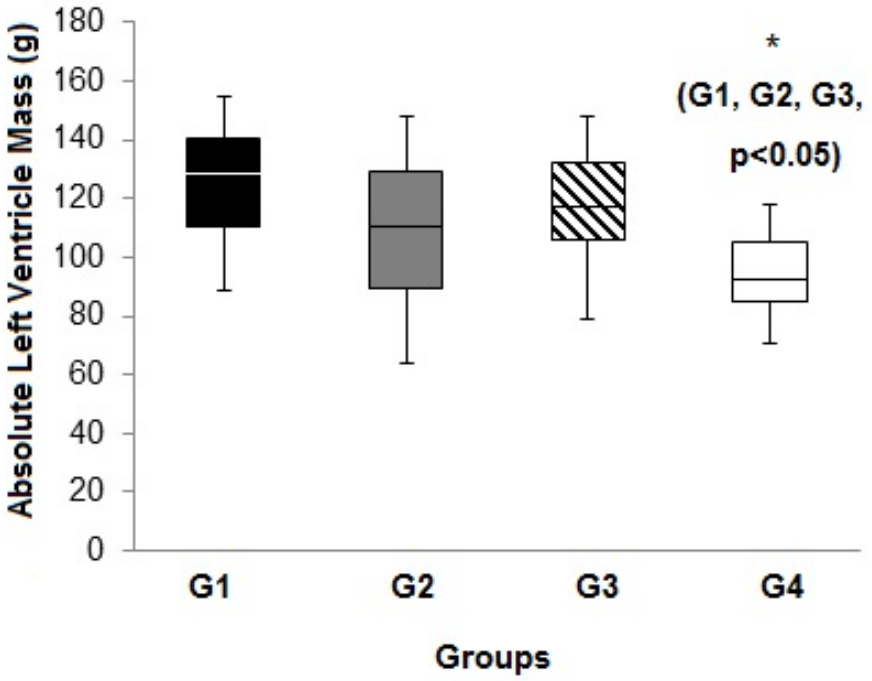

Figure 5-4 Box-plot of absolute LVM across groups: The mean LVM-N was found to be significantly higher in CVD groups (G1, G3) than controls (G1), (ANOVA, $P < 0.05$).

5.4.5 Aortic PWV and Left Ventricular Function

No significant correlation was found between PWV and LV parameters (Pearson correlation, $P > 0.05$, 2-tailed). Increased aortic PWV showed a negative trend with EF (ρ = -0.13, P = 0.20), EDV (ρ = -0.28, P = 0.22), ESV (ρ = -0.10, p=0.65), SV (ρ = -0.29, P = 0.18). For LVM, it correlated positively with PWV (ρ = -0.04, P=0.87) and is shown in Figure 5-5.

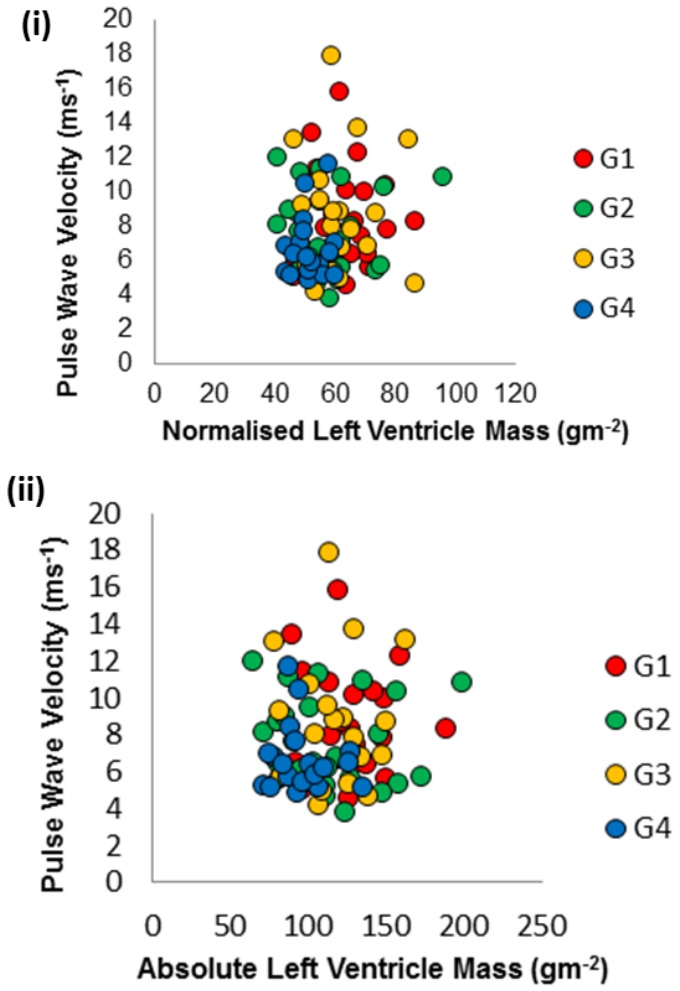

Figure 5-5 Scatter-plot of the relationship between aortic PWV and (i) normalised LVM and (ii) absolute LVM: PWV was plotted against LVM-N and LVM-A, however no significant correlation was found (Pearson correlation, $P > 0.05$).

5.4.6 Reclassification of Groups for either T2DM or Cardiovascular Disease

For part II of analysis, the original classification of their SUMMIT grouping will be used (G1 to G4) as shown in Table 5-7. New groups were also adapted into composite groups in respect to the presence or absence of T2DM and with or without CVD for analysis, groups; G5, G6, G7 and G8.

Table 5-7 Reclassification of SUMMIT groups: Original SUMMIT grouping are shown from G1 to G4. *G5 to G8 are new composite groups used in subsequent analysis.

Groups	Group description	Group size, *n*
Group 1	Participants with T2DM with CVD (G1)	*n* = 22
Group 2	Participants with T2DM without CVD (G2)	*n* = 28
Group 3	Participants with no T2DM and with CVD (G3)	*n* = 19
Group 4	Participants with no T2DM without CVD (G4)	*n* = 19
*Group 5	All participants with T2DM with and without CVD (G5)	*n* = 50
*Group 6	All participants with no T2DM with and without CVD (G6)	*n* = 38
*Group 7	All participants with CVD, with and without T2DM (G7)	*n* = 41
*Group 8	All participants without CVD, with and without T2DM (G8)	*n* = 47

The following relationships will be investigated using groups as defined in Table 5-7:

(i) Aortic PWV and T2DM

(ii) Left Ventricular Function and T2DM

(iii) Aortic PWV and Duration of T2DM

(iv) Left Ventricular Function and Duration of T2DM

(v) Aortic PWV and CVD

(vi) Left Ventricular Function and CVD

5.4.6 (i) Aortic PWV and T2DM

Using the reclassified G5, the presence of T2DM was investigated in terms of PWV. No significant relationship was found between T2DM population (G5: 8.06 ± 2.69 ms^{-1}) compared to the non-T2DM (G6: 7.85 ± 3.01 ms^{-1}), (unpaired t-test, P > 0.72).This is shown in Table 5-8 below and Figure 5-6.

Table 5-8 Mean aortic PWV of patients with and without T2DM: PWV was compared for T2DM (G5, G2, G1) versus non-T2DM controls (G6, G4, G3), irrespective of presence of CVD. No significant difference was found (unpaired t-test, *P* > 0.05).

T2DM Groups		PWV ms^{-1}	Non-T2DM Group		PWV ms^{-1}	*P*-value
G5:	All T2DM with and without CVD	8.06 ± 2.69, *n* = 50	G6:	All non-T2DM with and without CVD	7.85 ± 3.01, *n* = 38	NS, *P* = 0.72
G2:	T2DM with no CVD	7.58 ± 2.3, *n* = 28	G4:	Non-T2DM with no CVD	6.77 ± 1.8, *n* = 19	NS, *P* = 0.28
G1:	T2DM with CVD	8.68 ± 2.8, *n* = 23	G3:	Non-T2DM with CVD	8.93 ± 3.6, *n* = 19	NS, *P* = 0.80

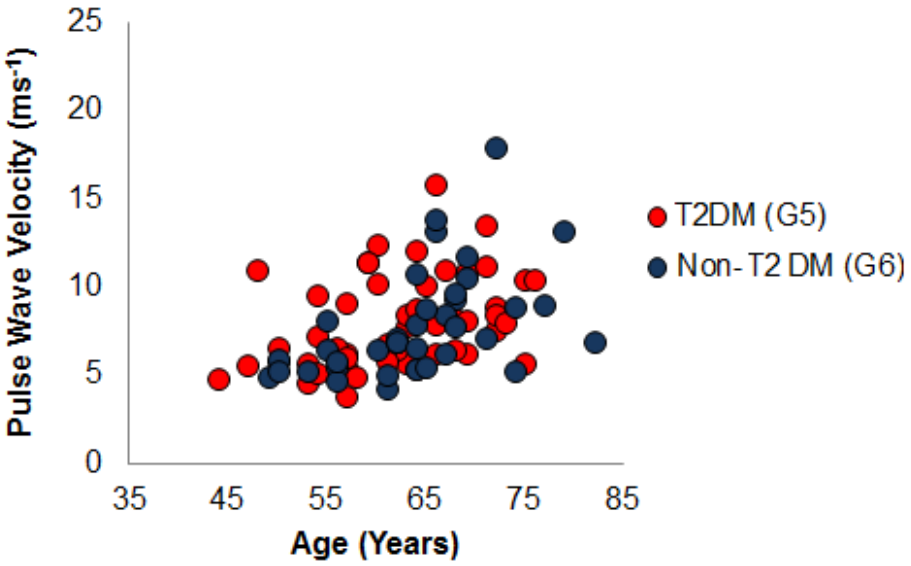

Figure 5-6 Scatter-plot of PWV and T2DM: Relationship of PWV with T2DM (G5, G2, G1) and without T2DM (G6, G4, G3), no significant difference was found (unpaired t-test, *P* > 0.05)

5.4.6 (ii) Left Ventricular Function and T2DM

No significant difference between mean LVM-N was found between T2DM (G5: 59.3 ± 11.6 gm^{-2}) and non- T2DM G6: (56.4 ± 9.9 gm^{-2}), (unpaired t-test, $P = 0.23$) as shown in Table 5-9.

In contrast, LVM-A was found to be significantly higher in T2DM (G5: 119.1 ± 29.2 g^{-2}) compared to the non-T2DM population (G6: 106.7 ± 23.3 g^{-2}), (unpaired t-test, $P = 0.03$). This is shown in Table 5-10 and Figure 5-7.

Table 5-9 Mean LVM-N of patients with and without T2DM: LVM-N was compared for T2DM (G5, G2, G1) versus non-T2DM controls (G6, G4, G3), irrespective of presence of CVD. No significant difference was found (unpaired t-test, $P > 0.05$).

	T2DM Groups	LVM-N (gm^{-2})		Non-T2DM Group	LVM –N (gm^{-2})	*P*-value
G5:	All T2DM with and without CVD	59.3 ± 11.6, $n = 50$	G6:	All non-T2DM with and without CVD	56.4 ± 9.9, $n = 38$	NS, $P = 0.23$
G2:	T2DM with no CVD	56.8 ±12.0, $n = 28$	G4:	Non-T2DM with no CVD	51.5 ± 5.3, $n = 19$	NS, $P = 0.07$
G1:	T2DM with CVD	62.5 ± 10.4, $n = 23$	G3:	Non-T2DM with CVD	61.5 ± 10.9, $n = 19$	NS, $P = 0.76$

Table 5-10 Mean LVM-A of patients with and without T2DM: PWV was compared for T2DM (G5, G2, G1) versus non-T2DM controls (G6, G4, G3), irrespective of presence of CVD. No significant difference was found (unpaired t-test, $P > 0.05$).

	T2DM Groups	LVM Abs (g)		Non-T2DM Group	LVM Abs (g)	*P*-value
G5:	All T2DM with and without CVD	119.1± 29.2 , n= 50	G6:	All non-T2DM with and without CVD	106.7 ± 23.3, n=38	**P*=0.04
G2:	T2DM with no CVD	114.1 ± 32.1, n=28	G4:	Non-T2DM with no CVD	95.9 ± 18.2, n=19	**P*=0.03
G1:	T2DM with CVD	125.4 ± 24.2, n=23	G3:	Non-T2DM with CVD	117.5 ± 23.2, n=19	NS, *P*=0.29

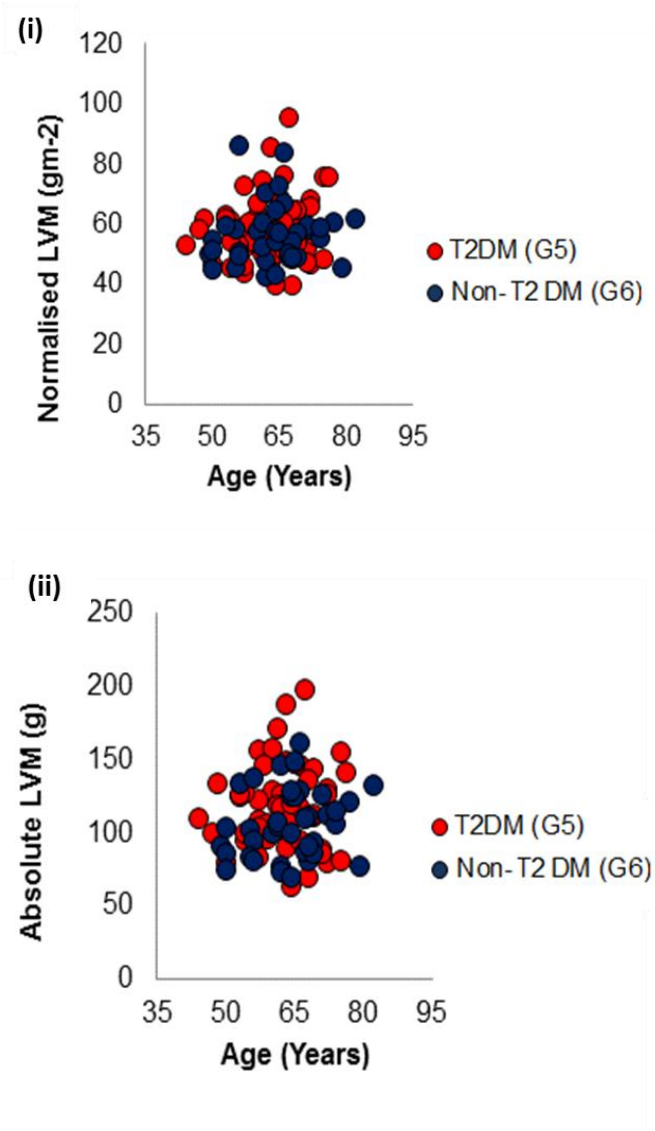

Figure 5-7 Scatter-plot of (i) normalised LVM, (ii) absolute LVM and T2DM: Mean LVM-N was not significantly different between T2DM and non-T2DM (unpaired t-test, $P > 0.05$). However a significant relationship was found between mean LVM-N (unpaired t-test, $P < 0.05$)

The rest of the LV parameters also did not show significant relationship between T2DM and non-T2DM population. EF (64.3 ± 10.0 vs. 64.7 ± 9.0%, $P = 0.74$), EDV (70.7 ± 12.9 vs. .72.4 ± 18.0 ml, $P = 0.21$) and SDV (25.6 ± 9.8 vs. 26.5 ± 14.3 ml, $P = 0.31$) and SV (45.1 ± 8.11 vs. 45.9 ± 8.2 ml, $P = 0.34$) were similar in both groups.

5.4.6 (iii) Aortic PWV and duration of T2DM

The duration of T2DM was defined from the date of clinical diagnoses. Duration of T2DM did not show a significant relationship with PWV (Pearson's correlation, $P = 0.80$). Likewise, when the duration was divided into tertiles (< 5 years, 6 – 10 years and < 11 years), no significant difference was seen with mean PWV (unpaired t-test, $P > 0.05$). Results are shown in Table 5-11 and in Figure 5-8.

Table 5-11 Aortic PWV and duration of T2DM with and without CVD: Duration of T2DM ranged from early onset >1 year to 14 years. For this analysis, T2DM duration was divided into 3 tertiles (< 5 years, 6 – 10 years and < 11 years). No significant difference was found between groups (unpaired t-test, $P > 0.05$).

Factors	G1: CVD and T2DM PWV ms^{-1}	G2: T2DM PWV ms^{-1}	*P*-value
< 5 years	8.85 ± 2.7, $n = 6$	7.10 ± 1.3, $n = 10$	NS, $P = 0.10$
6 – 10 years	8.89 ± 1.4, $n = 4$	8.07 ± 2.6, $n = 10$	NS, $P = 0.56$
> 11 years	7.75 ± 2.6, $n = 12$	7.57 ± 3.0, $n = 8$	NS, $P = 0.89$

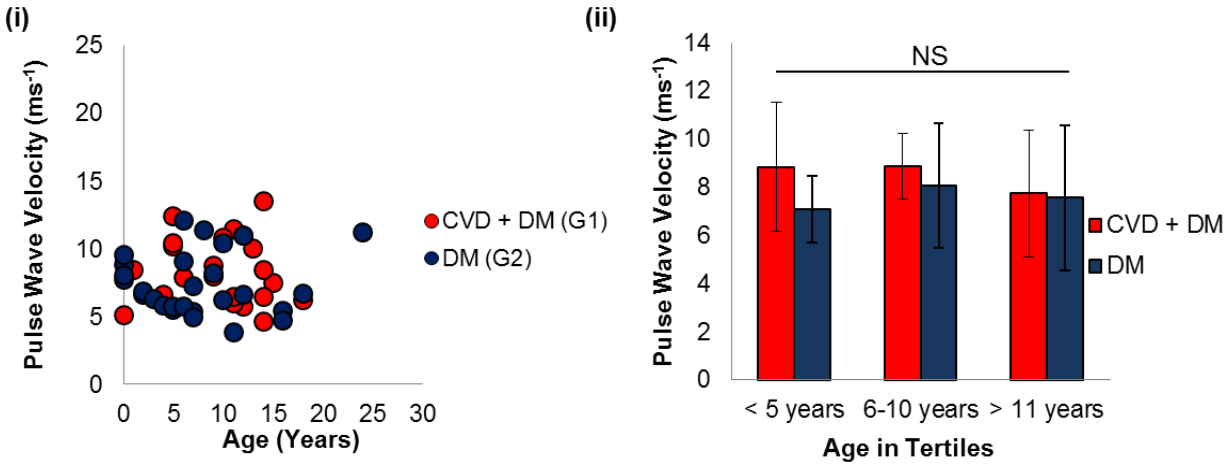

Figure 5-8 Aortic PWV for T2DM duration with and without CVD (i) years and (ii) tertiles: No significant mean difference was found between PWV and duration of T2DM, (unpaired t-test, $P > 0.05$).

5.4.6 (iv) Left Ventricular Function and duration of T2DM

Duration of T2DM also did not show a significant relationship with any of the LV parameters either absolute or normalised LVM (Pearson's correlation, P = NS). Likewise, when the duration was divided into tertiles, neither group (G1 and G2) showed any effect (t-test, $P > 0.05$), results are shown in Table 5-12 and Figure 5-9.

Table 5-12 LVM and duration of T2DM with and without CVD: Duration of T2DM ranged from early onset >1 year to 14 years. This table shows 3 tertiles (< 5 years, 6 – 10 years and > 11 years). No significant difference was found between groups (unpaired t-test, $P > 0.05$).

Factors	G1: CVD and T2DM LVM-N (gm^{-2})	G2: T2DM LVM-N (gm^{-2})	*P*-value
< 5 years	133.9 ± 37.2, $n = 6$	107.7 ± 30.4, $n = 10$	NS, $P = 0.15$
6 – 10 years	123.5 ± 16.1, $n = 4$	108.7 ± 31.0, $n = 10$	NS, $P = 0.39$
> 11 years	120.9 ± 20.0, $n = 12$	128.9 ± 34.8, $n = 8$	NS, $P = 0.49$

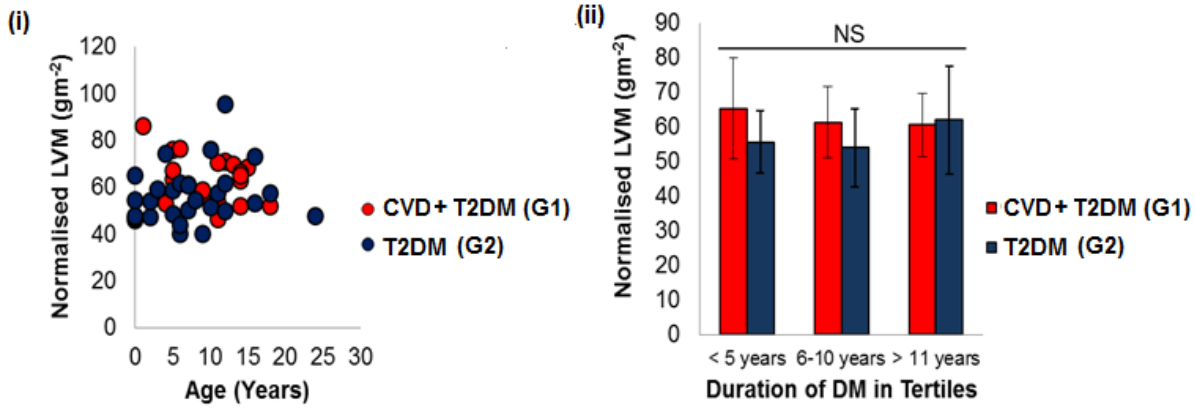

Figure 5-9 LVM-N for T2DM duration with and without CVD (i) years and (ii) tertiles: No significant mean difference was found between PWV and duration of T2DM, (unpaired t-test, $P > 0.05$)

5.4.6 (v) Aortic PWV and CVD

Overall, a significantly increased PWV was found in patients with CVD compared to controls (G7: 8.80 ± 3.19 vs. G8: 7.25 ± 2.2 ms^{-1}), (unpaired t-test, $P < 0.05$). Of the CVD group, patients with CHD and PVD show a significantly higher PWV than control participants, although it should be noted that PVD had a smaller sample size compared to CHD ($n = 6$ vs. $n = 32$). PWV in patients with stroke did not differ from controls (7.94 ± 1.54 vs. 7.25 ± 2.2 ms^{-1}, $P = 0.36$). The mean PWV in the CVD patient groups are displayed in Table 5-13.

Table 5-13 Aortic PWV in patients with CVD: Mean PWV for all CVD, CHD, PVD were found significantly higher than compared to non-CVD controls (unpaired t-test,*$P < 0.05$, **$P < 0.005$). PWV in stroke was not found to be significantly changed ($P > 0.05$).

Factors	CVD PWV ms^{-1}	Non-CVD PWV ms^{-1}	P-value
All CVD	8.80 ± 3.19, $n = 41$	7.25 ± 2.2, $n = 47$	*$P = 0.009$
CHD	8.88 ± 3.49, $n = 32$	7.25 ± 2.2, $n = 47$	*$P = 0.050$
PVD	10.68 ± 2.99, $n = 6$	7.25 ± 2.2, $n = 47$	*$P = 0.005$
Stroke	7.94 ± 1.54, $n = 8$	7.25 ± 2.2, $n = 47$	NS, $P = 0.360$

Abbreviations: PWV: Pulse Wave Velocity, CHD: Chronic Heart Disease, PVD: Peripheral Vascular Disease, NS: Not Significant

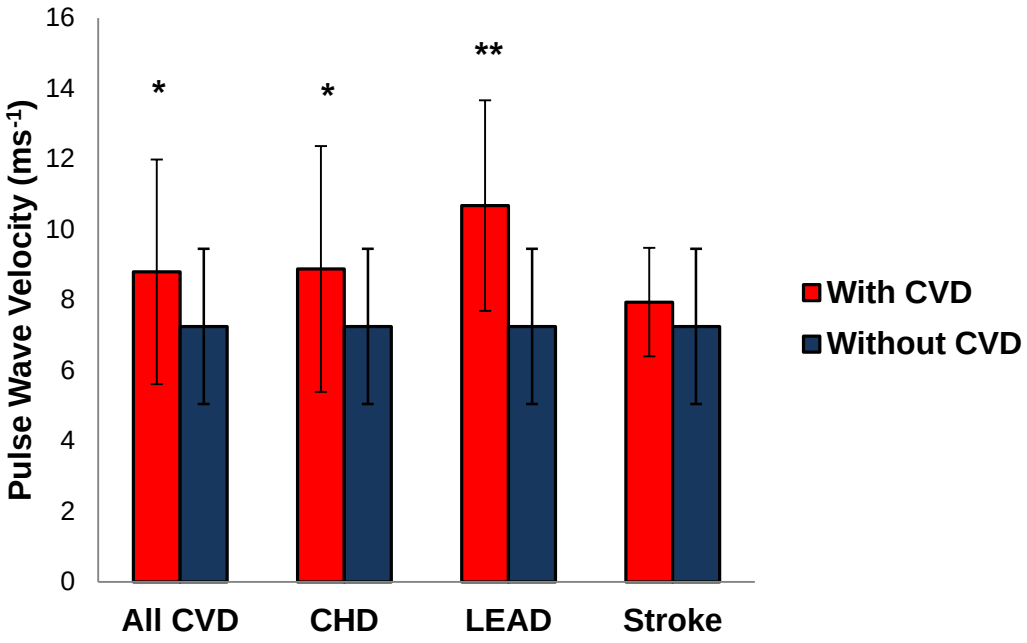

Figure 5-10 Aortic PWV in patients with CVD: Mean PWV for all CVD, CHD, PVD were found significantly higher than compared to non-CVD controls (unpaired t-test,*$P < 0.05$, **$P < 0.005$). PWV in stroke was not found to be significantly changed ($P > 0.05$)

5.4.6 (vi) Left Ventricle Function and CVD

For LV function, no significance was found with CVD and EF, EDV, ESV, and SV. LVM (both absolute and normalised) was found significantly higher in patients with CVD compared to controls without CVD, irrespective of T2DM (detailed for LVM-N in Table 5-14, and LVM-A in Table 5-15 and Figure 5-11).

For patients with CHD, LVM was significantly different as was EDV (G7 vs. G8; 148.2 ± 30.7 vs. 133.1 ± 27.9 ml $P = 0.03$), Figure 5-11. Patients with PVD and stroke, showed an elevated LVM, although they did not reach significance (ANOVA, $P = 0.08$, $P > 0.05$).

Table 5-14 LVM-N in patients with CVD: Mean LVM-N for all CVD and CHD were significantly higher than non-CVD controls (unpaired t-test, $^{**}P < 0.005$). LVM-N for PVD and stroke was not found to be significantly changed ($P > 0.05$).

Factors	CVD LVM-N gm^{-2}	Non-CVD LVM-N gm^{-2}	*P*-value
All CVD	61.9 ± 10.3, $n = 41$	54.7 ± 10.4, $n = 47$	$^{**}P = 0.001$
CHD	61.6 ± 10.2, $n = 32$	54.7 ± 10.4, $n = 47$	$^{**}P = 0.005$
PVD	62.6 ± 7.8, $n = 6$	54.7 ± 10.4, $n = 47$	NS, $P = 0.08$
Stroke	7.94 ± 1.54, $n = 8$	54.7 ± 10.4, $n = 47$	NS, $P = 0.06$

Abbreviations: CHD: Chronic Heart Disease, PVD: Peripheral Vascular Disease, NS: Not Significant

Table 5-15 LVM-A in patients with CVD: Mean LVM-A for CVD, CHD, PVD were significantly higher than non-CVD controls (unpaired t-test, $^{**}P < 0.005$). LVM-A for PVD and stroke was not found to be significantly changed ($P > 0.05$).

Factors	CVD LVM-N gm^{-2}	Non-CVD LVM-N gm^{-2}	*P*-value
All CVD	121.7 ± 10.3, $n = 41$	106.7 ± 29.1, $n = 47$	$^{*}P = 0.009$
CHD	121.5 ± 10.2, $n = 32$	106.7 ± 29.1, $n = 47$	$^{*}P = 0.016$
PVD	126.2 ± 26.9, $n = 6$	106.7 ± 29.1, $n = 47$	NS, $P = 0.13$
Stroke	118.8 ± 36.8, $n = 8$	106.7 ± 29.1, $n = 47$	NS, $P = 0.30$

Abbreviations: CHD: Chronic Heart Disease, PVD: Peripheral Vascular Disease, NS: Not Significant

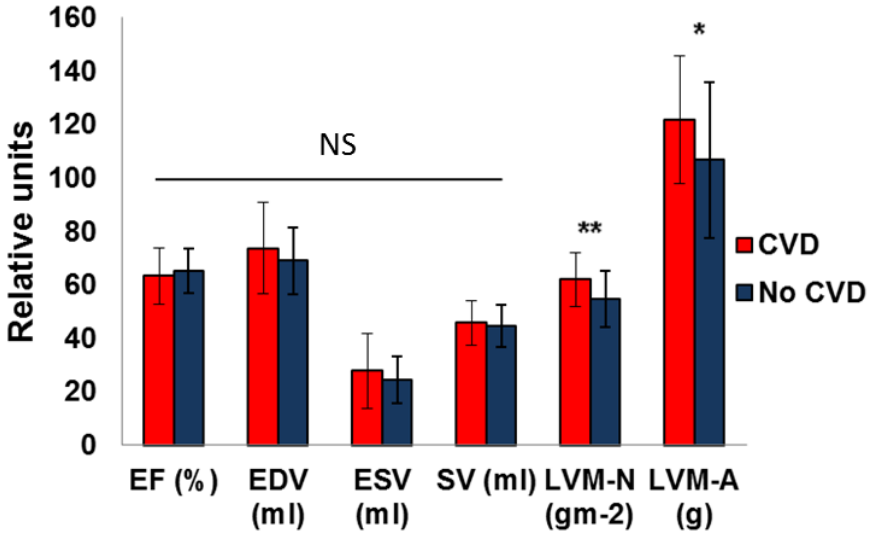

Figure 5-11 LV parameters with and without CVD: Mean differences were tested for all the LV parameters. A significant difference was found between LVM (ANOVA, *$P < 0.05$, ** $P < 0.005$).

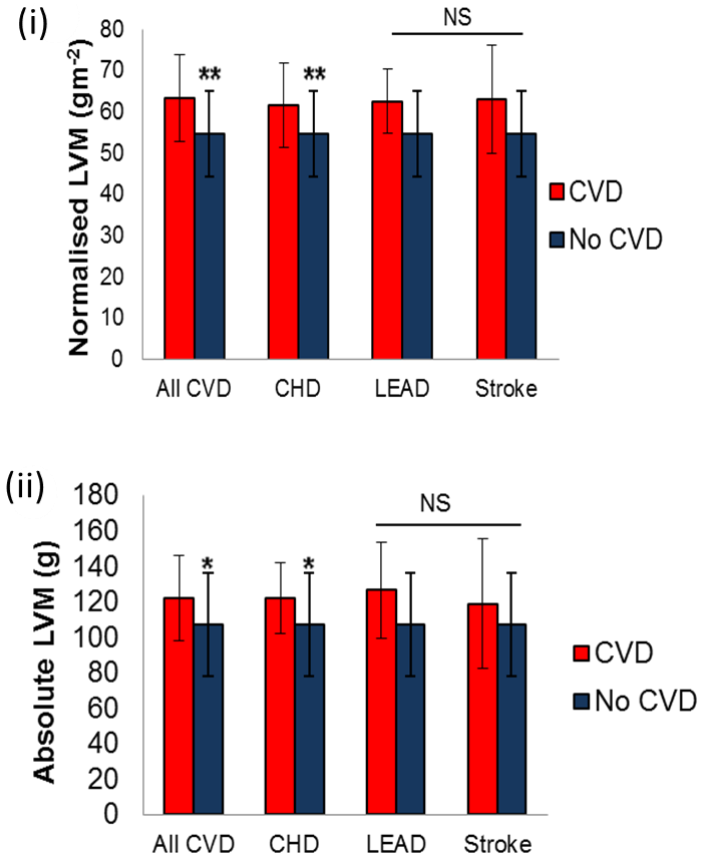

Figure 5-12 (i) Absolute and (ii) normalised LVM with and without CVD: Mean LVM was significantly increased for all CVD and CHD (ANOVA, *$P < 0.05$, ** $P < 0.005$).

5.4.7 SUMMIT Population Factors

Factors associated with Aortic PWV

Population factors associated with aortic PWV were evaluated by Pearson's correlation analysis (Table 5-16). Increased aortic PWV was associated positively with age, systolic BP and hypertension. No significant relationships were found between gender, waist to hip ratio, smoking, pulse pressure, and diastolic BP, height or BMI.

Table 5-16 Multiple correlation analysis of factors associated with aortic PWV: PWV was found to be significantly correlated with age, systolic BP and hypertension, (Pearson's correlation, $*P < 0.05$, $**P < 0.005$)

Factors	Pearson Correlation (ρ)	*P*-value
Age (years)	0.420	$**P < 0.001$
Gender (m/f)	0.726	NS, $P = 0.73$
Height (m)	-0.022	NS, $P = 0.84$
BMI (kgm^{-2})	-0.107	NS, $P = 0.33$
Waist to hip ratio	0.081	NS, $P = 0.46$
Smoking (y/n)	0.075	NS, $P = 0.11$
Pulse pressure (mmHg)	0.002	NS, $P=0.98$
Systolic BP	0.401	$**P < 0.001$
Diastolic BP	0.060	NS, $P = 0.57$
Hypertension	0.236	$*P = 0.036$

Factors Associated with Normalised LVM

Population factors associated with LVM-N were evaluated by Pearson's correlation analysis (Table 5-17). LVM-N was significantly positively associated with height, waist to hip ratio and hypertension. A significant negative correlation was found with gender, indicating that males have higher LVM-N than females. No significant relationships were found between age, smoking, systolic and diastolic BP. Interestingly, BMI was not found to be significant positive correlation in LVM-N compared to LVM-A. This may be the result of normalising the LVM-N with BSA.

Table 5-17 Multiple correlation analysis of factors associated with LVM-N: LVM-N was found to be significantly correlated with height, waist to hip ratio, hypertension and gender, (Pearson's correlation, $*P < 0.05$, $** P < 0.005$).

Factors	Pearson Correlation (ρ)	P-value
Age (years)	0.123	NS, $P = 0.26$
Gender (m/f)	-0.577	$**P < 0.001$
Height (m)	0.368	$**P < 0.001$
BMI (kgm^{-2})	0.059	NS, $P = 0.59$
Waist to hip ratio	0.385	$**P < 0.001$
Smoking (y/n)	0.140	NS, $P = 0.20$
Pulse pressure (mmHg)	-0.144	NS, $P = 0.19$
Systolic BP	0.196	NS, $P = 0.07$
Diastolic BP	0.068	NS, $P = 0.89$
Hypertension	0.363	$**P = 0.001$

Factors Associated with Absolute LVM

Population factors associated with LVM-A were evaluated by Pearson's correlation analysis (Table 5-18). LVM-A was significantly positively associated with height, BMI, waist to hip and hypertension. A significant negative correlation was found with gender, indicating that males have higher LVM than females. No significant relationships were seen with age, smoking, systolic and diastolic BP or pulse pressure.

Table 5-18 Multiple correlation analysis of factors associated with LVM-A: LVM-A was found to be significantly correlated with height, BMI, waist to hip hypertension and gender, (Pearson's correlations, $*P < 0.05$, $** P < 0.005$).

Factors	Pearson Correlation (ρ)	*P*-value
Age (years)	0.101	NS, $P = 0.35$
Gender (m/f)	-0.669	$**P < 0.001$
Height (m)	0.622	$**P < 0.001$
BMI (kgm^{-2})	0.276	$*P = 0.01$
Waist to hip ratio	0.523	$**P < 0.001$
Smoking (y/n)	0.072	NS, $P = 0.50$
Pulse pressure (mmHg)	-0.085	NS, $P = 0.44$
Systolic BP	0.142	NS, $P = 0.19$
Diastolic BP	0.027	NS, $P = 0.53$
Hypertension	0.336	$**P = 0.001$

5.4.7 (i) Age Related Variation in PWV

PWV has been shown to increase with vascular aging (Rose *et al*. 2010). A strong relationship between PWV and age was seen across all participants ($P < 0.001$). Although age has significant effect in all groups, it could be assumed that the effects of age on arterial stiffening is equal across all groups as no significant difference was found between groups regarding age (baseline characteristics, Table 5-4). Interestingly, a higher correlation was found in the patient groups (G1, G2 and G3) than the controls (G4) as displayed in Figure 5-13.

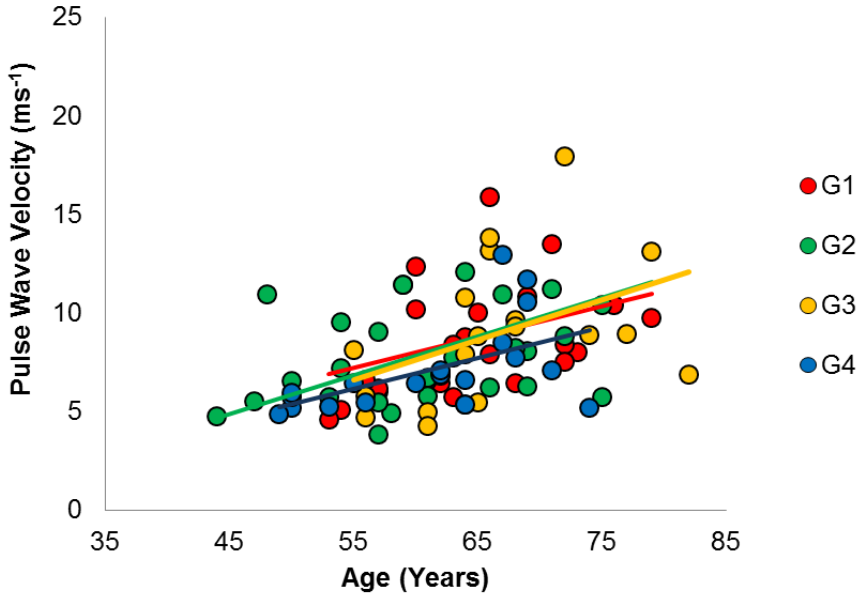

Figure 5-13 Regression analysis of aortic PWV and age: A significant correlation was seen between PWV and age (Pearson's correlation, $P < 0.001$).

5.4.7 (ii) Hypertension and Aortic PWV

The following Table 5-19 summarises PWV in hypertensive patients and normotensive individuals. Hypertensive was associated with a significantly raised PWV (unpaired t-test, $P = 0.03$). Although this relationship was not identified in the groups individually, (unpaired t-test, $P > 0.05$).

Table 5-19 Aortic PWV for hypertensive and normotensive participants: Aortic PWV was significantly elevated in hypertensive individuals compare to normotensives, (unpaired t-test, $P = 0.03$).

	Hypertensive	**Normotensive**	***P*-value**
All Groups	8.49 ± 3.1, *n*=53	7.17 ± 2.0, *n*=35	**P* = 0.03
CVD + T2DM (G1)	8.86 ± 2.9, *n*=18	7.61 ± 2.5, *n*=4	NS, *P* = 0.54
T2DM (G2)	7.61 ± 2.5, *n*=14	7.54 ± 2.2, *n*=14	NS, *P* = 0.94
CVD (G3)	9.15 ± 3.8, *n*=16	7.73 ± 2.1, *n*=3	NS, *P* = 0.55
Controls (G4)	7.59 ± 2.6, *n*=5	6.47 ± 1.46, *n*=14	NS, *P* = 0.25

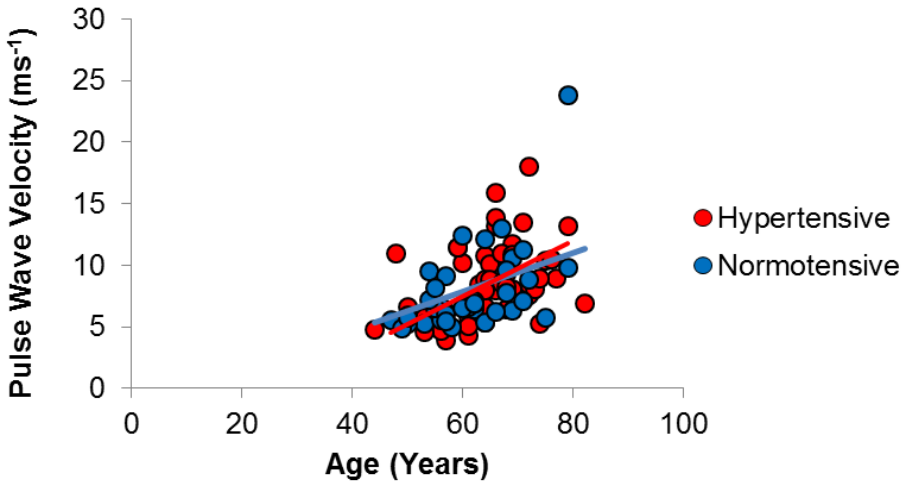

Figure 5-14 Regression analysis of aortic PWV and hypertension and normotensive participants.

5.4.7 (iii) Smoking Status and Aortic PWV

No significant relationship was found between smoking and PWV, (Pearson correlation, $P = 0.78$). Although not significant, PWV was found to be slightly higher in ex-smokers (8.20 ± 2.9, $n = 39$) and smokers (8.37 ± 3.9, $n = 8$) compared to non-smokers (7.81 ± 2.4, $n = 38$). The majority of non-smoking participants were in the T2DM and control group (G2, G4), the majority of ex-smokers were participants with CVD with and without T2DM (G1, G3). Out of all the groups, only 9% were current smokers.

5.4.7 (iv) Gender and Aortic PWV

Gender showed no significant relationship with aortic PWV, Pearson correlation, $P = 0.73$. Although, it was found to be highly significant factor for LVM (Pearson correlation, $P < 0.001$).

Table 5-20 Summary of key findings in Chapter 5

Investigation	Key Results
I. Summit Groups Analysis (5.4.1 – 5.4.5)	
Demographics and baseline characteristics	• No significant differences were seen regarding age, body weight, BMI, SBP, DBP, (ANOVA, $P > 0.05$). • Gender, BSA, waist circumference and hypertension differed significantly, (ANOVA, $P < 0.05$).
Aortic PWV between groups	• Mean PWV was found significantly differ between groups (ANOVA, $P < 0.05$). • Mean PWV of CVD groups (G1 and G3) were significantly greater than controls (G4), (post-hoc LSD test, $P < 0.05$).
LV function between groups	• No significant difference was seen between EF, EDV, ESV, SV between the 4 groups, (ANOVA, $P > 0.05$). • LVM was found to differ between the 4 groups (ANOVA, $P < 0.005$). • Mean LVM-N of CVD groups (G1 and G3) was significantly higher than controls (G4), (post-hoc LSD, $P < 0.005$), however no difference was found between either of the CVD groups (G1 vs. G3) or T2DM and controls (G2 vs. G4) (post-hoc LSD, $P > 0.05$). • Mean LVM-A was found to be increased in all the patient groups (G1, G2, and G3) than controls (G4), (post-hoc LSD, $P < 0.05$). There was no difference between patient groups, (post-hoc LSD, $P > 0.05$).
Aortic PWV and LV function	• No significant correlation was found between PWV and LV parameters (Pearson correlation, $P > 0.05$).

II. Reclassification of Groups for either Diabetes or Cardiovascular Disease (5.4.6)	
Aortic PWV with and without T2DM	• Mean PWV was not found to be significantly different with or without T2DM (G5 vs. G6), (unpaired t-test, $P > 0.05$).
LV Function with and without Diabetes	• Mean LVM-N was not found to be significantly different with or without T2DM (G5 vs. G6), (unpaired t-test, $P > 0.05$).
Aortic PWV and LVM and duration of T2DM	• No significant correlation was found between PWV and LV parameters with T2DM duration (Pearson correlation, $P > 0.05$).
Aortic PWV and CVD	• Mean PWV was found to be significantly different with or without CVD (unpaired t-test, $P < 0.05$).
Left Ventricle Function and CVD	• Mean LVM was found to be significantly different with or without CVD (unpaired t-test, $P < 0.05$).
III. Population factors (5.4.7)	
Factors associated with Aortic PWV	• PWV was associated positively with age, systolic BP and hypertension (Pearson correlation, $P < 0.05$). • No significant relationships were found between gender, waist to hip ratio, smoking, pulse pressure, and diastolic BP, height or BMI (Pearson correlation, $P > 0.05$).
Factors associated with LV Function	• For LVM-N, significant negative correlation was found with gender, indicating that males have higher LVM than females ($P < 0.05$), no significant relationships were found between age, smoking, systolic and diastolic BP ($P > 0.05$). • LVM-A was significantly positively associated with height, BMI, waist to hip and hypertension ($P > 0.05$), a significant negative correlation was found with gender, indicating that males have higher LVM than females ($P > 0.05$).

5.5 Discussion

In this study, aortic and cardiac function was evaluated by MRI in multiple cohorts of patients with and without T2DM, with and without the presence of CVD. Damage to the large arteries is a major contributor to high cardiovascular morality, with PWV proving to be a useful predicator of structural and functional changes of the arterial wall (Blacher *et al*, 2005). The primary finding highlights PWV as a stronger marker of CVD complications with and without T2DM, than merely just uncomplicated diabetes.

The present study differs to other MRI aortic PWV studies as it uses a heterogeneous complicated T2DM patient population with and without symptomatic CVD. In an uncomplicated T2DM group, a study by van der Meer *et al*. (2007) found PWV to be significantly increased in patients with diabetes as compared to healthy subjects. No significance was found in our study but this may be due to the variation in duration of diabetes (0 - 24 years) compared to their tighter selection criteria for diabetes duration (less than 5 years) and well-matched controls. However, we did see a significant increase in the CVD population with and without T2DM.

The quantitative parameters of LV function were found to be similar across the different patient groups apart from LVM. As expected, it was elevated in the two CVD groups in this this study, with and without T2DM. No relationship was found between aortic PWV and LV function; although in previous studies they have stated a negative relationship with diastolic function and increased PWV (van der Meer et al. 2007).

Delayed glycemic control and prolonged duration of diabetes perilously increase cardiovascular risk, with a direct relationship between the risk of developing cardiovascular complications and increasing hyperglycemia, especially for microvascular diseases (UKPDS 35 study, Stratton *et al*, 2000) . In our study, the duration of diabetes showed no association with PWV or cardiac function suggesting that CVD risk does not increase linearly with onset of diabetes. Although, it may be argued that the clinical baseline of patient diagnoses may not always be the beginning of the disease and it is difficult to factor the effect of different treatment regimens within the size of our current study group.

The patient groups were also analysed in terms of CVD (G1 and G3), which showed that irrespective of presence of diabetes, CHD and PVD have a positive relationship to PWV. No significance change was seen in stroke or T2DM. However, conclusive statements on the relationship between stroke and PVD and elevated PWV are limited due to the low sample size within each of these groups (n = 6 and n = 8, respectively). Further work in Chapter 7 will interrogate the interaction of PWV and PVD using multi-slice PWV.

It has been shown in normal volunteer studies that LV parameters can be influenced by age, BSA and gender. (Maceria *et al* 2006) In our study, the cardiac assessment, LVM and CO showed a significant relationship with PWV, while ESV, EDV and EF showed no correlation. These findings are comparable to previously study findings (Aquaro et al. 2013).

Vascular ageing results in dilatation and arterial stiffening due to elastin fibres weakening and mechanical stress over time. A linear relationship was found between ageing and PWV in a healthy population. In the patient groups, a linear relationship was also found but it was

significantly higher than the non-disease population. Interestingly, the T2DM cohort (G2) showed a similar relationship to PWV as the other two patient groups with CVD, (G1, G3). This may indicate that even though the T2DM cohort did not show significantly higher PWV than the healthy population, it may still have a slightly accelerated progression of arterial stiffness with age.

An overall increase in aortic stiffness was seen but it needs to be determined if stiffening can be specific to regional areas along the aorta. In a study by Hickson *et al*. (2010), age was shown to differentially affect regional aortic stiffness, with the greatest difference in the distal aorta in a healthy population. The PWV technique applied in this study is limited to only assessing three sites of the aorta; ascending aortic arch, descending aortic arch and the abdominal aorta. Therefore, we were unable to assess the effect of disease duration or progression with localised aortic stiffening. Another limitation due to the small cohorts, is the difficultly separating the effects of ageing on the vascular system from disease pathology.

Further development of this technique will involve application of a multi-site PWV technique, validated in a healthy population and applied to a patient population of PVD. This population was selected as it was underpowered in this study and there was greater availability of this patient group in comparison to CHD and stroke. Outcomes of these results are discussed in Chapters 6 and Chapter 7.

This study has shown that aortic PWV increases with hypertension and CVD. Although arterial stiffness is well established in T2DM and CVD, this study differed as the heterogeneous cohorts ranged from a healthy population, to patients with T2DM through to the later complicated T2DM and CVD.

Epidemiological studies highlight an increased cardiovascular risk in diabetic patients which is enhanced when in combination with other CVD risk factors such as hypertension, dyslipidemia, obesity and glucose intolerance. (Ong *et al*. 2007; Juutilainen *et al*. 2005) Hypertension is an established risk factor of CVD, and often shares a significant overlap with diabetes and systemic vascular diseases (Sowers *et al*. 2001). Regardless of diabetes, CVD or being a healthy participant, all patients with hypertension showed a significantly higher PWV than normotensive patients. The elevated aortic PWV correlates with both hypertensive status and presence of clinically apparent arterial disease, independent of one another and can support its importance as a maker of cardiovascular risk in hypertensive patients as seen in larger epidemiological studies (Blacher *et al*. 1999). Hypertension and diabetes are both associated with increased aortic PWV. However, the association of hypertension with diabetes may obscure the degree to which diabetes rather than hypertension contributes to an elevated PWV.

Conversely, smoking has been shown to exacerbate cardiovascular risk particularly in the case of PVD and CHD (Price 1999). In our cohorts, patients were divided into non-smokers, ex-smokers or current smokers but failed to show a significant correlation with PWV.

The pathological mechanism linking increased aortic stiffness to cardiovascular events is still relatively unclear. PWV leads to an early reflected wave return and higher systolic and lower diastolic central pressures contributing to the rise of left ventricular workload, subsequent hypertrophy and a decrease in coronary perfusion (Mitchell *et al*. 2010). Previous studies have established the prognostic value of this CVD marker by means of cross sectional and longitudinal studies such as Framingham and the Rio de Janerio (Cardoso *et al*. 2013).

We acknowledge some limitations to this study such as study design, cohort's size, age distribution and gender matching. The purpose of this study was to pilot and to gain an experimental insight of applying different MRI imaging markers in the quest to stratify between disease groups. As effect size was not estimated prior recruitment, it therefore insufficiently powered for subgroup analysis. This was particularly reflective in the patient CVD subgroup analysis of both the PVD and stroke group, and it is therefore difficult to make a definitive conclusion. Another limitation of MRI is the contraindications, cost and the timely acquisitions of MRI scans which consequently limits the size of the population in comparison to the more time efficient and cost effective CF-PWV technique.

PWV is a predictor of future fatal and non-fatal cardiovascular events in high risk diabetic patients over and beyond traditional cardiovascular risk factors including micro-macrovascular diabetes complications, metabolic control parameters and ambulatory BP levels (Cardoso *et al*. 2013). As this is a single time point cross sectional study, we are

unable to make comment on the prediction of future fatal and non-fatal CVD complications nor estimate a mortality index as previously performed in large population studies. A follow-up study would be interesting as a comparison for this population.

Otherwise, the strengths of our study were that it was the first to implement a comprehensive MRI protocol in a complicated T2DM patient population with and without symptomatic CVD. In this study, we investigated cardiac function alongside aortic PWV without the need of anatomical assumptions made in other PWV assessment methods. Most studies to date have employed ultrasound and applanation tonometry to assess PWV or vascular distensibility (Cruickshank 2002). As this study used MRI in assessing aortic stiffness, we were able to measure a local aortic PWV and make a direct measure of aortic path length. A local aortic PWV may also minimises influences of peripheral arteries, especially as it has been postulated, that diabetes has a preferential impact on central elastic arteries compared to muscular peripheral arteries (Kimoto *et al*. 2003).

5.6 Summary

PWV is a marker of arterial stiffness and aortic and cardiac function was defined in patients with and without T2DM and with and without CVD using a comprehensive CMR protocol. PWV was assessed using flow waveforms using MRI and was found to be significantly higher in CVD than T2DM.

Arterial stiffness, through its effect on the pulse wave and central aortic pressure, may be a key determinant of increased cardiovascular risk but was not found to be significantly elevated in patients with uncomplicated T2DM.

CHAPTER 6

Validation of Multi-Site PWV

6.1 Introduction

PC-MRI can interrogate blood velocity at multiple vessel regions within a single examination and provides a non-invasive method of estimating PWV along the entire aorta. The simplest method of deriving PWV from MR data is to determine the temporal shift between two flow waveforms, which can be achieved through-plane to the aorta, at two locations (typically the aortic arch and the descending aorta). This has been the most commonly used technique in the literature (Ibrahim *et al*. 2010; van der Meer *et al*. 2007; Westenberg *et al*. 2011) and has been applied in Chapters 4 and 5. For the purposes of this chapter, it will be referred to as conventional-PWV (C-PWV).

Recently, the use of more than two waveforms has been shown to result in higher PWV accuracy-than C-PWV, even at the expense of lower temporal resolution (Kröner *et al*. 2012). To date, the use of a multi-site PWV method (MS-PWV) has been limited a to healthy ageing population (Rogers *et al*. 2001; Hickson *et al*. 2010) and a population with Marfan syndrome (Kröner *et al*. 2012; Westenberg *et al*. 2011).

The aim of this chapter was to estimate MS-PWV from number of sample points along the aorta in a cohort of young healthy volunteers and to compare it with the C-PWV technique and to also test the scan to scan variability of MS-PWV.

6.2 Study Aims

The aims of the research presented in this chapter are:

i. To derive multi-slice PC-MRI data (with through-plane velocity encoding) to measure flow and PWV calculated over 6-8 different anatomical sites from the aortic arch to the renal bifurcation.
ii. To compare MS-PWV with the two slice C-PWV method.
iii. To determine scan to scan variation of MS-PWV by repeating the scan setup.

6.3 Methods

6.3.1 Demographics and Baseline Characteristics

For this study, a cohort of young healthy participants (YHV), under 40 years of age, were recruited (n = 22). They had a mean age of 29 ± 6 years and with 10 males and 12 females. All MR examinations were performed with setup as described in Chapter 3.

6.3.2 Image Acquisition and Analysis

The MRI study protocol for this study was designed to assess cardiac and aortic function via the C-PWV and MS-PWV method (full protocol Appendix A). The results of the LV cardiac function are later discussed in Chapter 7.

The protocol was divided into two parts (as detailed below). When Part I was completed the volunteer was asked to leave the MRI table for a short break and then returned for Part II. The second part only acquired MS-PWV for the purpose of testing scan to scan repeatability.

Part I:

i. Acquisition of the cine images acquired in 2 and 4 chamber orientations and a stack of cine images acquired in the short axis from base to apex to assess cardiac function.

ii. Aortic flow quantification with C-PWV at the aortic arch and just above the renal bifurcation for calculation of PWV.

iii. Multi-site aortic flow quantification (5 to 8 sites, depending on the length of the aorta) for calculation of MS-PWV.

Part II

i. Volunteer set-up with chest coil again, and multi-slice aortic flow quantifications are repeated as before with new set-up.

The scan parameters for the C-PWV are the same as described in Chapter 3.2. The multi-site acquisition was a breath-hold PC-MRI sequence, with lower temporal and spatial resolution than the C-PWV technique. Comparisons of the scan parameters for both PC-MRI sequences are detailed in Table 6-1.

Table 6-1 Phase contrast pulse sequence parameters for C-PWV and MS-PWV

Parameter (3.0T *Siemens*)	**Conventional 2-Slice PC**	**Multi-site PC**
Repetition time (ms)	14	22.85
Echo time (ms)	4.83	1.83
Field of view (mm)	350	350
Flip angle	20°	30°
Slice thickness (mm)	8	6
Resolution	256 x 256	144x192
No of segments	3	3
No of averages	1	1
Number of phases	128	128
VENC ($cm.sec^{-1}$)	150	150
Average scan time	240- 360 sec (4- 6 mins)	20-30 sec

Multiple images of the aorta were acquired in axial oblique orientation from the aortic arch (starting at the ascending aorta at the level of the pulmonary bifurcation) and ending at the descending aorta (immediately proximal to the renal arteries) using a consistent gap of 3cm as shown in

Figure 6-1 between slices. Image analysis was completed using the same software as the previous methodology described in Chapter 3.3.2. The transit-time was calculated for each of the flow waves at each location (Figure 6-2) and the slope of these interval times at

different regions, along with the distance between slices were used to calculate mean MS-PWV of the aorta.

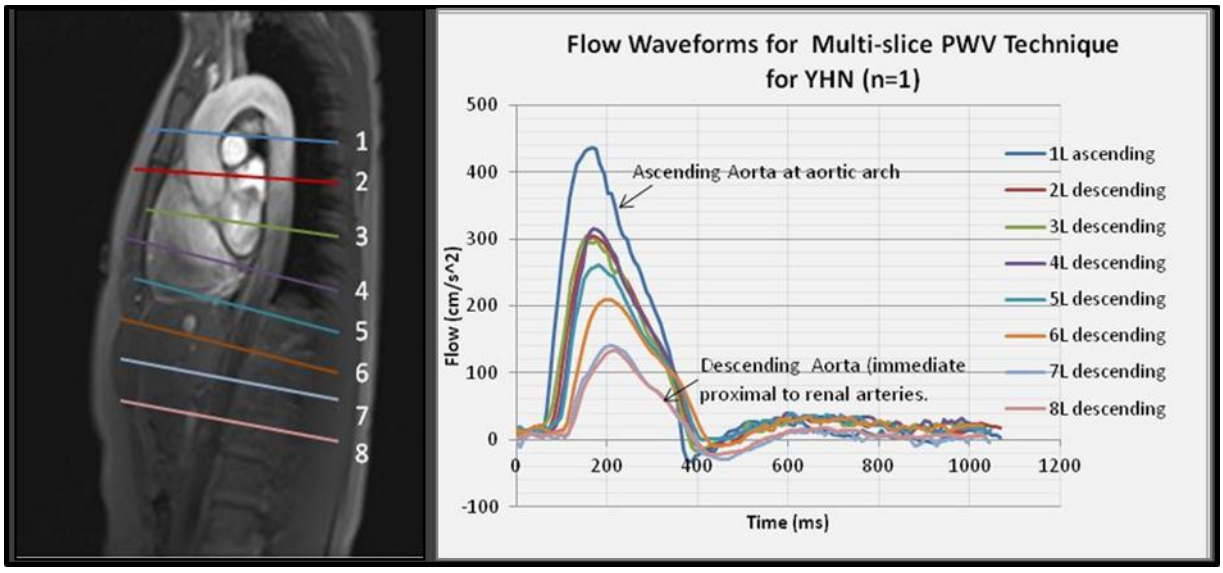

Figure 6-1 Multi-site PWV acquisition at different intervals along the aorta. Left Image is a FLASH 'Candy Stick' View of the aorta a right image is multi-slice waveforms for PWV assessment for a YHV

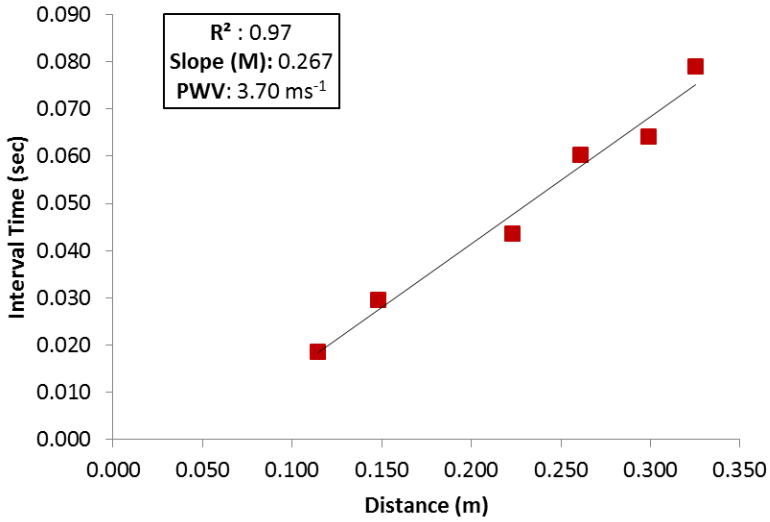

Figure 6-2 Interval times (sec) versus distance (m) of each slice position: The inverse slope of time and distance represents mean PWV (ms^{-1}) value.

6.3.3 Statistical Analysis

Between group differences were calculated using a paired t-test and repeated measures ANOVA. Significance was assumed at $P < 0.05$.

6.4 Results

6.4.1 Validation of C-PWV and MS-PWV

The mean aortic PWV for the YHV was found not to be significant different between C-PWV and MSPWV techniques (paired t-test, $P = 0.14$). These PWV ranges are displayed in Table 6-2 and Figure 6-3.

Table 6-2 Mean PWV results: C-PWV and MS-PWV on young healthy volunteers (YHV) and for a repeated MS-PWV scan on the same day**.**

	C-PWV (ms^{-1})	MS-PWV (ms^{-1})	Repeated MS-PWV (ms^{-1})
YHV	4.22 ± 0.6	4.52 ± 0.7	4.82 ± 0.8

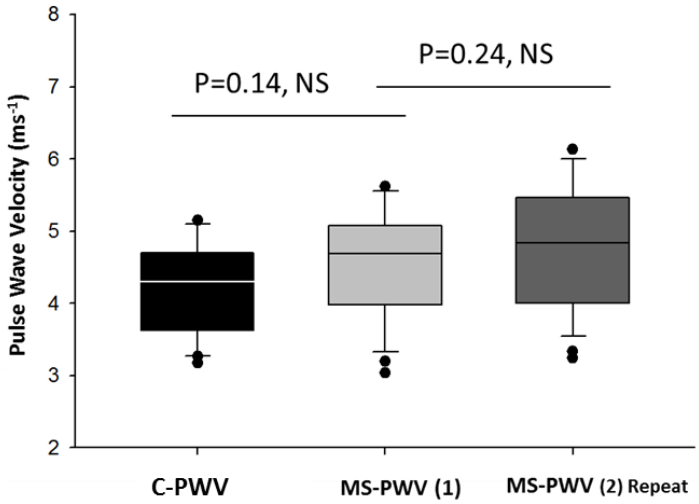

Figure 6-3 Means plot with SDs for both PWV techniques, C-PWV and MS-PWV (t-test, $P > 0.05$). A repeat scan was also performed with MS-PWV to test its scan to scan variation. No significant difference was found between the first MS-PWV and the repeat scan (t-test, $P > 0.05$)

6.4.2 Reproducibility of MS-PWV

Reproducibility of MS-PWV was examined by repeating the multi-site PC-MRI acquisition on the same day. No significant difference was seen between either acquisition (paired t-test, P =0.24). Bland-Altman and regression analysis were performed to investigate the difference between the techniques and linear relationship with each other (C-PWV and MS-PWV 1, and MS-PWV (1) and MS-PWV (2) as represented in Figure 6-4. A weak regression was seen between the C-PWV and MS-PWV (R^2 =0.04).

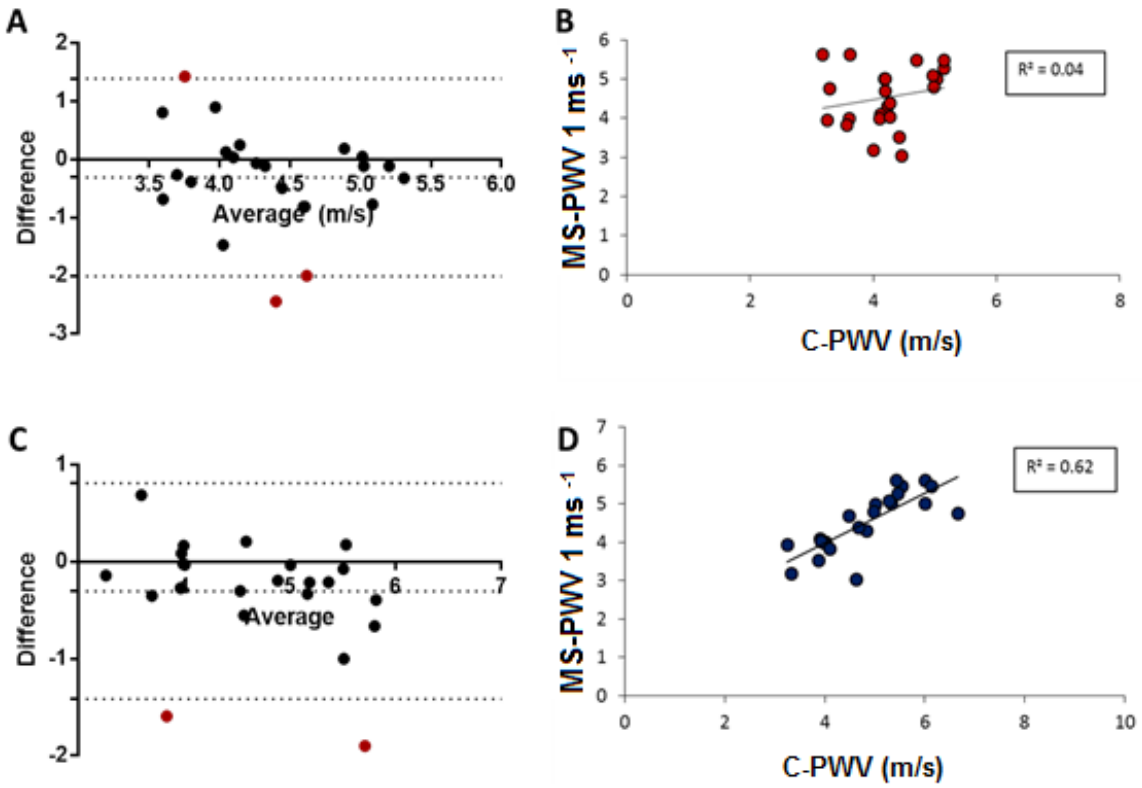

Figure 6-4 Bland-Altman (95% upper and lower confidence intervals) and regression analysis: Where **(**A), (B): comparing C-PWV and MS-PWV 1, and (C), (D): comparing MS-PWV 1 and MS-PWV 2.

6.5 Discussion

In this present study, the performance of MS-PWV, in comparison to the conventional MR-PWV method, was evaluated in a cohort of YHV. The main findings of this study were (i) no significant difference was seen between C-PWV and MS-PWV and (ii) MS-PWV was found to be repeatable on a scan to scan basis.

The mean PWV for both groups (C-PWV, MS-PWV) and (MS-PWV 1, MS-PWV2) were shown not to be significantly different. The mean C-PWV was slightly lower than the MS-PWV (4.22 versus 4.52 ms^{-1}, $P = 0.14$). There was high reproducibility seen with MS-PWV ($R^2 = 0.66$), and no significant change in mean PWV.

The C-PWV provides a higher temporal resolution while the multi-site technique provides increased spatial sampling density secondary to more sampling locations along the aorta. Kröner *et al*. (2012) showed by adding more than two slice locations along the aorta, increased the accuracy of PWV. The purpose of this study was to compare our MS-PWV with the C-PWV, already implemented in clinical research studies (SUMMIT) and to investigate if MS-PWV was a viable technique for use in a patient population with PVD (Chapter 7).

Reproducibility is an important factor for any new technique with research applications, particularly in the case of longitudinal studies. In this case, it is important to know if a patient is scanned on a different day with a different set-up, the potential error in set-up will not result in a false-positive change in aortic PWV. It has been previously shown that C-

PWV shows agreement with invasive pressure measurements and can be reproduced with high reproducibility (Grotenhuis *et al*. 2009; Ibrahim *et al*. 2010) and the results of this study show that MS-PWV is a repeatable technique.

The advantages of MS-PWV over a C-PWV include the improvement of PWV accuracy from multiple points along the aorta, its reduced acquisition time post-planning, average 12 minutes for C-PWV versus 4 minutes MS-PWV (6 - 8 acquisition with a 25 second breath-hold) and increased likelihood of earlier detection of heterogeneous processes such as atherosclerotic disease.

A limitation of this work was reproducibility of C-PWV was not evaluated with MS-PWV on the second scan. This was due to time restraints of having a long protocol. The total scan length for these volunteers was approximately 40 minutes for the first part of the scan and 15 minutes for the second part. Additionally, the volunteers were given time to leave the scanner table before the repeat set-up and localiser and planning sequences had to be repeated.

Even though MS-PWV has a shorter acquisition time in comparison to C-PWV; the analysis time of multiple image stacks was substantially increased. The lower temporal resolution also made the boundaries of the aortic wall more difficult to segment by the software so more manual adjustment is was necessary.

Another limitation is the lower temporal resolution of the MS-PWV sequence and the requirement for a breath-hold during sequence acquisition. We stated earlier in the initial validation work (Chapter 4), that lowering the temporal resolution reduces our reproducibility compared to a higher temporal resolution image. However, due to the acquisition of more sampling points, the error is reduced over multiple sites, although there was a slightly higher SD in the MS-PWV than the C-PWV in this healthy volunteer study.

6.6 Summary

In conclusion, this chapter investigated the use of a breath-hold multi-site approach to calculate PWV. MS-PWV was found comparable with C-PWV technique, even on a scan to scan basis. No apparent advantages were seen in this YHV population, but possibly with increased atheroma burden, a multi-site approach may offer provide better evaluation of aortic stiffening, thus allowing a more accurate PWV.

The following Chapter 7 will examine the MS-PWV in older population and patients with known PVD.

CHAPTER 7

Multi-Site Aortic PWV in Peripheral Vascular Disease

7.1 Introduction

As previously demonstrated in Chapter 7, CMR can interrogate multiple vessel regions within a single examination and provides a non-invasive method of estimating PWV along the entire aorta. MS-PWV technique was found to be repeatable and comparable with C-PWV in a young population. The aim of this chapter is to apply this MS-PWV technique to an older population and a patient cohort of PVD, to examine if a multi-site approach may be beneficial when there's an increased likelihood of disturbances to wave reflections and increased atheroma burden.

7.2 Study Aims

The aims of the research presented in this chapter are:

i. To estimate aortic PWV technique using a multi-site approach in a cohort of YHV, (< 40 years), an OPV (> 40 years) and a patient population with clinically diagnosed PVD.
ii. To further investigate aortic PWV ranges in relation to disease severity of PVD
iii. To investigate the relationship with LV function and disease severity of PVD

7.3 Methods

7.3.1 Demographics and Baseline Characteristics

For this study, a cohort of YHV, (as previously described in Chapter 7), OPV and a patient cohort with clinically diagnosed PVD were recruited (n = 70 in total). All MRI examinations were performed with setup as described in Chapter 3. A breakdown of the demographics of each of the groups is shown in Figure 7-1.

Table 7-1 Description of cohorts YHV, OPV and PVD

CMR data	YHV	OPV	PVD
Sample Size	22	22	26
Age	29 ± 6	61.1 ± 6	72 ± 7
Gender	10M:12F	10M: 12F	17M: 9F

The PVD patients were also classified into mild/moderate and severe after assessment of a peripheral angiogram by an experienced radiologist. This division of PVD severity is displayed in Table 7-2.

Table 7-2 Breakdown of PVD patients into disease severity for MS-PWV assessment

CMR data	Mild/ Moderate PVD	Severe PVD	ANOVA
Sample Size	17	9	NA
Age	63 ± 10	72 ± 7	NS, P=0.69
Gender	11M: 6F	6M: 3F	NA

7.3.2 Image Acquisition and Analysis

MRI study protocol was designed to assess cardiac and aortic function (as described in Chapter 3). Aortic PWV was estimated via the MS-PWV method and scan parameters are outlined in Chapter 6. The YHV results (MS-PWV and LV) from the previous chapter are continued in this chapter. OPV received full cardiac, WBA and MS-PWV assessment, as defined in Chapter 4.

PVD patients, as defined from clinical diagnosis, were recruited from an ongoing study and received a similar MRI protocol as SUMMIT study (Chapter 5), assessing LV function, WBA and MS-PWV.

7.3.3 Statistical Analysis

Descriptive statistics was used for the analysis of the demographic of the cohorts with data expressed as mean ± SD. Between group differences were calculated using an analysis of variance (ANOVA) test, with LSD post-hoc adjustment applied for multi-comparisons with both PWV and LV function. Significance was assumed at $P < 0.05$.

7.4 Results

7.4.1 MS-PWV between Groups

The calculated mean MRI PWV for the YHV cohort (4.5 ± 0.7 ms^{-1}) was significantly slower relative to the mean PWV for the OPV cohort (6.5 ± 1.5 ms^{-1}, $P = 0.003$) and the PVD cohort (8.6 ± 3.1 ms^{-1}, $P = 0.002$) as shown in Table 7-3. A box-plot of the MS-PWV from each of the cohorts is shown in Figure 7-1, ANOVA test with LSD correction applied.

Table 7-3 Aortic PWV between cohorts: Mean PWV was found to be significantly different between YHV, OHV, PVD (ANOVA, *$P < 0.001$).

CMR data	Group 1 YHV	Group 2 OPV	Group 3 PVD	ANOVA Sig.
PWV (ms^{-1})	4.5 ± 0.7, n=22	6.5 ± 1.5, n=22	8.6 ± 3.1, n=26	*$P < 0.001$

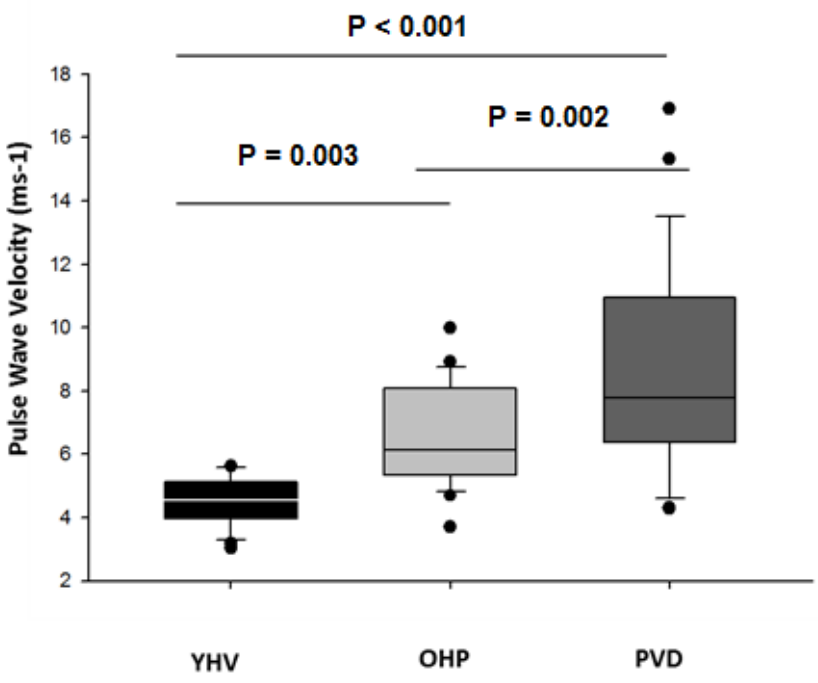

Figure 7-1 Box-plot of aortic PWV between cohorts: Mean PWV was found to be significantly different between YHV, OHV, PVD (ANOVA, $P < 0.001$).

7.4.2 MS-PWV and Peripheral Vascular Disease

PVD patients were divided into clinical severity as verified by MRA of the peripheral vasculature. Mean PWV was significantly slower in both the mild/moderate PVD patients compared to the severe PVD group (7.6 ms^{-1} versus 10.8 ms^{-1}, P = 0.02). The division of the groups can be seen in Table 7-4.

Table 7-4 Aortic PWV and PVD severity: Mean PWV was found to be significantly different between different classifications of PVD (ANOVA, *P = 0.02).

CMR data	Mild/ Moderate PVD	Severe PVD	ANOVA Sig.
PWV (ms^{-1})	7.6 ± 2.5, n = 17	10.8 ± 3.4, n = 9	*P = 0.02

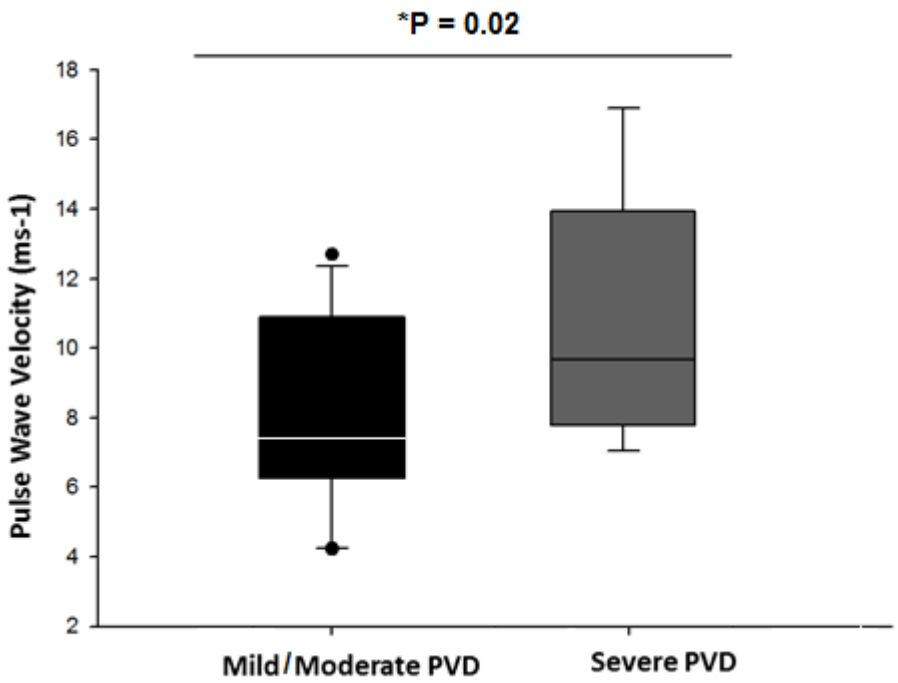

Figure 7-2 Box-plot of Aortic PWV and PVD severity: Mean PWV was found to be significantly different between mild/moderate versus severe PVD (ANOVA, *P = 0.02).

7.4.3 Left Ventricle Function between Groups

The LV analysis was completed for all YHV and OPV. Four patients from PVD group were excluded from the analysis due to poor image quality (n = 3) and uncompleted scan (n = 1). The results for the final participants are shown in the Table 7-5 below.

The means and SD are presented in Table 7-5 for each of the LV parameters. The ANOVA revealed a significant difference between the SV (P = 0.002). LSD post-hoc analysis revealed that for SV was significantly lower in PVD than in YHV and OPV (P = 0.001 and P = 0.013 respectively).

EDV also showed a trend towards significance (P = 0.06), with LSD post-hoc analysis revealing that EDV was significantly higher in YHV in comparison to PVD patients (P = 0.02).

Table 7-5 LV function between groups: Mean PWV was found to be significantly different between different classifications of PVD (ANOVA, *P < 0.05).

CMR data	YHV (n = 22)	OPV (n = 22)	PVD (n=22)	ANOVA Sig.
EF (%)	66.1 ± 6.1	65.5 ± 6.8	64.8 ± 8.6	NS, P = 0.86
EDV-N (ml)	80.5 ± 8.6	77.6 ± 13.7	71.1 ± 14.0	NS, P = 0.06
ESV-N (ml)	27.3 ±6.3	27.2 ± 8.3	26.2 ± 11.3	NS, P = 0.90
SV-N (ml)	53.2 ± 7.4	50.4 ± 7.9	44.9 ± 5.8	* P = 0.002
LVM-N (gm^{-2})	61.6 ± 10.7	56.3 ± 11.1	61.8 ± 9.7	NS, P = 0.16

Abbreviations: EDV-N: Normalised End Diastolic Volume, ESV-N: Normalised End Systolic Volume, SV-N: Normalised Stroke Volume, LVM-N: Normalised Left Ventricular Mass.

7.4.4 LV Function and Peripheral Vascular Disease

The LV analysis was also divided into grades of severity. The results for the PVD patients are shown in the Table 7-6 below. The means and SDs are presented in Table 7-6 for each of the LV parameters. The ANOVA revealed no significant difference between the different severity grades of PVD ($P > 0.05$).

Table 7-6 LV function and PVD severity: Mean PWV was found to not to be significantly different between different classifications of PVD (ANOVA, $P > 0.05$).

CMR data	Mild/ Moderate PVD (*n* = 17)	Severe PVD (*n* = 6)	ANOVA Sig.
EF (%)	64.8 ± 8.8	62.8 ± 8.6	NS, $P = 0.59$
EDV-N (ml)	71.8 ± 9.4	68.3 ± 12.8	NS, $P = 0.85$
ESV-N (ml)	26.8 ± 12.2	26.5 ± 11.4	NS, $P = 0.93$
SV-N (ml)	44.9 ± 5.8	41.8 ± 6.9	NS, $P = 0.18$
LVM-N (gm^{-2})	61.4 ± 9.2	61.0 ± 12.9	NS, $P = 0.72$

Abbreviations: EDV-N: Normalised End Diastolic Volume, ESV-N: Normalised End Systolic Volume, SV-N: Normalised Stroke Volume, LVM-N: Normalised Left Ventricular Mass.

7.5 Discussion

Following on from the previous study, this study evaluated MS-PWV in three different cohorts; YHV, OPV and PVD. The main findings of this study show (i) mean MS-PWV was significantly different across the three cohorts, YHV, OPV and PVD, (ii) MS-PWV correlated with age and PVD disease severity and (iii) stroke volume was reduced in PVD compared to YHV and OPV.

Both degenerative stiffness and arteriosclerosis of the arterial beds tend to coexist resulting in a progressive, diffuse and age-related disease process of vascular beds (Cavalcante *et al*. 2011). As previously mentioned in 1.1, the origins of the SMCs of the basal, ascending and the descending aorta have been shown to have regional diversity. This may contribute to the susceptibility of site-localisation of vascular disease, and promote heterogeneous arterial stiffness (Cheung et al. 2012).

The mean PWV differed between the YHV, OPV, and with PVD (4.5 ms^{-1}, 6.5 ms^{-1} and 8.6 ms^{-1}, $P < 0.001$) indicating that age and disease was a distinguishable factor. The PVD patients were divided into three groups by disease severity after MR angiographic data of the peripheral vessels. In terms of disease severity, MS-PWV showed diagnostic capability to differentiate between mild/ moderate PVD from severe PVD burden (7.6 ms^{-1} versus 10.8 ms^{-1}, $P = 0.02$). However, it was unable to distinguish mild/ moderate burden, as the mild PVD phenotype in this group, and the extent of the disease heterogeneity in this group (4.5 $ms^{-1}$and 6.5 ms^{-1}, $P > 0.05$).

As this was a novel exploration, and there are no prior MR-PWV values for a PVD cohort, the MS-PWV technique was compared to LV function, an established clinical reference. In the PVD cohort, this study showed a marked decrease in SV and increase in EDV compared to the healthy participants. Interestingly, no significant changes in LVM were evident between PVD or in relation to increasing severity and overall burden. This may suggest that even though these patients had elevated arterial stiffness, structural remodelling of the LV had not significantly changed. This may suggest that there may be potential role for aortic PWV within this population, evaluating overall cardiovascular burden before the onset of cardiac dysfunction.

Limitations of Study

A limitation of the study is the absence of an age matched control groups. The OPV were participants in the TASCFORCE study (as described in *Preface*), and the mean age was lower than the PVD cohort. Ideally, this group would have been age and gender matched to the patent population. Secondly, this study included the use of a breath-hold PC-MRI acquisition. However, some PVD patients found it difficult to hold their breath in comparison to the YHV and OPV, resulting in breathing artefacts on several image sets. It also should be noted that PVD patients are more commonly classified using the ankle brachial index (ABI). As we did not have this data, we used peripheral angiograms and clinical report to classify the patients, which may be more subjective than ABI.

Finally, in this study we estimated the mean PWV over the entire aorta using different sites. As this was a multi-site acquisition, we could of also investigated PWV in different aortic

regions such as the ascending, distal or proximal aorta. This would have provided analysis of how arterial stiffness varies over the aorta in both a healthy population and a PVD cohort. This work will be further expanded in future work for this cohort.

7.6 Conclusion

In conclusion, this study utilised a MS-PWV technique in an ageing and PVD population. Atherosclerosis is a heterogeneous pathophysiological process occurring in various focal points and different vascular beds; to which arterial stiffening may also vary along the aortic length. Sampling from multiple points along the aorta may provide a more sensitive measure of aortic stiffness, particularly in the earlier stages of disease.

CHAPTER 8

Discussion and Further Work

8.1 Aim of Thesis

The aim of this thesis was to examine the use of MR-PWV (i) to investigate whether PWV can be used as a surrogate MRI marker of macrovascular disease in a heterogeneous population with and without CVD, and (ii) whether these markers can provide greater risk prediction of CVD risk compared to established MRI parameters of ventricular function.

8.2 Key Findings

In summary, the studies in this thesis show that MR-PWV is affected by both the extent and severity of atherosclerotic burden and CVD.

- MR-PWV when applied to a complicated T2DM population with and without symptomatic CVD; PWV yields an important distinction between the CVD groups which was not apparent with other parameters including LVM. In contrast, PWV was unable to distinguish between T2DM populations before the onset of symptomatic CVD.
- A developed technique, MS-PWV, has shown to be comparable with the C-PWV technique in a cohort of YHV.
- In cohorts of YHV, OPV and PVD, MS-PWV found a significant difference in mean PWV in a between an ageing population and patients with symptomatic PVD.

- Using MRA, PVD was classified into a score system where the degree of severity was attributed; mild, moderate and severe, MS-PWV was significantly higher in severe PVD compared to mild or moderate PVD. However, it was unable to distinguish between mild onset and moderate PVD burden.

This thesis provides a novel insight into the process of arterial stiffening though a non-invasive MRI assessment of arterial stiffness and subsequent cardiovascular health throughout different disease cohorts. It differs from current published work by examining MR-PWV in a heterogeneous T2DM and CVD population, whilst previous studies have examined either T2DM or CVD patients in isolation.

Secondly, a multi-site arterial assessment approach was used to determine aortic PWV in a PVD population, a novel application. Modification of the conventional MR-PWV imaging protocols allowed to account for site variation along the aorta, a known phenomenon of atherosclerosis.

8.2.1 Clinical Implications of MRI Derived Aortic PWV

In order to become a useful CVD screening tool, MR-PWV ideally needs to be able to predicate major macro and microvascular disease in asymptomatic patients, where such values supplement existing risk scores models (Greenland *et al*. 2010). The techniques discussed in this thesis have shown value in detecting symptomatic CVD. However, it cannot be determined if MR-PWV has the potential to be implemented as a screening tool for asymptomatic population without sufficient longitudinal data.

To this need, new evidence is beginning to emerge from larger studies such as the multi-ethnic study of atherosclerosis (MESA). This is the first longitudinal study to used MR-

PWV as a screening tool, covering a 10 year period with 226 participants (Liu *et al*. 2012). Also, an even larger subgroup of the Dallas Heart Study (DHS), consisting of 2122 participants underwent CMR measures of arterial stiffness, to which it was found to have an association with adverse cardiovascular events (Maroules *et al*. 2014).

In conclusion, taken together with the high cost, and limited availability, MR-PWV is mainly confined to a research setting, and may not be applicable for routine CVD risk monitoring in the population. For MR-PWV to gain clinical diagnostic value, it is necessary for it to gain increasing evidence in larger, longitudinal studies and thus providing a definable prognostic range for normal and abnormal arterial stiffness. Alternatively, it may serve as a suitable target for pharmaceutical interventions studies such as the lipid lowering drugs statins. In the meantime, what remains to be shown is whether vascular stiffness has potential to be a therapeutic target. It can be argued, results from MESA and DHS and forthcoming studies may provide the evidence base behind the widespread adaptation and value of this technique.

8.3 Limitations

Commercial Software for Estimating PWV

A major limitation inhibiting the routine use of MR-PWV, is the lack of a PWV commercially software package. The majority of the studies to date have either used a flow quantification software analysis programme, estimating transit times manually or an ‘in-house’ developed software. The second difficulty is defining a ‘standardised’ approach for image acquisition for calculating PWV. This thesis has only investigated through-plane 2D PC-MRI, however recent work from Leiden University have derived PWV from an in-

plane PC-MRI acquisition, stating that it showed a stronger correlation with invasive pressure measurements (Westenberg *et al*. 2012).

Research based MRI Sequences

The studies within this thesis were confined to using 2D PC-MRI for flow quantification as we were restricted to commercial sequences that were readily available in on the scanner. However, there are a plethora of other MRI techniques that could have been applied such as Fourier velocity encoding (FVE) motion-mode (M-mode) imaging and 4D PC-MRI methods (Markl *et al*. 2010).

For instance, the advantage of using FVE M-mode imaging is its high temporal resolution (~ 3 to 5 ms, in comparison to 2D-PC-MRI at ~ 10 – 30 ms). It is acquired through a pencil-beam acquisition and is therefore restricted to research sites as its not commercially available technique (Taviani *et al*. 2010).

Availability and Resources

Although, good accuracy and direct aortic flow measures are achievable with MR-PWV, it presents other difficulties in a clinical setting. MRI scans are generally associated with high cost, poor accessibility and have many restrictions on patient's eligibility (e.g. pacemakers, metal implants). Therefore, predominately restricting arterial stiffness derived by MRI to a research setting.

8.4 Future Work

In Chapter 5, we determined MR-PWV for different cohorts of patients with and without CVD as part of a multi-centre SUMMIT study. This same cohort of patients also received vascular function tests in the vascular and inflammatory unit, including CF-PWV. Preliminary analysis was performed between both PWV techniques and interestingly showed good correlation in healthy control cohorts, but weaker correlation in the CVD patients. One hypothesis for this difference may potentially be due to the error in distance measurement between the two sites. With ageing, the aorta is thought to become elongated and more tortuous (Sugawara *et al*. 2008). Additionally, in the case of vessel occlusion, there is an increase likelihood of collateral vessels that shunt blood supply around a blockage in the CVD cohorts. Both of these factors may in theory contribute to extended distance between the carotid and femoral sites, not accountable with the traditional tape measure approximation. With the aid of whole body MRA, these vessels are easily identifiable and correspondingly, a definite distance between the sites can be defined. Further analysis will include estimating this distance discrepancy and examining its outcome to the overall CF-PWV value.

Other Haemodynamic Factors

As discussed previously, haemodynamic factors are a strong predictor of the early stages of disease progression. This thesis focused on estimation of PWV through the analysis of flow quantification at various sites along the aorta. While this is a clinically validated measurement, there may be further data of diagnostic value currently uncovered, for example flow patterns, forward and backward flow and wave reflections that may provide

further insight into the pathophysiological processes of altered PWV. It would be interesting if we could further understand these wave characteristics and investigate the relevance to disease pathology.

General Developments in Flow MRI

Emerging techniques such as 4D flow, in which spatial encoding is combined with 3D velocity encoded PC-MRI, is still developing in the field of MR research (Markl, Frydrychowicz, *et al*. 2012). It provides a comprehensive analysis of blood flow dynamics using a full volumetric region of interest and is not confined to standardising slice placement in patients with tortuous vessels, and allows multiple waveforms to be sampled at the same time (Figure 8-1). Likewise, it provides the opportunity of deriving other clinically interesting haemodynamic parameters, including WSS, pressure gradients across stenosis and other flow related parameters (Goubergrits *et al*. 2014; Markl, Wallis, *et al*. 2012). In the future, these techniques may evolve into additional diagnostic information that may contribute to earlier detection of disease or assist with surgical planning decisions.

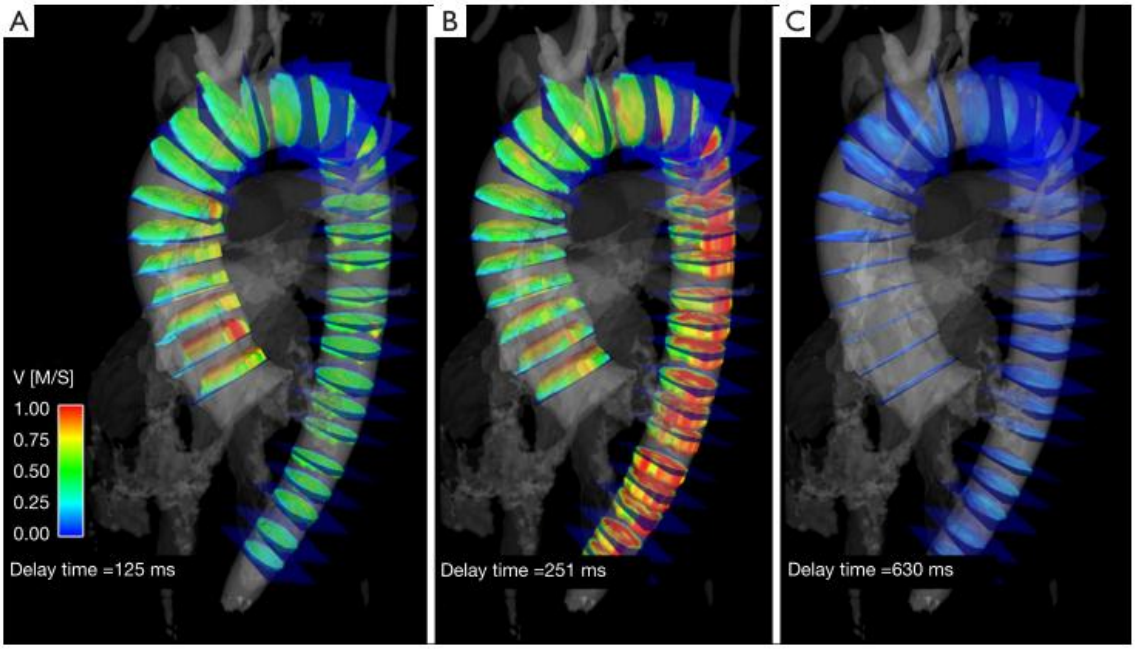

Figure 8-1 4D phase contrast MRI: The assessment of PWV of a healthy volunteer is shown in 3 out of 20 cardiac phases with delay time 125 ms, 251 ms and 630 ms. The velocity data is highlighted using velocity vectors and overlaid on the anatomical data (greyscale). As reproduced from (Wentland *et al*. 2014).

8.5 Conclusion

Aortic PWV, as derived from MRI is associated with both the extent and severity of atherosclerosis and CVD. PWV was able to distinguish symptomatic CVD, which was not apparent in cardiac function parameters. In order for MR-PWV to be used as a screening tool, it needs to be able to predicate major macro and micro-vascular disease in asymptomatic patients. Future work from risk prediction and longitudinal studies is necessary to evaluate the prognostic value of MR-PWV.

APPENDIX A

MRI Study Protocols

(i) Summit Study MRI protocol

		tfl_loc_multi_@c_CARDIAC LOC		00:18
		tfl_loc_2-chamber_iPAT		00:02
		tfl_loc_4-chamber_iPAT		00:02
		tfl_loc_short-axis_iPAT		00:10
		trufi_freqScout_ES3.4_4CH		00:10
		tf2d14_retro_iPAT_ES3.4_4CH		00:12
		tf2d14_retro_iPAT_ES3.4_2CH		00:12
		tf2d14_retro_iPAT_ES3.2_SA_Multi ...		00:12
		psir_FLASH_single-shot_2CH		00:06
		psir_FLASH_single-shot_4CH		00:06
		----- Left Atrial Assessment -----		
		tf2d14_retro_iPAT_ES3.2_LA_5mm		00:18
		NEW_T2STAR_256_2ph_9seg_TD1...		00:14
		deselect injection icon		
		-----Whole body angio second part-----		
		lll_fl3d-cor_legs_pre		00:16
		ll_fl3d-cor_abdomen_pre		00:14
		inject gad		
		l_care_bolus_cor	46	01:30
		ll_fl3d-cor_abdomen_post	46	00:14
		lll_fl3d-cor_legs_post	45	00:16
		----- Axial HASTE -----		
		t2_haste_tra_p2_mbh_320		01:18
		fl2d8_retro_iPAT_candystick		00:11
		-----Flow quant for pulse wave velocity--...		
		fl5_150_tp_retro_bh_TEST		00:15
		-----1ST BP-----		
		Cine_PC_AX_venc150_Pulm_Bifurc_...		06:42
		-----2ND BP-----		
		Cine_PC_AX_venc150_Abdo_Renals		06:42
		-----3RD BP-----		
		-----Final TI Scout-----		
		TI-Scout_SA_final		00:18
		-----Extra Sequences-----		
		T2star_GRE_SA_iPAT2		00:09
		T2star_GRE_SA_iPAT2_High_Res		00:12
		fl2d8_retro_iPAT_LA_4mm		00:22
		T2star_GRE_SA_iPAT2_multi-ph		00:12

(ii) Healthy Volunteer Multi-site PWV MRI Protocol

	tfl_loc_multi_iPAT3	00:14
	tfl_loc_2-chamber_iPAT	00:02
	tfl_loc_4-chamber_iPAT	00:02
	tfl_loc_short-axis_iPAT	00:10
	trufi_freqScout_ES3.4_4CH	00:11
	tf2d14_retro_iPAT_ES3.4_4CH	00:12
	tf2d14_retro_iPAT_ES3.4_2CH	00:12
	tf2d14_retro_iPAT_ES3.2_SA_Multi ...	00:12
	NEW_T2STAR_256_2ph_9seg_TD1...	00:11
	t2_haste_tra_p2_mbh_320	00:52
	t2_haste_CORp2_mbh_320	00:52
	fl2d8_retro_iPAT_candystick	00:12
	fl2d8_retro_COR_candystick	00:12
	Cine_PC_AX_venc150_Pulm_Bifurc_...	03:35
	Cine_PC_AX_venc150_Abdo_Renals 1ST BP	03:34
	Cine_PC_AX_venc150_3_SEG_Aorta 2ND BP	00:14
	tse_9_db_t1_iPAT	00:11

(iii) Older Healthy Population (TASCFORCE) MRI Protocol

(iv) Peripheral Vascular Disease Study MRI Protocol

		Position 230mm above feet		
		l_flash_feet		00:13
		ll_flash_legs		00:13
		lll_flash_abdomen		00:11
		l_fl3d-cor_feet_pre		00:20
		ll_fl3d-cor_legs_pre		00:15
		lll_fl3d-cor_abdomen_pre		00:13
		inject gad		
		lll_care_bolus_cor	7	01:30
		lll_fl3d-cor_abdomen_post	7	00:13
		ll_fl3d-cor_legs_post	6	00:15
		l_fl3d-cor_feet_post	5	01:01
		tfl_loc_multi_@c_CARDIAC LOC		00:15
		tfl_loc_2-chamber_iPAT		00:01
		tfl_loc_4-chamber_iPAT		00:01
		tfl_loc_short-axis_iPAT		00:08
		trufi_freqScout_ES3.4_4CH		00:10
		tf2d14_retro_iPAT_ES3.4_4CH		00:04
		tf2d14_retro_iPAT_ES3.4_2CH		00:04
		tf2d14_retro_iPAT_ES3.2_SA_Multi ...		00:04
		NEW_T2STAR_256_2ph_9seg_TD1...		00:11
		t2_haste_tra_p2_mbh_320		01:18
		fl2d8_retro_iPAT_candystick		00:04
		fl2d8_retro_COR_candystick		00:04
		1ST BP		
		Cine_PC_AX_venc150_3_SEG_Aorta		00:08

APPENDIX B

Conference Presentations

- **DB Cassidy,** SJ Gandy, F Khan, P Martin, RS Nicholas, JG Houston, 'Can Magnetic Resonance Pulse Wave Velocity Measurements Characterise Aortic Cardiovascular Disease?', International Conference of Medical Physics, Oral Presentation, Brighton, September 2013.
- **DB Cassidy**, SJ Gandy, S Duce, S Matthew, P Martin, RS Nicholas, JG Houston , 'The Fatty Heart: CMRI Study of Diabetes and Cardiovascular Disease', Oral Presentation, International Conference of Medical Physics, Brighton, September 2013.
- **DB Cassidy**, SJ Gandy, S Duce, F Khan, P Martin, RS Nicholas, JG Houston, 'Investigating the Role of Epicardial Fat as an Imaging Biomarker in Type-2 Diabetes', Poster, International Union of Physiological Sciences, Poster Presentation, Birmingham, July 2013.
- **DB Cassidy,** SJ Gandy, S Duce, S Matthew, P Martin, RS Nicholas, JG Houston, 'Diabetes and Myocardial Fat in the Paradigm of Cardiovascular Disease', Oral and Poster Presentation, UK Radiology Congress, Liverpool, June 2013.
- **DB Cassidy,** SJ Gandy, S Duce, S Matthew, P Martin, RS Nicholas, JG Houston Preliminary Investigation into the Benefits of Imaging Myocardial Fat', Scottish Heart and Arterial Risk Prevention, Oral and Poster Presentation, Dunkeld, November 2012.
- **DB Cassidy,** SJ Gandy, P Martin, RS Nicholas, JG Houston 'Investigation of Magnetic Resonance Pulse Wave Velocity Measurements: Can it Characterise Aortic Cardiovascular Disease?', UKRC abstract, Oral Presentation, Manchester, June 2012.

- **DB Cassidy,** SJ Gandy, P Martin, RS Nicholas, JG Houston 'Multi-Slice CINE Phase Contrast Pulse Wave Velocity Measurements for Characterising Aortic Cardiovascular Disease', SINAPSE Annual Scientific Meeting, Poster Presentation, Royal College of Physicians and Surgeons, Glasgow, May 2012.
- **DB Cassidy,** SJ Gandy, P Martin, RS Nicholas, JG Houston 'Characterising Aortic Cardiovascular Disease Using Novel MRI Pulse Wave Velocity Techniques',. Scottish Society of Experimental Medicine SSEM, Poster Presentation, Dundee, May 2012.
- **DB Cassidy,** SJ Gandy, P Martin, RS Nicholas, JG Houston 'Multi-Slice CINE Phase Contrast Pulse Wave Velocity Measurements for Characterising Aortic Cardiovascular Disease' International Society of Magnetic Resonance in Medicine ISMRM, Poster Presentation, Melbourne, Australia, May 2012.
- **DB Cassidy,** SJ Gandy, P Martin, RS Nicholas, JG Houston 'Can Magnetic Resonance Pulse Wave Velocity Measurements Characterise Aortic Cardiovascular Disease?' Scottish Cardiovascular Forum, Oral Presentation, Dundee, Feb 2012.
- **DB Cassidy,** SJ Gandy, P Martin, RS Nicholas, JG Houston 'Using Magnetic Resonance Pulse Wave Velocity Measurement to Predict Levels of Aortic Stiffening' Medical Research Institute Symposium, Poster Presentation, Dundee, Dec 2011
- **DB Cassidy,** SJ Gandy, P Martin, RS Nicholas, JG Houston 'Technical Validation of Cardiac MRI Pulse Wave Velocity Measurements', SINAPSE Annual Scientific Meeting, Poster presentation, Dundee, May 2011.

REFERENCES

ADA, 2008. Standards of medical care in diabetes--2008. *Diabetes care*, 31 Suppl 1, pp.S12–54..

Adams, R.J. et al., 2003. Coronary risk evaluation in patients with transient ischemic attack and ischemic stroke: a scientific statement for healthcare professionals from the Stroke Council and the Council on Clinical Cardiology of the American Heart Association/American Stroke A. *Circulation*, 108(10), pp.1278–90.

Aquaro, G.D. et al., 2013. Age-dependent changes in elastic properties of thoracic aorta evaluated by magnetic resonance in normal subjects. *Interactive cardiovascular and thoracic surgery*, 17(4), pp.674–9.

Balter, S., 1987. An introduction to the physics of magnetic resonance imaging. *Radiographics*, pp.371–383.

Ben-Shlomo, Y. et al., 2014. Aortic pulse wave velocity improves cardiovascular event prediction: an individual participant meta-analysis of prospective observational data from 17,635 subjects. *Journal of the American College of Cardiology*, 63(7), pp.636–46.

Bérard, E. et al., 2013. Pulse wave velocity, pulse pressure and number of carotid or femoral plaques improve prediction of cardiovascular death in a population at low risk. *Journal of human hypertension*, 27(9), pp.529–34.

Blacher, J. et al., 1999. Aortic Pulse Wave Velocity as a Marker of Cardiovascular Risk in Hypertensive Patients. *Library*, 33(5), pp.1111–7.

Blacher, J. & Safar, M.E., 2005. Large-artery stiffness, hypertension and cardiovascular risk in older patients. *Nature clinical practice. Cardiovascular medicine*, 2(9), pp.450–5.

Bland, J.M. & Altman, D.G., 1999. Measuring agreement in method comparison studies. *Statistical Methods in Medical Research*, 8(2), pp.135–160.

Bock, J. et al., 2010. 4D phase contrast MRI at 3 T: effect of standard and blood-pool contrast agents on SNR, PC-MRA, and blood flow visualization. *Magnetic resonance in medicine : official journal of the Society of Magnetic Resonance in Medicine / Society of Magnetic Resonance in Medicine*, 63(2), pp.330–8.

Bots, M.L. et al., 2014. Common Carotid Intima-Media Thickness Measurements Do Not Improve Cardiovascular Risk Prediction in Individuals With Elevated Blood Pressure: The USE-IMT Collaboration. *Hypertension*, 63(6), pp.1173–81.

Bramwell, J.C. & Hill, A.., 1922. VELOCITY OF TRANSMISSION OF THE PULSE-WAVE. *The Lancet*, 199(5149), pp.891–892.

Brandts, A. et al., 2012. The effect of hypertension on aortic pulse wave velocity in type-1 diabetes mellitus patients: assessment with MRI. *The international journal of cardiovascular imaging*, 28(3), pp.543–50.

Burnett, J.R., 2004. Lipids, lipoproteins, atherosclerosis and cardiovascular disease. *The Clinical biochemist. Reviews / Australian Association of Clinical Biochemists*, 25(1), p.2.

Butlin, M. et al., 2008. Determining pulse wave velocity using MRI: a comparison and repeatability of results using seven transit time algorithms. *Artery Research*, 2(3), p.99.

Cardoso, C.R.L. et al., 2013. Prognostic Impact of Aortic Stiffness in High-Risk Type 2 Diabetic Patients: The Rio de Janeiro Type 2 Diabetes Cohort Study. *Diabetes care*.

Cavalcante, J.L. et al., 2011. Aortic Stiffness. *Journal of the American College of Cardiology*, 57(14), pp.1511–1522. Available at:

Cheung, C. et al., 2012. Europe PMC Funders Group Generation of human vascular smooth muscle subtypes provides insight into embryological origin-dependent disease susceptibility. , 30(2), pp.165–173.

Chilton, R.J., 2004. Pathophysiology of Coronary Heart Disease: A Brief Review. *J Am Osteopath Assoc*, 104(9_suppl), p.5S–8.

Cruickshank, K., 2002. Aortic Pulse-Wave Velocity and Its Relationship to Mortality in Diabetes and Glucose Intolerance: An Integrated Index of Vascular Function? *Circulation*, 106(16), pp.2085–2090.

Davignon, J. & Ganz, P., 2004. Role of endothelial dysfunction in atherosclerosis. *Circulation*, 109(23 Suppl 1), pp.III27–32.

Dogui, A. et al., 2011. Measurement of aortic arch pulse wave velocity in cardiovascular MR: Comparison of transit time estimators and description of a new approach. *Journal of magnetic resonance imaging : JMRI*, 33(6), pp.1321–9.

Franklin, S.S. et al., 1997. Hemodynamic Patterns of Age-Related Changes in Blood Pressure : The Framingham Heart Study. *Circulation*, 96(1), pp.308–315.

Franklin, S.S. et al., 1999. Is pulse pressure useful in predicting risk for coronary heart Disease? The Framingham heart study. *Circulation*, 100(4), pp.354–60.

Franklin, S.S. & Wong, N.D., 2013. Hypertension and Cardiovascular Disease: Contributions of the Framingham Heart Study. *Global Heart*, 8(1), pp.49–57.

Futterman, L.G. & Lemberg, L., 1998. Fifty percent of patients with coronary artery disease do not have any of the conventional risk factors. *American journal of critical care : an official publication, American Association of Critical-Care Nurses*, 7(3), pp.240–4.

Gandy, S.J. et al., 2008. Comparison of the reproducibility of quantitative cardiac left ventricular assessments in healthy volunteers using different MRI scanners: a multicenter simulation. *Journal of magnetic resonance imaging : JMRI*, 28(2), pp.359–65.

Gatehouse, P.D. et al., 2005. Applications of phase-contrast flow and velocity imaging in cardiovascular MRI. *European radiology*, 15(10), pp.2172–84.

Goff, D.C. et al., 2014. 2013 ACC/AHA Guideline on the Assessment of Cardiovascular Risk: A Report of the American College of Cardiology/American Heart Association

Task Force on Practice Guidelines. *Journal of the American College of Cardiology*, 63(25 Pt B), pp.2935–59.

Goubergrits, L. et al., 2014. MRI-based computational fluid dynamics for diagnosis and treatment prediction: Clinical validation study in patients with coarctation of aorta. *Journal of magnetic resonance imaging : JMRI*.

Greenland, P. et al., 2010. 2010 ACCF/AHA guideline for assessment of cardiovascular risk in asymptomatic adults: a report of the American College of Cardiology Foundation/American Heart Association Task Force on Practice Guidelines. *Journal of the American College of Cardiology*, 56(25), pp.e50–103.

Grotenhuis, H.B. et al., 2009. Validation and reproducibility of aortic pulse wave velocity as assessed with velocity-encoded MRI. *Journal of magnetic resonance imaging : JMRI*, 30(3), pp.521–6.

Grundy, S.M. et al., 1999. Assessment of cardiovascular risk by use of multiple-risk-factor assessment equations. *Journal of the American College of Cardiology*, 34(4), pp.1348–1359.

Hackam, D.G. & Anand, S.S., 2003. Emerging risk factors for atherosclerotic vascular disease: a critical review of the evidence. *JAMA : the journal of the American Medical Association*, 290(7), pp.932–40.

Haffner, S.M. et al., 1998. Mortality from coronary heart disease in subjects with type 2 diabetes and in nondiabetic subjects with and without prior myocardial infarction. *The New England journal of medicine*, 339(4), pp.229–34.

Hahn, C. & Schwartz, M.A., 2009. Mechanotransduction in vascular physiology and atherogenesis. *Nature reviews. Molecular cell biology*, 10(1), pp.53–62.

Haimovici, H., 1991. The role of arterial tissue susceptibility in atherogenesis. *Texas Heart Institute journal / from the Texas Heart Institute of St. Luke's Episcopal Hospital, Texas Children's Hospital*, 18(1), pp.81–3.

Hansen, T.W. et al., 2006. Ambulatory arterial stiffness index predicts stroke in a general population. *Journal of hypertension*, 24(11), pp.2247–53.

Hashemi, R.H., Bradley, W.G. & Lisanti, C.J., 2012. *MRI: The Basics*, Lippincott Williams & Wilkins.

Heiberg, E. et al., 2010a. Design and validation of Segment--freely available software for cardiovascular image analysis. *BMC medical imaging*, 10, p.1.

Heiberg, E. et al., 2010b. Design and validation of Segment--freely available software for cardiovascular image analysis. *BMC medical imaging*, 10(1), p.1.

Hennion, D.R. & Siano, K.A., 2013. Diagnosis and treatment of peripheral arterial disease. *American family physician*, 88(5), pp.306–10.

Hickson, S.S. et al., 2010. The relationship of age with regional aortic stiffness and diameter. *JACC. Cardiovascular imaging*, 3(12), pp.1247–55.

Huybrechts, S.A.M. et al., 2011. Carotid to femoral pulse wave velocity: a comparison of real travelled aortic path lengths determined by MRI and superficial measurements. *Journal of hypertension*, 29(8), pp.1577–82.

Ibrahim, E.-S.H. et al., 2010. Measuring aortic pulse wave velocity using high-field cardiovascular magnetic resonance: comparison of techniques. *Journal of cardiovascular magnetic resonance : official journal of the Society for Cardiovascular Magnetic Resonance*, 12(1), p.26.

Joly, L. et al., 2009. Pulse wave velocity assessment by external noninvasive devices and phase-contrast magnetic resonance imaging in the obese. *Hypertension*, 54(2), pp.421–6.

Jung, B. et al., 2004. Measurement of left ventricular velocities: phase contrast MRI velocity mapping versus tissue-doppler-ultrasound in healthy volunteers. *Journal of cardiovascular magnetic resonance : official journal of the Society for Cardiovascular Magnetic Resonance*, 6(4), pp.777–83.

Juutilainen, A. et al., 2005. Type 2 diabetes as a "coronary heart disease equivalent": an 18-year prospective population-based study in Finnish subjects. *Diabetes care*, 28(12), pp.2901–7.

Kau, T. et al., 2007. Aortic development and anomalies. *Seminars in Interventional Radiology*, 24(212), pp.141–152.

Kawasaki, T. et al., 1987. Non-invasive assessment of the age related changes in stiffness of major branches of the human arteries. *Cardiovascular research*, 21(9), pp.678–87.

Kilner, P.J. et al., 2010. Recommendations for cardiovascular magnetic resonance in adults with congenital heart disease from the respective working groups of the European Society of Cardiology. *European heart journal*, 31(7), pp.794–805.

Kimoto, E. et al., 2003. Preferential stiffening of central over peripheral arteries in type 2 diabetes. *Diabetes*, 52(2), pp.448–52.

Kröner, E.S.J. et al., 2012. Evaluation of sampling density on the accuracy of aortic pulse wave velocity from velocity-encoded MRI in patients with Marfan syndrome. *Journal of magnetic resonance imaging : JMRI*, 36(6), pp.1470–6.

Lancet, 2014. Cardiovascular disease, chronic kidney disease, and diabetes mortality burden of cardiometabolic risk factors from 1980 to 2010: a comparative risk assessment. *The lancet. Diabetes & endocrinology*.

Laurent, S., Cockcroft, J., Bortel, L. Van, et al., 2006. Expert consensus document on arterial stiffness : methodological issues and clinical applications. , pp.2588–2605.

Laurent, S., Cockcroft, J., Van Bortel, L., et al., 2006. Expert consensus document on arterial stiffness: methodological issues and clinical applications. *European heart journal*, 27(21), pp.2588–605.

Lee, J.M.S. et al., 2007a. Multi-modal magnetic resonance imaging quantifies atherosclerosis and vascular dysfunction in patients with type 2 diabetes mellitus. *Diabetes & vascular disease research : official journal of the International Society of Diabetes and Vascular Disease*, 4(1), pp.44–8.

Lee, J.M.S. et al., 2007b. Multi-modal magnetic resonance imaging quantifies atherosclerosis and vascular dysfunction in patients with type 2 diabetes mellitus. *Diabetes & vascular disease research : official journal of the International Society of Diabetes and Vascular Disease*, 4(1), pp.44–8.

Lee, V.S., 2006. *Cardiovascular MRI: Physical Principles to Practical Protocols*, Lippincott Williams & Wilkins.

Leroux-Berger, M. et al., 2011. Pathologic calcification of adult vascular smooth muscle cells differs on their crest or mesodermal embryonic origin. *Journal of bone and mineral research : the official journal of the American Society for Bone and Mineral Research*, 26(7), pp.1543–53.

Libby, P. & Theroux, P., 2005. Pathophysiology of coronary artery disease. *Circulation*, 111(25), pp.3481–8.

Liberati, A. et al., 2009. The PRISMA statement for reporting systematic reviews and meta-analyses of studies that evaluate health care interventions: explanation and elaboration. *PLoS medicine*, 6(7), p.e1000100.

Liu, C.-Y. et al., 2012. Aortic size, distensibility, and pulse wave velocity changes with aging: longitudinal analysis from Multi-Ethnic Study of Atherosclerosis (MESA). *Journal of Cardiovascular Magnetic Resonance*, 14(Suppl 1), p.P126.

Lloyd-Jones, D.M. et al., 2004. Framingham risk score and prediction of lifetime risk for coronary heart disease. *The American journal of cardiology*, 94(1), pp.20–4. Available at: http://www.sciencedirect.com/science/article/pii/S0002914904004370

Lloyd-Jones, D.M. et al., 2006. Prediction of lifetime risk for cardiovascular disease by risk factor burden at 50 years of age. *Circulation*, 113(6), pp.791–8.

Majesky, M.W., 2007. Developmental basis of vascular smooth muscle diversity. *Arteriosclerosis, Thrombosis, and Vascular Biology*, 27, pp.1248–1258.

Mancia, G. et al., 2007. 2007 Guidelines for the Management of Arterial Hypertension: The Task Force for the Management of Arterial Hypertension of the European Society of Hypertension (ESH) and of the European Society of Cardiology (ESC). *Journal of hypertension*, 25(6), pp.1105–87.

Mancia, G. et al., 2014. 2013 ESH/ESC Practice Guidelines for the Management of Arterial Hypertension. *Blood pressure*, 23(1), pp.3–16.

Markl, M., Frydrychowicz, A., et al., 2012. 4D flow MRI. *Journal of magnetic resonance imaging : JMRI*, 36(5), pp.1015–36.

Markl, M., Wallis, W., et al., 2012. Analysis of pulse wave velocity in the thoracic aorta by flow-sensitive four-dimensional MRI: reproducibility and correlation with

characteristics in patients with aortic atherosclerosis. *Journal of magnetic resonance imaging : JMRI*, 35(5), pp.1162–8.

Markl, M. et al., 2010. Estimation of global aortic pulse wave velocity by flow-sensitive 4D MRI. *Magnetic resonance in medicine : official journal of the Society of Magnetic Resonance in Medicine / Society of Magnetic Resonance in Medicine*, 63(6), pp.1575–82.

Markl, M. & Leupold, J., 2012. Gradient echo imaging. *Journal of magnetic resonance imaging : JMRI*, 35(6), pp.1274–89.

Maroules, C.D. et al., 2014. Cardiovascular outcome associations among cardiovascular magnetic resonance measures of arterial stiffness: the Dallas heart study. *Journal of cardiovascular magnetic resonance : official journal of the Society for Cardiovascular Magnetic Resonance*, 16(1), p.33.

Mathers, C.D. & Loncar, D., 2006. Projections of global mortality and burden of disease from 2002 to 2030. *PLoS medicine*, 3(11), p.e442.

McRobbie, 2007. *MRI from Picture to Proton [Paperback]*, Cambridge University Press; 2 edition. Available at: http://www.amazon.co.uk/MRI-Picture-Proton-Donald-McRobbie/dp/052168384X

Van der Meer, R.W. et al., 2007. Magnetic resonance assessment of aortic pulse wave velocity, aortic distensibility, and cardiac function in uncomplicated type 2 diabetes

mellitus. *Journal of cardiovascular magnetic resonance : official journal of the Society for Cardiovascular Magnetic Resonance*, 9(4), pp.645–51.

Mitchell, G.F. et al., 2010. Arterial stiffness and cardiovascular events: the Framingham Heart Study. *Circulation*, 121(4), pp.505–11.

Mohiaddin, R.H. & Longmore, D.B., 1989. MRI studies of atherosclerotic vascular disease: Structural evaluation and physiological measurements. *Br. Med. Bull.*, 45(4), pp.968–990.

Montgomery, J.E. & Brown, J.R., 2013. Metabolic biomarkers for predicting cardiovascular disease. *Vascular health and risk management*, 9, pp.37–45.

Moratal, 2008. k-Space tutorial: an MRI educational tool for a better understanding of k-space. *Biomedical Imaging and Intervention Journal*, 4(1), p.e15.

Mowat, D.H., Haites, N.E. & Rawles, J.M., 1983. Aortic blood velocity measurement in healthy adults using a simple ultrasound technique. *Cardiovascular research*, 17(2), pp.75–80.

Muller, J.E., Tofler, G.H. & Stone, P.H., 1989. Circadian variation and triggers of onset of acute cardiovascular disease. *Circulation*, 79(4), pp.733–743. Available at: http://circ.ahajournals.org/cgi/doi/10.1161/01.CIR.79.4.733

Nayak, K.S. et al., 2004. Real-time cardiac MRI at 3 tesla. *Magnetic resonance in medicine : official journal of the Society of Magnetic Resonance in Medicine / Society of Magnetic Resonance in Medicine*, 51(4), pp.655–60.

Nichols WW, O.M., 2011. *McDonald's Blood Flow in Arteries, Sixth Edition: Theoretical, Experimental and Clinical Principles*, CRC Press.

Nissen, S.E. et al., 2004. Effect of intensive compared with moderate lipid-lowering therapy on progression of coronary atherosclerosis: a randomized controlled trial. *JAMA : the journal of the American Medical Association*, 291(9), pp.1071–80.

Papavassiliu, T. et al., 2005. Effect of endocardial trabeculae on left ventricular measurements and measurement reproducibility at cardiovascular MR imaging. *Radiology*, 236, pp.57–64.

Pereles, F.S. et al., 2001. Usefulness of segmented trueFISP cardiac pulse sequence in evaluation of congenital and acquired adult cardiac abnormalities. *AJR. American journal of roentgenology*, 177(5), pp.1155–60.

Price, J., 1999. Relationship between smoking and cardiovascular risk factors in the development of peripheral arterial disease and coronary artery disease; Edinburgh Artery Study Edinburgh Artery Study. *European Heart Journal*, 20(5), pp.344–353.

Qian, M. et al., 2014. Pulsatile Flow Characterization in A Vessel Phantom With Elastic Wall Using Ultrasonic Particle Image Velocimetry Technique: The Impact of Vessel Stiffness on Flow Dynamics. *IEEE transactions on bio-medical engineering*, 9294(c), pp.1–7.

Della Rocca, D.G. & Pepine, C.J., 2010. Endothelium as a predictor of adverse outcomes. *Clinical cardiology*, 33(12), pp.730–2.

Roes, S.D. et al., 2008. Assessment of aortic pulse wave velocity and cardiac diastolic function in subjects with and without the metabolic syndrome: HDL cholesterol is independently associated with cardiovascular function. *Diabetes care*, 31(7), pp.1442–4.

Rogers, W.J. et al., 2001. Age-associated changes in regional aortic pulse wave velocity. *Journal of the American College of Cardiology*, 38(4), pp.1123–9.

Rose, J.-L. et al., 2010. Influence of age and sex on aortic distensibility assessed by MRI in healthy subjects. *Magnetic resonance imaging*, 28(2), pp.255–63.

Ruddy, J.M. et al., 2008. Regional heterogeneity within the aorta: Relevance to aneurysm disease. *The Journal of Thoracic and Cardiovascular Surgery*, 136(5), pp.1123–1130.

Saeed, M., Wendland, M.F. & Higgins, C.B., 2000. Blood pool MR contrast agents for cardiovascular imaging. *Journal of magnetic resonance imaging : JMRI*, 12(6), pp.890–8.

Safar, O.R., 2006. *Arterial Stiffness in Hypertension, Volume 23*, Elsevier.

Salvi, P. et al., 2008. Comparative study of methodologies for pulse wave velocity estimation. *Journal of human hypertension*, 22(10), pp.669–77.

Schirmang, T.C. et al., 2009. Peripheral arterial disease: update of overview and treatment. *Medicine and health, Rhode Island*, 92(12), pp.398–402.

Scott, J., 2004. Pathophysiology and biochemistry of cardiovascular disease. *Current opinion in genetics & development*, 14(3), pp.271–9.

Slark, J. & Sharma, P., 2009. Cerebrovascular Disease and its Relationship to Other Vascular Beds : A Comprehensive Review of the Literature. , pp.1–8.

Smith, S.C. et al., 2006. AHA/ACC guidelines for secondary prevention for patients with coronary and other atherosclerotic vascular disease: 2006 update endorsed by the National Heart, Lung, and Blood Institute. *Journal of the American College of Cardiology*, 47(10), pp.2130–9.

Sowers, J.R., Epstein, M. & Frohlich, E.D., 2001. Diabetes, Hypertension, and Cardiovascular Disease : An Update. *Hypertension*, 37(4), pp.1053–1059.

Stanisz, G.J. et al., 2005. T1, T2 relaxation and magnetization transfer in tissue at 3T. *Magnetic resonance in medicine : official journal of the Society of Magnetic Resonance in Medicine / Society of Magnetic Resonance in Medicine*, 54(3), pp.507–12.

Stratton, I.M., 2000. Association of glycaemia with macrovascular and microvascular complications of type 2 diabetes (UKPDS 35): prospective observational study. *BMJ*, 321(7258), pp.405–412.

Strijkers, G.J. et al., 2007. MRI contrast agents: current status and future perspectives. *Anti-cancer agents in medicinal chemistry*, 7(3), pp.291–305.

Suever, J.D. et al., 2011. Reproducibility of pulse wave velocity measurements with phase contrast magnetic resonance and applanation tonometry. *The international journal of cardiovascular imaging*, pp.1–6.

Sugawara, J. et al., 2008. Age-associated elongation of the ascending aorta in adults. *JACC. Cardiovascular imaging*, 1(6), pp.739–48.

Taviani, V. et al., 2010. Accuracy and repeatability of fourier velocity encoded M-mode and two-dimensional cine phase contrast for pulse wave velocity measurement in the descending aorta. *Journal of magnetic resonance imaging : JMRI*, 31(5), pp.1185–94.

Vasan, R.S. et al., 2001. Impact of high-normal blood pressure on the risk of cardiovascular disease. *The New England journal of medicine*, 345(18), pp.1291–7.

Vermeersch, S.J. et al., 2009. Distance measurements for the assessment of carotid to femoral pulse wave velocity. *Journal of hypertension*, 27(12), pp.2377–85.

Vermeersch, S.J., Dynamics, B. & Society, L., 2010. Determinants of pulse wave velocity in healthy people and in the presence of cardiovascular risk factors: "establishing normal and reference values". *European heart journal*, 31(19), pp.2338–50.

Vinereanu, D., 2006. Risk factors for atherosclerotic disease: present and future. *Herz*, 31 Suppl 3, pp.5–24.

Vlachopoulos, C., 2010. Prediction of cardiovascular events and all-cause mortality with arterial stiffness: a systematic review and meta-analysis. *Journal of the American College of Cardiology*, 55(13), pp.1318–27.

Wang, T.J. et al., 2006. Multiple biomarkers for the prediction of first major cardiovascular events and death. *The New England journal of medicine*, 355(25), pp.2631–9.

Waugh, S.A. et al., 2009. Optimization of the contrast dose and injection rates in whole-body MR angiography at 3.0T. *Journal of magnetic resonance imaging : JMRI*, 30(5), pp.1059–67.

Weishaupt, D., Köchli, V.D. & Marincek, B., 2003. *How does MRI work?: An Introduction to the Physics and Function of Magnetic Resonance Imaging*, Springer.

Wentland, A.L., Grist, T.M. & Wieben, O., 2014. Review of MRI-based measurements of pulse wave velocity: a biomarker of arterial stiffness. *Cardiovascular diagnosis and therapy*, 4(2), pp.193–206.

Westenberg, J.J.M. et al., 2011. Age-related and regional changes of aortic stiffness in the marfan syndrome: Assessment with velocity-encoded MRI. *Journal of magnetic resonance imaging : JMRI*, 531, pp.526–531.

Westenberg, J.J.M. et al., 2012. Bramwell-Hill modeling for local aortic pulse wave velocity estimation: a validation study with velocity-encoded cardiovascular magnetic resonance and invasive pressure assessment. *Journal of cardiovascular magnetic resonance : official journal of the Society for Cardiovascular Magnetic Resonance*, 14(1), p.2.

Westenberg, J.J.M. et al., 2010. Improved aortic pulse wave velocity assessment from multislice two-directional in-plane velocity-encoded magnetic resonance imaging. *Journal of magnetic resonance imaging : JMRI*, 32(5), pp.1086–94.

Wieben, O., Francois, C. & Reeder, S.B., 2008. Cardiac MRI of ischemic heart disease at 3 T: potential and challenges. *European journal of radiology*, 65(1), pp.15–28.

Wilkinson, I.B. & McEniery, C.M., 2004. Arterial stiffness, endothelial function and novel pharmacological approaches. *Clinical and experimental pharmacology & physiology*, 31(11), pp.795–9.

Wood, R. et al., 2012. 1.5 tesla magnetic resonance imaging scanners compared with 3.0 tesla magnetic resonance imaging scanners: systematic review of clinical effectiveness. *CADTH technology overviews*, 2(2), p.e2201.

Young, 1808. The Croonian Lecture: On the Functions of the Heart and Arteries. *Phil. Trans. R. Soc. Lond*, p.99.

Yu, H.-Y. et al., 2006. Quantification of the pulse wave velocity of the descending aorta using axial velocity profiles from phase-contrast magnetic resonance imaging. *Magnetic resonance in medicine : official journal of the Society of Magnetic Resonance in Medicine / Society of Magnetic Resonance in Medicine*, 56(4), pp.876–83.